

**BIOCHEMICAL AND STRUCTURAL  
STUDIES OF HUMAN METHIONINE  
SYNTHASE REDUCTASE**

A thesis submitted to the University of Manchester  
for the degree Doctor of Philosophy in the Faculty  
of Life Sciences

**2010**

**Xiaodong Lou**

# CONTENTS

CONTENTS	1
ABSTRACT	7
DECLARATION	8
COPYRIGHT STATEMENT	8
ABBREVIATIONS	9
ACKNOWLEDGEMENTS	11

## CHAPTER ONE

### INTRODUCTION

1.1.	General aims of this project	13
1.2.	Cofactors in biology	15
1.3.	Diflavin reductase	22
1.3.1.	The structure and function of the diflavin reductases family	22
1.3.2.	Examples of diflavin enzymes NOS and CPR	28
1.3.2.1.	NOS	28
1.3.2.2.	CPR	31
1.4.	Methionine synthase reductase	35
1.4.1.	Cloning and mapping of the cDNA of the methionine synthase reductase	35
1.4.2.	Molecular and functional properties of human MSR	36
1.4.3.	Electron transfer on human MSR	39
1.4.4.	Complex formation between human MSR and human MS	41
1.5.	Methionine Synthase	43
1.5.1.	The catalytic reaction of <i>E. coli</i> MS as a basis for understanding human MS	43
1.5.2.	Mechanism of reductive activation of <i>E. coli</i> MS	44
1.5.3.	Function modules of <i>E. coli</i> MS	45
1.5.4.	A working model for <i>E. coli</i> MS	47

1.5.5.	Human methionine synthase	48
1.6.	The molecular basis for the autosomal recessive disorders related with MSR	48

## CHAPTER TWO

### MATERIALS AND METHODS

2.1.	Materials	53
2.2.	Media	53
2.3.	Recombinant DNA techniques	53
2.3.1.	Isolation of plasmid DNA	53
2.3.2.	Transformation of <i>E. coli</i> cells	53
2.3.3.	Construction of MSR expression plasmids	55
2.3.3.1.	Construction of plasmid pET41aMSR containing cDNA encoding the MSR gene, a GST tag and a (His) <sub>6</sub> tag.	55
2.3.3.2.	Construction of a plasmid containing MSR cDNA encoding the MSR fused to a GST tag for expression in <i>Pichia pastoris</i> .	57
2.3.4.	Agarose gel electrophoresis	58
2.3.5.	Polymerase Chain Reaction (PCR)	59
2.3.6.	Sources of DNA	61
2.3.7.	Site-directed mutagenesis	61
2.4.	Protein expression and purification	62
2.4.1.	Protein analysis	62
2.4.1.1.	Protein concentration	62
2.4.1.2.	SDS-PAGE electrophoresis	63
2.4.2.	Expression of wild-type MSR, MSR mutant proteins, and MS activation Domain	64
2.4.3.	Purification of MSR and MS	65
2.4.3.1.	Purification of wild-type FAD/NADPH binding domain of MSR and mutant Proteins	65

2.4.3.2. Purification of wild-type full-length MSR and its mutant forms	66
2.4.3.3. Purification of the activation domain of MS	67
2.5. Crystallogenesis, X-ray diffraction and model building	68
2.5.1. Crystallogenesis of the FAD/NADPH binding domain of MSR	69
2.5.2. X-ray diffraction on the FAD/NDAPH binding domain of MSR	69
2.5.3. Structure determination and refinement of the model for the FAD/NADPH binding domain	69
2.5.4. Crystallogenesis on the activation domain of MS	69
2.6. Kinetic studies	70
2.6.1. Steady-state kinetic studies with the FAD/NADPH binding domain of MSR	71
2.6.2. Steady-state kinetic studies with the wild-type full-length MSR and its mutant Forms	72
2.6.3. Steady-state inhibition studies with wild-type and the mutant forms of the FAD/NADPH- binding domain of MSR	72
2.6.4. Pre-steady-state kinetic studies on the wild-type FAD/NADPH binding domain of MSR and mutants	73
2.6.5. Redox titrations of the flavin cofactors in FAD/NADPH binding domain of MSR	75
2.7. Fluorescence studies on the wild-type MSR and mutants	77
2.8. Electron spin echo (ESE) studies on the wild-type full-length MSR	78
2.8.1. Sample preparation for ESE	78
2.8.2. EPR	79
2.8.2.1. Theory of EPR	79
2.8.2.2. EPR experiments and conditions	80
2.8.3. ENDOR	80
2.8.3.1. Theory of ENDOR	80
2.8.3.2. ENDOR experiments and conditions	81

2.8.4. ESEEM	81
2.8.4.1. Theory of ESEEM	81
2.8.4.2. Sample preparation and equipment	82
2.8.5. ELDOR	82
2.8.5.1. Theory of ELDOR	82
2.8.5.2. Sample preparation and equipment	83

## **CHAPTER THREE**

### **STRUCTURAL STUDIES ON THE**

### **WILD-TYPE FAD/NADPH BINDING DOMAIN OF MSR**

3.1. Introduction	86
3.2. Results	87
3.2.1. Expression of the FAD/NADPH binding domain of MSR	87
3.2.2. Purification of the FAD/NADPH-binding domain of MSR	88
3.2.3. Kinetic studies on the FAD/NADPH binding domain of MSR	90
3.2.3.1. Spectral properties of the FAD/NADPH-binding domain of MSR	90
3.2.3.2. Steady-state reduction properties of the FAD/NADPH binding domain of MSR	91
3.2.3.3. Pre-steady-state reduction properties of the FAD/NADPH binding domain	92
3.2.3.3.1. Photodiode array spectroscopy analysis of reduction of the FAD/NADPH binding domain by NADPH	90
3.2.3.3.2. Single-wavelength analysis on FAD/NADPH binding domain of MSR	94
3.2.4. Crystallization, X-ray diffraction, structure elucidation and molecular Modelling	95
3.2.5. Description and analysis of the structural model of the FAD/NADPH-binding domain of MSR	98
3.2.5.1. Overall domain structure of the FAD/NADPH binding domain of MSR	98
3.2.5.2. The hinge region and connecting domain	99

3.2.5.3. The FAD binding region and FAD binding site	100
3.2.5.4. The NADPH binding domain and NADPH binding site	102
3.3. Discussion	104

## **CHAPTER FOUR**

### **COMPARISON OF THE MUTANTS WITH THE WILD TYPE OF MSR**

4.1. Introduction	110
4.2. Results	113
4.2.1. Site-directed mutagenesis of the FAD/NADPH binding domain of MSR	113
4.2.2. The purification of the mutants	114
4.2.2.1. The purification of the mutants D652A, D652R, D652N of FADPH- binding domain of MSR	114
4.2.2.2. The purification of the mutants D652A, D652R, D652N, W679A, W697H of the full-length MSR	116
4.2.3. Kinetic studies on mutants	121
4.2.3.1. Kinetic studies on the FAD/NADPH binding domain of MSR	121
4.2.3.1.1. Steady-state kinetic studies on the FAD/NADPH binding domain mutants D652A, D652R, D652N	121
4.2.3.1.2. Steady-state inhibition studies on the FAD/NADPH binding domain mutants D652A, D652R and D652N.	122
4.2.3.1.3. Pre-steady-state kinetic studies on the FAD/NADPH binding domain mutants D652A, D652R, D652N	125
4.2.3.1.4. Redox potential studies on the FAD/NADPH binding domain mutants D652A, D652R, and D652N.	127
4.2.3.2. Kinetic studies on the full length MSR mutants D652A, D652R, D652N, W697A and W697H	131
4.2.3.2.1. Steady-state kinetic studies on the full length MSR mutants D652A, D652R, D652N, W697A and W697H	131
4.2.3.2.2. Pre-steady-state kinetic studies on the full length MSR mutants D652 A, W697A and W697H	133

4.2.3.3. Fluorescence on the wild-type and one mutant of full-length MSR	135
4.3. Discussion	136

## **CHAPTER FIVE**

### **EPR, ENDOR, ESEEM and ELDOR on MSR**

5.1. Introduction	140
5.2. Results	141
5.2.1. EPR spectroscopy	141
5.2.2. ESEEM spectroscopy	143
5.2.3. ENDOR spectroscopy	149
5.2.4. ELDOR	149
5.3. Discussion	151

## **CHAPTER SIX**

### **THE CRYSTALLOGRAPHY OF THE ACTIVATION DOMAIN OF METHIONINE SYNTHASE**

6.1. Introduction	157
6.2. Results	159
6.2.1. Expression and purification of the activation domain of MS	159
6.2.2. Crystallography of the activation domain of MS	160
6.2.3. The construction of two MSR expression plasmids.	161
6.2.3.1. The construction of pET41a and its expression of MSR.	161
6.2.3.2. The construction of pMSRGST	162
6.3. Discussion	164

## **CHAPTER SEVEN**

### **DISCUSSION**

7.1. Discussion	167
7.2. Further investigation	169

<b>REFERENCES</b>	171
-------------------	-----

Word Count: The total word count with figure legends and reference is 42,658

## ABSTRACT

### BIOCHEMICAL AND STRUCTURAL STUDIES OF HUMAN METHIONINE SYNTHASE REDUCTASE

Human methionine synthase reductase (MSR) is a 78-kDa diflavin enzyme involved in folate and methionine metabolism. It regenerates the cofactor of methionine synthase (MS), from cob(II), to the active cob (I) form in MS. MSR and one of its FAD/NADPH binding domains were cloned and expressed as GST fusion proteins in *Escherichia coli*. Two expression plasmids for full-length MSR, which contain a N-terminal GST tag and a C-terminal (His)<sub>6</sub> tag, were constructed and validated by sequencing and restriction enzyme digestion and successfully expressed in *E. coli* and *Pichia pastoris*. Subsequently, crystals of the FAD/NADPH binding domain of MSR that diffracted to 1.9 Å, both with and without NADP<sup>+</sup> were produced and the crystal structures were solved by molecular replacement methods. In addition, the activation domain of human MS was expressed in *E. coli* and purified and the crystallization conditions were determined. Based on structural information, site-directed mutagenesis of the two positions Asp<sup>652</sup> and Trp<sup>697</sup> of MSR was performed. The variants D652A, D652R and D652N of the FAD/NADPH binding domain of MSR and the variants D652A, D652R, D652N, W696A and W697H of the full-length MSR were cloned and expressed in BL21 *E. coli* cells. These variants of MSR were purified by affinity chromatography, anion exchange chromatography and gel filtration chromatography. The kinetic properties of these variants of MSR were investigated using steady-state kinetic studies, steady-state inhibition studies, stopped-flow pre steady-state kinetic and redox potential studies. Compared with the data for the wild type MSR, the turnover number of the variants all decreased, the catalytic ability became lower and the midpoint potential of the cofactor FAD shifted to a more positive potential. Both 2'5'-ADP and NADP<sup>+</sup> were competitive inhibitors for variants of MSR. However, 2'5'-ADP was a relatively stronger inhibitor than NADP<sup>+</sup>. All the data on variants of MSR suggested the Asp<sup>652</sup> and Trp<sup>697</sup> residues are important structural and functional determinants in MSR, in particular related to coenzyme binding and hydride transfer. To examine their dynamic properties, EPR, ENDOR and ESEEM were used to investigate the existence of the semiquinone flavin cofactors, FAD and FMN, and the hyperfine coupling arising from the interaction of some nuclei with the unpaired electron spin. ELDOR spectroscopy was applied to measure the distance between the FAD and FMN in MSR following the binding of 2', 5'-ADP, NADP and the activation domain of MS to further analyse conformational properties of MSR in solution.

**The University of Manchester**

**Xiaodong Lou**

**Doctor of Philosophy**

**30.09.2010**



## DECLARATION

No portion of the work referred to in thesis has been submitted in support of an application for another degree or qualification of this or any other university or other institute of learning.

## COPYRIGHT STATEMENT

- i.** The author of this thesis (including any appendices and/or schedules to this thesis) owns any copyright in it (the “Copyright”) and s/he has given The University of Manchester the right to use such Copyright for any administrative, promotional, educational and /or teaching purpose.
- ii.** Copies of this thesis, either in full or in extracts, may be made **only** in accordance with the regulations of the John Rylands University Library of Manchester. Details of these regulations may be obtained from the Librarian. This page must form part of any such copies made.
- iii.** The ownership of any patents, designs, trademarks and any and all other intellectual property rights except for the Copyright (the “ Intellectual Property Right”) and any reproductions of copyright works, for example graphs and tables (“Reproductions”), which may be described in this thesis, may not be owned by the author and may be owned by third parties. Such Intellectual Property rights and Reproductions cannot and must not be made available for use without the prior written permission of the owner(s) of the relevant Intellectual Property Rights and/or reproductions.
- iv.** Further information on the conditions under which disclosure, publication and exploitation of this thesis, the Copyright and any Intellectual Property Rights and/or Reproductions described in it may take place is available from the Head of School of (or the Vice-president) and the Dean of the Faculty of Life Sciences, for Faculty of Life Sciences’ candidates.

## ABBREVIATIONS

MSR	Methionine synthase reductase
MS	Methionine synthase
AdoMet	S-adenosylmethionine
AdoHcy	S-adenosylhomocysteine
FAD	Flavin adenine dinucleotide
FMN	Flavin mononucleotide
NADP <sup>+</sup>	Nicotinamide adenine dinucleotide phosphate
GST	Glutathione-S-transferase
NOS	Nitric oxide synthase
CPR	Cytochrome P450 reductase
NR1	Novel reductase 1
TB	Terrific broth medium
PMSF	Phenylmethanesulphonylfluoride
IPTG	Isopropyl- $\beta$ -D-thiogalactopyranoside
$k_{cat}$	Catalytic turnover number
$K_m$	Michaelis-Menten constant
$K_d$	Dissociation constant
SDS-PAGE	Sodium dodecyl sulfate-polyacrylamide gel electrophoresis
TEMED	<i>N,N,N',N'</i> -tetramethylethylenediamine
DTT	Dithiothreitol
$T_m$	Primer melting temperature
UV	Ultraviolet

**This thesis is dedicated to my wonderful wife Yuehong Wu  
and British Samaritan Dr Karl Fisher for all of the support  
and the encouragement they have given me.**

## **ACKNOWLEDGEMENTS**

I would like to thank my supervisor Professor Nigel Scrutton for giving me the opportunity to complete my PhD studies in his laboratory and for his guidance. I would also like to thank my committee members and specially Dr. Stephen Rigby for his considerable assistance on EPR experiments.

Special thanks go out to Dr. Karl Fisher, Dr Kirsty Mclean, Dr Adrian Dunford and Dr James Belcher for their guidance, support and encouragement they have given me throughout my studies. I would thank Dr Helen Toogood, Dr Kirsten Wolthers and Dr. Derren Leys for their advice on my research. A warm thank to all of the members of the Scrutton, Munro and Leys groups for their smile and encouragement.

## **CHAPTER ONE**

### **INTRODUCTION**

## 1.1. General aims of this project

In this section a brief overview of the general aims of the project is given prior to reviewing the background literature that supports the research project. The overall aim of the research programme was to develop more detailed understanding of the thermodynamic, structural and kinetic properties of two key human enzymes involved in methionine biosynthesis, methionine synthase reductase (MSR) and its protein partner methionine synthase (MS).

In the case of MSR, a reductionist approach was taken by studying the properties of the wild-type full length MSR enzyme the wild type isolated FAD/NADP-binding domain of MSR (residues from 163 to 698) [1], and selected mutants of MSR (full length and FAD/NADP-binding domain). The variants of MSR that were studied include mutants of the FAD/NADP-binding domain of MSR D652A, D652R, D652N and the mutants of the full-length MSR D652A, D652R, D652N, W697A and W697H, each designed to study protein interactions and function of the natural coenzyme (NADPH) binding site in MSR. Studies with MS focused on its activation domain (AD) which comprises residues 925 to 1265 [2]. The advantage of working with the isolated domains is that the spectral changes associated with individual cofactors (FAD or FMN) can be used to illustrate redox changes of one flavin cofactor without interference from other cofactors. Rapid kinetic methods can also be used to accurately follow the electron transfer reactions involving these flavin cofactors. In this project, both MSR and MS were available as recombinant proteins and expressed in *E. coli* or methylotrophic yeast cells (*Pichia pastoris*). A key aspect of this study is the purification, crystallization, structure determination and functional analysis of the FAD/NADP-binding domain of human MSR.

Purification of the FAD/NADP-binding domain of MSR was carried out by affinity chromatography and anion exchange chromatography to facilitate crystallization. The structure of the protein at 1.9 Å resolution was determined using crystals grown from the purified FAD/NADP-binding domain of MSR [3]. The structure was solved via the molecular replacement method [4]. Based on this structure, variants of the FAD/NADP-binding domains and full length MSR were prepared containing alterations at the positions of residues Asp<sup>652</sup> and Trp<sup>697</sup> in wild-type protein to study interactions with NADPH. Changes in the steady-state turnover properties, pre-steady-state kinetic behaviour, substrate specificity and redox potentials of the flavin cofactors of the mutants were analysed and compared with the wild-type protein.

Electron paramagnetic resonance (EPR) spectroscopy was also used to identify and characterise the radical states of the cofactors (semiquinone FAD and semiquinone FMN) [5]. Electron spin echo envelope modulation (ESEEM) spectroscopy [6] and electron nuclear double resonance (ENDOR) spectroscopy [7] were also employed to identify hyperfine couplings between the nuclei and unpaired electrons in the flavin semiquinone moieties. Finally, pulsed electron electron double resonance (ELDOR) spectroscopy [7] was used to measure the distance between the two unpaired electrons in the flavin semiquinones in the reduced MSR and to demonstrate the dynamic nature of the MSR protein. Combined, the results of these analytical techniques were used to illustrate a mechanism of electron transfer that involves ‘conformational sampling’ i.e. domain motion similar to that seen in other dynamic proteins such as human cytochrome P450 reductase [8].

In the case of MS, the purification and crystallization of the wild-type activation domain of MS is reported. This was performed to initiate structural studies

of the MS-MSR protein complex. The purification procedure and crystallization conditions reported should enable future studies aimed at co-crystallisation of these proteins for structural determination

Collectively, the work described in this thesis has provided more in-depth understanding of the electron transfer mechanisms and dynamics in the MSR-MS protein complex and makes a significant contribution to our knowledge of this complex redox system.

Prior to more in depth discussion of the MS-MSR system, the general role of organic and inorganic cofactors in biology is discussed (**Section 1.2**). This section is followed by a brief overview of the chemistry and biology of flavin-dependent systems (**Section 1.3**).

## 1.2 Cofactors in biology

A cofactor is a non-protein chemical compound bound to a protein [9]. Most cofactors are associated with enzymes and they are required for the biological activity of the protein. Generally, they can be divided in two groups: organic cofactors [10] (such as flavin and heme) and inorganic cofactors [11] (such as the metal ions  $Mg^{2+}$  and  $Cu^{2+}$ ). Typically, most organic cofactors are small organic molecules, less than 1000 Da in mass [12]. Those that bind tightly to the enzyme are called prosthetic groups [13] (e.g. flavins, cobalamin, heme); those more loosely bound to enzymes are termed coenzymes [14] (e.g. nicotinamide coenzymes). There is, however, no strict division between these two groups. Some common cofactors are listed in **Table 1.1**. Metal ions are the most common inorganic cofactors in enzymes [15]. In humans, they include iron [16], manganese [16], cobalt [16], copper [16], zinc [16], and selenium [16]. It is worth noting that calcium ions exist in many enzymes (e.g. nitric oxide synthase) [17]. Here calcium conformationally



activates the enzyme in its calmodulin complex. Calcium is generally considered as a cell signalling molecule rather than a cofactor.

Name of ion inorganic cofactors	Examples of enzymes containing ion cofactors
Copper	Cytochrome oxidase [18]
Ferrous or ferric iron	Catalase [19]
Magnesium	Glucose-6-phosphatase [20]
Manganese	Arginase [21]
Molybdenum	Nitrate reductase [22]
Nickel	Urease [23]
Selenium	Glutathione peroxidase [24]
Zinc	DNA polymerase [25]

**Table 1.1 Common inorganic cofactors found in biology and examples of enzyme systems in which they are found.**

Vitamins and derivatives		Chemical group(s) transferred	Distribution
Cofactor	Vitamin		
Thiamine pyrophosphate [26]	Thiamine (B <sub>1</sub> )	2-carbon groups	Bacteria, archaea and eukaryotes
NAD <sup>+</sup> and NADP <sup>+</sup> [27]	Niacin (B <sub>3</sub> )	Electrons/hydride ions	Bacteria archaea and eukaryotes
Pyridoxal phosphate [28]	Pyridoxine(B <sub>6</sub> )	Amino and carboxyl	Bacteria archaea and eukaryotes
Lipoamide [29]	Lipoic acid	Electrons, acyl groups	Bacteria archaea and eukaryotes
Cobalamin [30]	Vitamin B <sub>12</sub>	Methyl groups, hydrogen, alkyl groups	Bacteria archaea and eukaryotes
Biotin [31]	Biotin	CO <sub>2</sub>	Bacteria archaea and eukaryotes
Coenzyme A [32]	Pantothenic acid(B <sub>5</sub> )	Acetyl group	Bacteria archaea and eukaryotes
Flavin mononucleotide [33]	Riboflavin (B <sub>2</sub> )	Electrons	Bacteria archaea and eukaryotes
Flavin adenine Dinucleotide [33]	Riboflavin (B <sub>2</sub> )	Electrons	Bacteria archaea and eukaryotes
Coenzyme F420 [34]	Riboflavin (B <sub>2</sub> )	Electrons	Bacteria archaea and eukaryotes
<b>Non-vitamins</b>			
Adenosine triphosphate [35]		Phosphate group	Bacteria archaea and eukaryotes
S-adenosyl methionine [36]		Methyl group	Bacteria archaea and eukaryotes
Coenzyme B [37]		Electrons	Methanogens

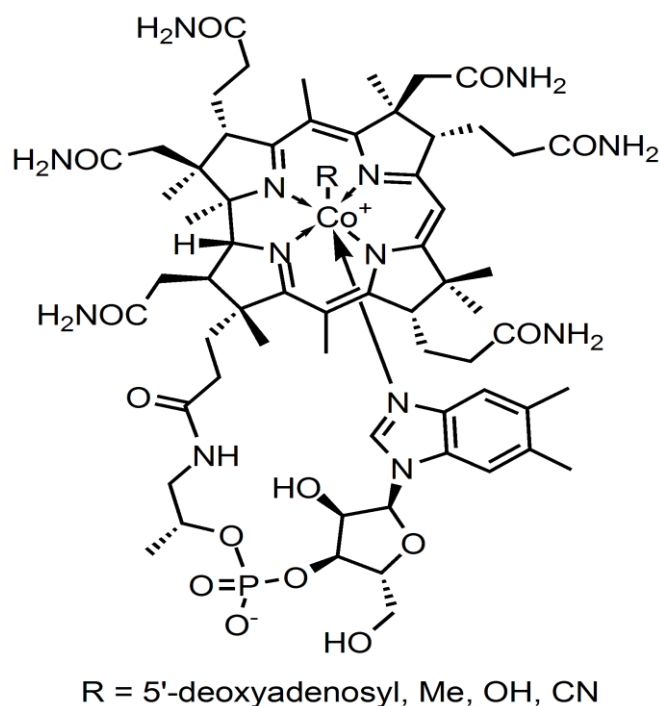
Coenzyme M [38]	Methyl group	Methanogens
Coenzyme Q [39]	Electrons	Bacteria archaea and eukaryotes
Heme [40]	Electrons	Bacteria archaea and eukaryotes
Glutathione [41]	Electrons	Bacteria archaea and eukaryotes
Molybdopterin [42]	Oxygen atom	Bacteria archaea and eukaryotes

**Table 1.2 Examples of organic cofactors in biology, the chemical groups transferred and their distribution across organisms.**

Three organic cofactors, NADPH, flavin and cobalamin, deserve more detailed mention in relation to the work described in this thesis as they are present in MSR and MS. NADPH, FAD and FMN are required for the functioning of MSR and adenosylcobalamin is the cofactor found in MS.

NADPH is the reduced form of nicotinamide adenine dinucleotide phosphate (NADP<sup>+</sup>). NADP<sup>+</sup> differs from NAD<sup>+</sup> by an additional phosphate group at the 2' position of the ribose ring that carries the adenine moiety [43]. In plants, NADP<sup>+</sup> is reduced by ferredoxin-NADP<sup>+</sup> reductase in the last step of the electron transfer chain of the light reaction of photosynthesis [44]. The reduced form, NADPH, acts as a reducing agent for the biosynthetic reactions in the Calvin cycle [45] and photosynthesis [46]. In animals, NADPH comes mainly from the oxidative phase of the pentose phosphate pathway [47]. NADPH provides the reducing equivalents for biosynthetic reactions and oxidation-reductions involved in protection against reactive oxygen species. It also provides the reducing power for anabolic pathways, such as lipid synthesis [48]. NADPH is also responsible for generating free radicals in immune cells through the action of the enzyme NADPH oxidase, a complex flavin-dependent heme protein [49]. These radicals can be used to destroy pathogens in the respiratory burst. In addition, NADPH is the source of reducing equivalents for cytochrome P450 hydroxylation [50] of aromatic compounds [51], steroids [52],

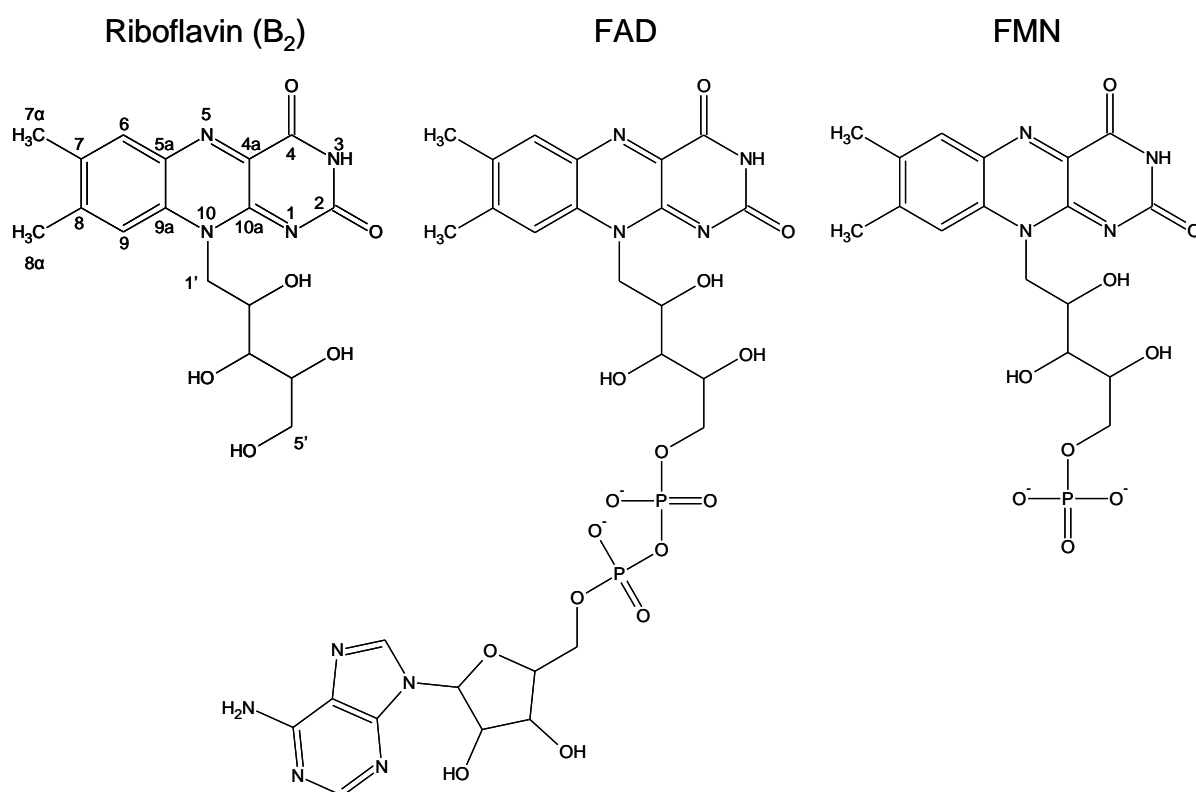
alcohols [53] and drugs [54]. In MSR, NADPH binds to the enzyme to transfer hydride to cofactor FAD. These electrons are then transferred to FMN and ultimately onto MS as part of a natural re-activation process.



**Figure 1.1** The structure of cobalamin skeleton [55]

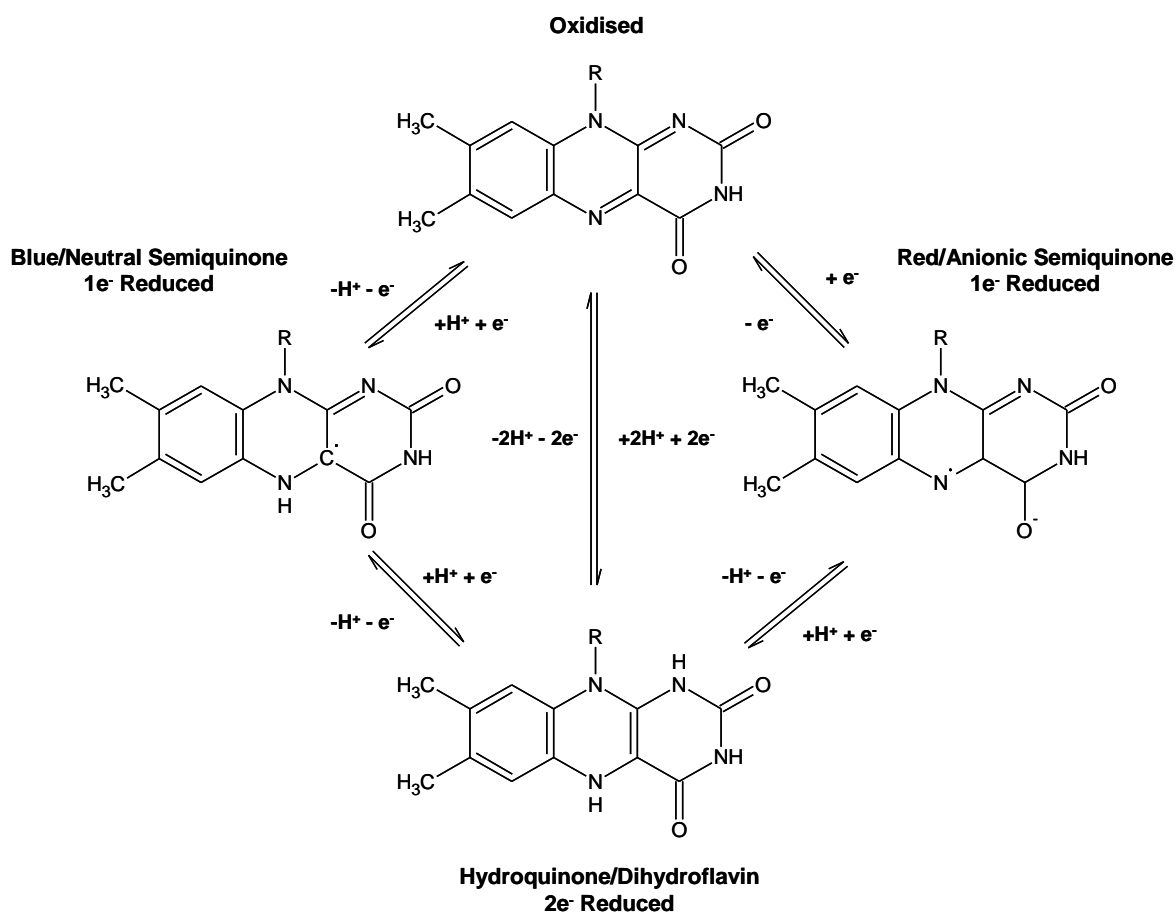
Cobalamin, the cofactor for MS, exists in a variety of enzymes. The structure of cobalamin was first solved in 1961 using crystallographic methods [56]. In the centre of the cobalamin structure is a Co atom covalently bound to four nitrogen atoms originating from a reduced tetrapyrrole (**Figure 1.1**). A characteristic feature of the corrin ring is its face up conformation and a nucleotide side chain links with the D part of the corrin ring. If this nucleotide side chain terminates at dimethylbenzimidazole, this cofactor is called cobalamins [55]; when this nucleotide side chain terminates at aminopropanol, this cofactor is cobinamides [55]. With any other nucleotides, all resulting cofactors are called cobamides [55]. The ligands, such as  $\text{CH}_3^+$  and 5-deoxyadenosyl, coordinate to the upper position of the Co atom, to

generate methylcobalamin and adenosylcobalamin, respectively [55]. The cobalt in the cobalamin exists in three oxidation states, I, II and III. Two of these states (I, III) always occur in the B<sub>12</sub>-dependent methyltransferase enzymes, such as corrinoid Fe/S protein [57], CoM methyltransferases [57, 58] and MS. In mammals, only two kinds of cobalamin-dependent enzymes exist, those being methyleneglutarate mutase [58] and MS. MS is the best characterised enzyme in this group. The cofactor of MS, cobalamin, receives a methyl group from methyltetrahydrofolate to form methylcobalamin, and then transfers this methyl group to homocysteine (see **Section 1.5**).



**Figure 1.2 Chemical structure of vitamin B<sub>2</sub> (riboflavin) and flavoprotein cofactors flavin mononucleotide (FMN) and flavin adenine dinucleotide (FAD).** The flavin precursor riboflavin is shown (on the left) with atomic numbering of the isoalloxazine tricyclic ring moiety and N10 bound ribityl chain. Phosphorylation of B<sub>2</sub> at the 5'-hydroxyl of the ribityl chain yields the cofactor FMN (on the right). FMN undergoes phosphoryladylation to give the cofactor FAD (centre).

Flavin is an essential cofactor in flavoenzymes, such as CPR [59], MSR [60], and NOS [17]. The structure of riboflavin consists of an isoalloxazine ring and a ribityl side chain attached to the central N10 position on the pyrazine moiety (**Figure 1.2**) [61]. When the riboflavin is phosphorylated by flavokinase at the 5-hydroxyl group, the cofactor is termed flavin mononucleotide (FMN). When the FMN is linked with an AMP group, the product is named flavin adenine dinucleotide (FAD). The isoalloxazine ring group in flavin usually serves as a reversible reduction-oxidation catalyst in many biological redox reactions; the side chain is related to the binding of the flavin ring system to protein. In flavoproteins, both noncovalent binding of the flavin to protein and covalent binding to an amino acid residue via 8- or 6-position of the isoalloxazine ring system is found [61]. Flavin has important UV/visible absorption features with peaks at 360 nm and 450 nm in the oxidized form of flavin and the extinction coefficients for the FMN and FAD are 12,500 and 11,300  $\text{M}^{-1}\text{cm}^{-1}$ , respectively [62]. With flavin bound to the protein moiety, these two extinction coefficients can range from 10,500 to 15,400  $\text{M}^{-1}\text{cm}^{-1}$  [61]. These absorption characteristics prove useful in studies of flavoproteins as the spectral properties change substantially on reduction to either the semiquinone (one electron reduced) or hydroquinone (two electron reduced) forms of the cofactor (**Figure 1.3**) [63]. Because flavin is an essential cofactor for the mechanisms of many enzymes, the observed spectral changes will show useful information on the reaction mechanism and the binding of substrates and products. The binding of substrate analogues and inhibitors can also be monitored by following the changes in the flavin absorption spectrum [63]. Also, the spectral properties are useful during the purification of flavoproteins, since they can be used to locate protein in purification fractions that contain the flavoprotein of interest.



**Figure 1.3 The three redox states of the heterocyclic isoalloxazine ring system of flavin.**

An important property of flavin is that it can be reduced to a two electron reduced form (hydroquinone), and one electron reduced form (semiquinone) [63]. The flavin semiquinone can be protonated to form the neutral, blue semiquinone, or it can be deprotonated to form the anionic, red semiquinone. These two radical species can be distinguished by their UV-visible spectral properties: the neutral semiquinone radical has a characteristic long wavelength absorbance at 580-620 nm ( $\epsilon = 4,000 \text{ M}^{-1} \text{ cm}^{-1}$ ) while the anionic semiquinone radicals have a strong absorbance around 380 nm ( $\epsilon = 16,000 \text{ M}^{-1} \text{ cm}^{-1}$ ) [63] and an additional sharp peak at 400 nm. It has been confirmed that the stabilisation of these radicals is related to the enzymatic function of the flavoprotein. Although flavin semiquinone exists in cationic, neutral

and anionic forms, only the neutral and anionic forms are found in flavoproteins [64]. The transient detection of flavin semiquinones in enzyme systems is a useful probe of the catalytic mechanisms of flavoproteins. Also, the type of flavin radical populated in enzymes is not only affected by the external factors, such as pH [64], but also by the binding of substrates, substrate analogues and inhibitors. Changes of the spectral features of flavin radicals in flavoprotein under different conditions can therefore provide some basic information about the reaction mechanisms of flavoproteins.

Flavin enzymes are involved in a wide range of biological processes including redox catalysis [65], light emission [66] and DNA repair [67]. According to the functions of these flavoenzymes, they can be classified into several different groups: electron transferases [68], photolyases [69], synthases [70], dehydrogenases [71], disulphide reductases [72, 73], oxidases [75] and monooxygenases [74]. Most flavoenzymes contain a single FAD or FMN; but some such as CPR and NOS, which are related to MSR (the subject of this PhD thesis) contain both FAD and FMN, and belong to the same family, namely the diflavin reductases.

### **1.3 Diflavin reductase enzymes**

#### **1.3.1 The structure and function of the diflavin reductases family**

Diflavin reductases are enzymes that have emerged as a result of gene fusion of an ancestral NADP<sup>+</sup>-dependent ferredoxin reductase [75] and a flavodoxin [76]. The enzymes in this family contain tightly bound flavin cofactors, including a FAD group in the ferredoxin reductase module and FMN in the flavodoxin-like domain. In mammalian systems, this family includes the enzymes cytochrome P450 reductase (CPR) [77], the isoforms of nitric oxide synthase (NOS) [78], and the cytoplasmic

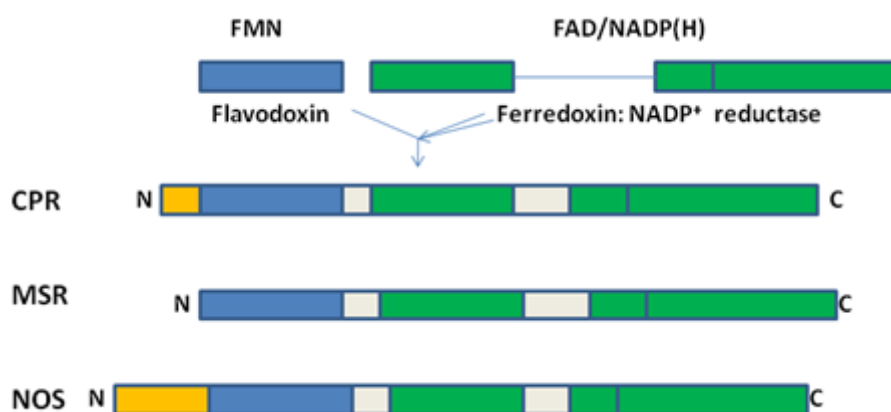
protein novel oxidoreductase 1 (NR1) [79] and MSR. Bacterial members of this family include flavocytochrome P450 BM3 (CYP102) [80] and sulphite reductase [81].

The general catalytic function of these enzymes is to provide reducing equivalents from NAD(P)H via the flavin cofactors to the respective heme domains where a variety of redox reactions are carried out [82]. In the main, this involves reaction with molecular oxygen in the classical P450 enzymes [82] and the NOS enzymes [83], but also involves long range electron transfer to non-heme dependent centres such as cobalamin (the MSR-MS system). The tightly bound cofactors FAD and FMN are intimately involved in the transfer of the reducing equivalents from nicotinamide coenzyme to either the heme domains (or alternative redox acceptors as in MS). In the first step of the reaction two electrons are transferred from NADPH to FAD as a hydride anion; these electrons are subsequently transferred from FAD hydroquinone to FMN in sequential one electron transfer reactions setting up a quasi-equilibrium of different reduced forms of the flavoprotein reductase (Figure 1.9). These series of reactions are similar for all members of the family and have enabled detailed comparisons of the thermodynamics and kinetics of electron transfer in these systems [68]. Ultimately, FMN acts as the electron donor to downstream heme domains or alternative electron acceptors.

A variety of natural and artificial electron acceptors can function with the reductases in this enzyme family. Ferricyanide and  $\text{NADP}^+$  can directly receive electrons from the reduced FAD cofactor through a series of one electron transfers (ferricyanide) or by formal hydride transfer ( $\text{NADP}^+$ ). The physiological electron acceptors [84] (e.g. P450 enzymes, heme oxygenase domains of NOS etc) accept electrons from the reduced FMN domain. Also the non physiological acceptors



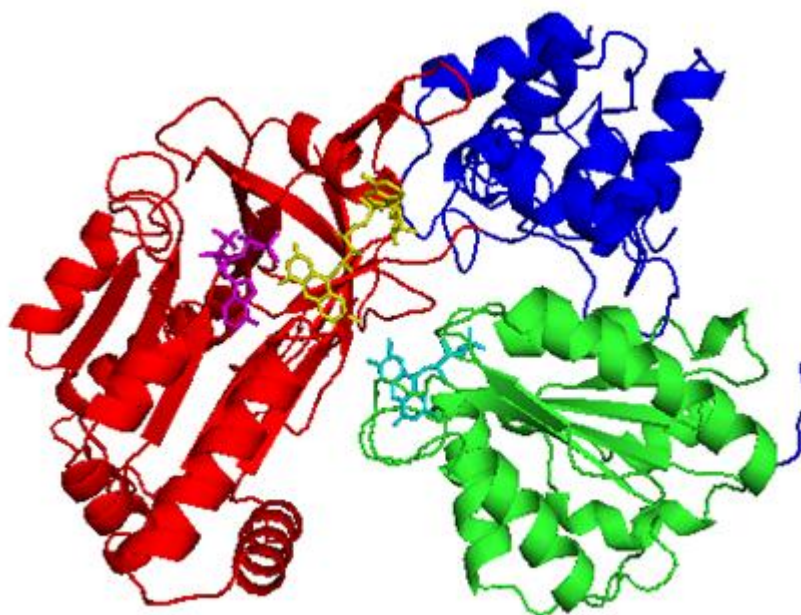
dichlorophenolindophenol (DCPIP) [85], menadione [86] and cytochrome *c* [87], only receive electrons from the reduced FMN. Electron transfer in CPR occurs across protein molecules from the reductase to a separate heme-containing oxygenase domain [88]. By comparison, NOS is a self-sufficient enzyme with two major functional domains (reductase and oxygenase domains) fused into a single polypeptide chain [17]. Like CPR, MSR is a discrete reductase component and needs to interact with the separate cobalamin-bound MS component to transfer electrons [60]. Sulfite reductase consists of two subunits. The  $\alpha$ -subunit is a 66-kDa FAD-FMN-containing protein and the  $\beta$ -unit contains siroheme and a  $\text{Fe}_4\text{S}_4$  cluster. The flavoprotein subunits transfer electrons from NADPH to the heme catalytic site to finish the reduction of sulfite to sulphide [89].



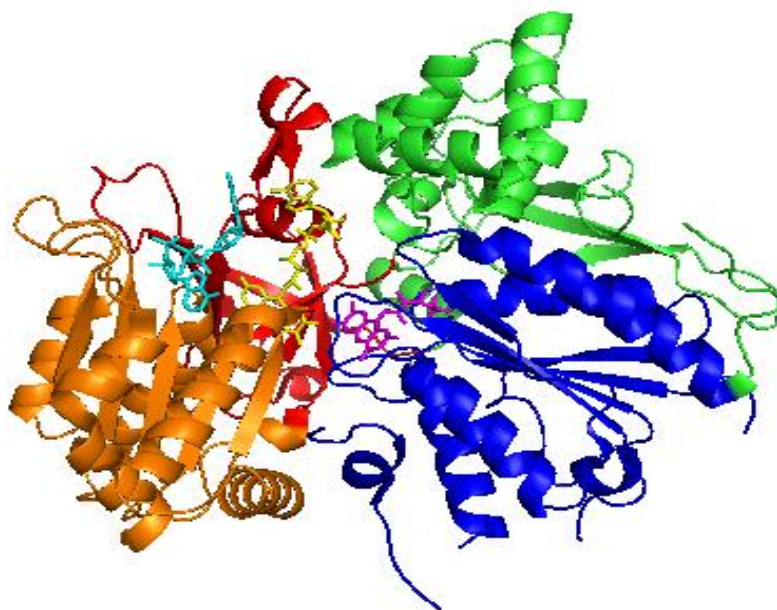
**Figure 1.4 Comparison of the domain architecture of diflavin reductase family.** FAD/NADPH binding domain, Green; FMN binding domain, blue; the connecting domain, white; the N-terminal membrane anchor of CPR and NOS, yellow. This alignment indicated that the members of this family have similar structure, which consists of two different domains, one binds FMN and another binds FAD and NADPH. The FMN binding domain is located on N-terminal and homologous to flavodoxin, while the FAD/NADPH binding domain is homologous to ferredoxin reductase and locates in the C-terminal of the protein.

On comparing alignments of amino acid sequences of the known members of the diflavin oxidoreductase family, it is clear that the overall three dimensional structures of these proteins are similar. A common structural feature is that the FMN-

binding domain is located at the N-terminus of the proteins and that the FAD and NADPH binding domains (ferredoxin-NADP<sup>+</sup> reductase module) are located at the C-terminus. Reported crystallographic structures of CPR [90], NOS reductase [77] and other family members (e.g. sulphite reductase) [91] have confirmed that the FMN-binding domain is homologous to the structure of flavodoxin [92] and that the FAD/NADPH-binding domain resembles the structure of ferredoxin-NADP<sup>+</sup> reductase [93]. There is also a connecting domain that separates the FMN-binding and FAD-binding domains in the diflavin oxidoreductases. This connecting domain is assumed to be involved in the control and modulation of electron transfer between the flavin cofactors through conformational control and recent kinetic [77] and spectroscopic studies [94] of human CPR have confirmed the dynamic nature of this molecule. The crystal structures of CPR and NOS have also been used to argue that domain dynamics are important in controlling electron transfer in these systems, consistent with for example EPR [95], kinetic [96] and spectroscopic studies [97] also conducted on the NOS enzymes. A hinge region between the connecting domain and the FMN-binding domain, which is partially disordered in crystal structures, is also in agreement with the dynamic characteristics of these enzymes. In CPR and other diflavin reductases this hinge is typically 14-24 residues long [90]. Sequence alignments however suggest that this hinge region is much longer in MSR (up to 82 residues in length). This suggests that large-scale domain motion of the FMN-binding domain is a feature of the structure of human MSR.



**Figure 1.5 Three dimensional structure of rat cytochrome P-450 oxidoreductase [1].** CPR is divided into: an FAD/NADPH-binding domain (red) with NADP<sup>+</sup> (magenta) and FAD (yellow); a connecting domain (blue); an FMN-binding domain (green) with FMN (cyan).

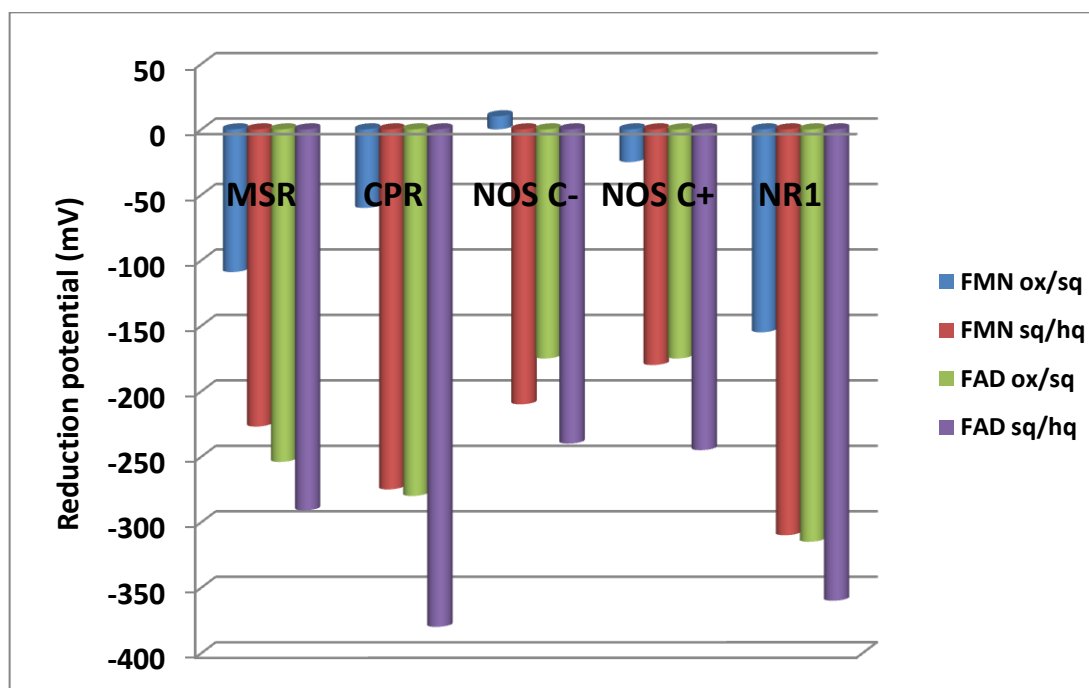


**Figure 1.6 Three dimension structure of nNOS reductase [98].** The deposited PDB only contained one monomer in the asymmetric unit as shown. The structure is divided in four domains: an FAD- binding domain (blue, residue 750 to 942) with FMN (magenta); a connecting domain (green, residue 943 to 989 and 1039 to 1170); an FAD binding domain (Red, residues 990 to 1038 and 1171 to 1231) with FAD (yellow) and NADPH-binding domain (orange, residues 1232-1396) with NADP<sup>+</sup> (cyan).

Other structural similarities in the orientation of the flavin cofactors and binding sites in this family have also been found. In CPR, the binding pockets for the isoalloxazine rings of FAD and FMN are mainly hydrophobic. Both sides of the isoalloxazine rings form  $\pi$ - $\pi$  stacking interactions with aromatic amino acid residues in the protein. The isoalloxazine ring of FMN is partially shielded by the phenyl rings of Tyr<sup>140</sup> and Tyr<sup>178</sup> on the *re*- and *si*-side respectively [99] and the isoalloxazine ring of FAD is sandwiched between Tyr<sup>455</sup> and Tyr<sup>456</sup> on the *si*-side and Trp<sup>677</sup> on the *re*-side. A similar structural organisation has been reported for other members such as mammalian NOS [79] and *E. coli* sulfite reductase [91]. Additionally, the binding sites for NADP<sup>+</sup>/NADPH in these enzymes is relatively conserved and typically are occupied by an aromatic amino acid (either tyrosine, tryptophan or phenylalanine), which is relatively dynamic and allows access to the FAD when the nicotinamide group of NADPH binds to the enzyme. Such dynamical character has been seen in kinetic (fluorescence) and structural studies of family members [100].

Clearly, the main physiological function of the diflavin reductases is to transfer electrons to redox partners or domains attached to the reductases. To further understanding of the electron transfer mechanisms thermodynamic studies have been conducted for many members to define the gradient of electron flow in these proteins. The direction of the net electron transfer is determined from the reduction potentials of the electron donor and acceptors (i.e. the flavin centres). Electrons move spontaneously from the atoms or molecules with more negative reduction potential to the atoms or molecules with more positive reduction potential. The reduction potentials of the flavin cofactors have been measured under equilibrium

anaerobic titration experiments and a summary of available data are shown in **Figure 1.7**.



**Figure 1.7 Flavin reduction potentials for some members of the diflavin reductase enzyme family.** These data include the midpoint reduction potentials for both the oxidised/semiquinone and semiquinone/hydroquinone couples of FAD and FMN for MSR [101], CPR [102], rat neuronal NOS in calmodulin-free (C<sup>-</sup>) and calmodulin-bound forms (C<sup>+</sup>) [103] and novel reductase 1(NR1) [79].

These reduction potentials show that the thermodynamic gradient for electron transfer is from NADPH → FAD → FMN. However, there are some key differences across family members. Also, some of the measured potentials deserve further comment. For example, the redox potential for the FMN semiquinone in NOS is -49 mV, and the redox potential for heme is -220 mV. However, during NOS turnover the FMN semiquinone is able to donate electrons to the heme iron. It has been suggested that the potentials in these measured equilibrium conditions are not the same as those that exist under catalytic conditions.

### 1.3.2 Examples of diflavin enzymes NOS and CPR

#### 1.3.2.1 NOS

Nitric oxide synthase, which catalyzes the oxidation of one of the L-arginine guanidinium N atoms to nitric oxide (NO), comprises an N-terminal heme domain and an FMN/FAD reductase domain at the C-terminus which contains FAD, FMN and NADPH binding sites. Electrons are transferred from NADPH to FAD then FMN, and further to the heme domain. There are three kinds of NOS isoforms, endothelial NOS (eNOS), neuronal NOS (nNOS) and inducible NOS (iNOS). A particular characteristic for NOS is that it has one redox cofactor and a regulatory protein, calmodulin (CaM). Constitutive NOS proteins which include nNOS and eNOS are expressed in mammals constitutively and collectively are controlled by CaM with a dependence on the concentration of  $\text{Ca}^{2+}$  (which binds to CaM). In contrast, CaM binds to the iNOS as a permanent additional subunit. Hence, the iNOS is not regulated by CaM binding, and regulation is achieved only through transcriptional control [104].

The size of NOS ranges from 135 kDa to 160 kDa, but it has no activity in its monomeric form. The dimer form of NOS has activity and is tightly dimerised by its heme domains. The crystal structures of the heme domains of the three NOS isoforms show some similarity with  $\text{H}_4\text{B}$  molecules binding at the dimer interface. Additionally, a Zn ion is found at the dimer interface and is ligated by two cysteine residues from each monomer [17].

Kinetic and spectroscopic studies have been carried out to investigate the redox potential, electron transfer and cofactor binding properties of the NOS enzymes. Direct anaerobic titration has been applied to determine the midpoint reduction potentials for the flavin cofactors in the reductase domain of nNOS in CaM-free and bound forms [103]. For the CaM-free form, the FMN potentials are  $-49 \pm 5$  mV (ox/sq) and  $-274 \text{ mV} \pm 5$  mV (sq/hq); the FAD potentials are  $-232 \pm 7$  mV (ox/sq)

and  $-280 \pm 6$  mV (sq/hq) [103]. These data are confirmed by the existence of the blue (neutral) semiquinone, which is attributed to the accumulation of FMN semiquinone rather than the FAD semiquinone. For the CaM-bound form of nNOS, the midpoint potential is identical to that of CaM-free form with a small alteration at the midpoint potential of FMN (ox/sq) in  $-30 \pm 4$  mV [79]. In comparison to the midpoint potential of heme of nNOS ( $-239$  mV, L-Arg-free;  $-220$  mV, L-Arg-bound [103]), it is clear that electron transfer from FMN hydroquinone to heme in nNOS is thermodynamically feasible. Stopped-flow kinetic studies have also been completed to investigate the electron transfer in the reductase domain of nNOS [97]. The resulting time-dependent photodiode array spectra were analysed by the global single value decomposition (SVD) analysis method. Together with single wavelength absorption and NADPH fluorescence data, the authors identified four resolvable kinetic steps: the first step represents rapid formation of an equilibrium between an NADPH-enzyme charge transfer species and two-electron-reduced enzyme bound to  $\text{NADP}^+$ ; the second and third steps were to further reduction of the flavins and the release of  $\text{NADP}^+$ ; the fourth step represents the accumulation to the equilibrium final state of the reduced enzyme. Stopped-flow flavin fluorescence studies over long time bases indicated a slow kinetic phase, which was attributed to enzyme disproportion and/or conformational change. No di-semiquinones are detected in stopped-flow studies after the first hydride transferred from NADPH to nNOS reductase. This suggests the internal electron transfer is relatively slow and is probably gated by  $\text{NADP}^+$  release. An important aspect of nNOS function is related to the role of CaM binding. CaM binding activates the enzyme and is believed to trigger the release of  $\text{NADP}^+$  and facilitate electron transfer through conformation change [105]. The binding of NADPH induces a conformational change to restrict

the access of FMN with the electron acceptor of nNOS. It is hypothesised that the binding of NADPH induces a ‘conformational lock’ in the reductase domain and thereby prevents efficient electron transfer to either the oxygenase domain or other electron acceptors. CaM binding on the other hand unlocks this complex at elevated  $\text{Ca}^{2+}$  concentrations and reorients the two domains to trigger interdomain electron transfer and NO synthesis.

### **1.3.2.2 CPR**

The cytochrome P450 is a heme-containing monooxygenase and it is critical to animal physiology and drug metabolism. In mammalian systems, numerous different isoforms of cytochrome P450s catalyse the oxidization of some endogenous compounds such as steroids, eicosanoids and a diverse range of xenobiotics. Because the P450s require the delivery of two electrons for catalytic function, so an efficient electron delivery system is critical to P450 catalysis. Depending on the type of reductase system, cytochrome P450 can be grouped into two classes [106]. Class I ( $\beta$ -class) P450 includes most bacterial systems and mitochondrial forms, in which electrons from NADPH are transferred to FAD in the ferredoxin reductase then passing through the small iron-sulfur containing ferredoxin to P450; Class II (E-class) includes the majority of eukaryotic P450s often referred to as microsomal P450s. Microsomal P450s have a single redox partner, cytochrome P450 reductase.

Cytochrome P450 reductase, CPR, is the best characterized diflavin reductase, which is bound to the endoplasmic reticulum of eukaryotic cells. The size of CPR ranges from 75 kDa to 85 kDa [107] in monomeric form depending on the source. It is an essential component of microsomal cytochrome P450 dependent



monooxygenases systems and catalyses the transfer of electrons from NADPH to FAD, FMN then to cytochrome P450.

The three dimensional structure of CPR consists of four structural domains: from N terminus to C terminus, these are the FMN-binding domain, the connecting domain, the FAD-binding domain and the NADPH-binding domain [90]. The structure of the FMN-binding domain is similar to the structure of flavodoxin. The structure of the FAD/NADP-binding domain is similar to that of ferredoxin-NADP<sup>+</sup> reductase (FNR). The connecting domain is responsible for the relative orientation of the other domains and the proper alignment of the two flavin cofactors for efficient electron transfer. The position of the two flavin isoalloxazine rings is juxtaposed at a distance of about 3.5Å [90]. The binding pockets of the isoalloxazine rings of FAD and FMN are hydrophobic and are separated on both sides of the oxidised NADP-bound structure by the methyl groups of the FMN towards the FAD. This structure suggests there is a flexible hinge between the flavin domains and that the FMN-binding domain of CPR moves back-and-forth during the reduction and oxidation process.

The crystal structure of CPR has revealed the electron transfer occurs directly between the cofactors with no amino acid residues participating in the redox chemistry. In the electron transfer process, a charge transfer complex is formed. This complex can be identified by an absorbance band above 500 nm and is assumed to reflect a direct interaction between the flavin (FAD) isoalloxazine ring with the pyridinium ring of NADPH, which leads to a rapid hydride ion transfer. Studies by Isenberg and Szent-Gyorgyi [108] have shown that riboflavin in free solution can form charge transfer complexes with amino acids with distinctive absorption properties that are similar to the charge-transfer spectra for FAD-NADPH interaction

formed in CPR amino acids. Also, studies with bis-nucleotide analogs containing covalently attached nicotinamide and isoalloxazine rings show that a charge transfer complex absorbance maximum and the band intensity depend on pH, solvent polarity and the distance between the aromatic rings. In addition, CPR has also demonstrated that the interaction of NADPH with CPR can affect the reduction potential of the flavin cofactors and help to stabilize the reduced flavin. This is confirmed by the studies of the semiquinone form of CPR which is much more stable after interaction with NADPH than with NADH [109].

Different parts of the NADPH coenzyme make different contributions to the binding reaction with CPR. With rat CPR the 2'-phosphate part contributes 5 kcal/mol to the binding energy of NADPH; this 2'-phosphate is not only critical for the binding of NADPH to CPR but is also important for the fast hydride transfer from the nicotinamide ring to FAD [110]. Although the distance between the 2'-phosphate group to the nicotinamide ring is about 10-12 Å, the phosphate group is believed to induce distal conformation changes required for reorganization and optimal binding. Different forms of NADPH, such as the reduced form and oxidized form have different binding affinities for CPR. For example, the neutral reduced nicotinamide ring interacts with the oxidized form of CPR in a tight binding complex, but the positively charged oxidized nicotinamide does not bind tightly. It is thought that there are two steps in the binding of NADPH to CPR: the first step is the recognition of the 2'-phosphate group which controls the affinity of the enzyme for NADPH. The second step is the effect of the binding of the 2'-phosphate group which 'turns on' the recognition system of the nicotinamide ring portion of the coenzyme. This might involve movement of a tryptophan residue that is positioned

close to the FAD isoalloxazine ring in the crystal structure of the oxidised form of CPR.

Temperature-jump relaxation studies have been used to investigate the affect of NADPH binding on internal electron transfer in CPR [111]. It was found that NADPH binding triggers conformational changes which slow down the rate of internal electron transfer between the CPR flavin domains. This conformational change is also sensitive to solution viscosity changes suggesting the involvement of domain motion [111].

The redox potential of flavin in full-length human CPR has been determined in solution without its membrane spanning domain by anaerobic redox titration methods [102]. The midpoint potential of the flavin cofactors for CPR are: FMN,  $-66 \pm 8$  mV (ox/sq),  $-269 \pm 10$  mV (sq/hq); FAD,  $-283 \pm 5$  mV (ox/sq),  $-382 \pm 8$  mV (sq/hq). These data confirm the electron transfer direction is from NADPH to FAD then FMN. This direction is consistent with what is known of the potentials for the other members of the diflavin reductase family.

The reduction of NADPH for the FAD and FMN redox centres in human CPR has been studied by rapid-mix stopped-flow spectroscopy. The reduction of the isolated FAD/NADP-binding domain has three kinetically resolvable steps. In the first step, there is a rapid formation ( $\sim 500$  s<sup>-1</sup>) [94] of a charge-transfer species between the oxidised FAD and NADPH; in the second step, a second charge-transfer species is formed in isomerisation with an intense absorption in a long wavelength region; in the third step, a second hydride is transferred from NADPH to FAD with a further change in the tryptophan fluorescence of the FAD/NADP-binding domain. The hydride transfer to FAD is reversible and the reduction of NADP<sup>+</sup> by FADH<sub>2</sub> is more rapid (8 s<sup>-1</sup>) relative to the reduction by NADPH (3 s<sup>-1</sup>) [94]. This is consistent

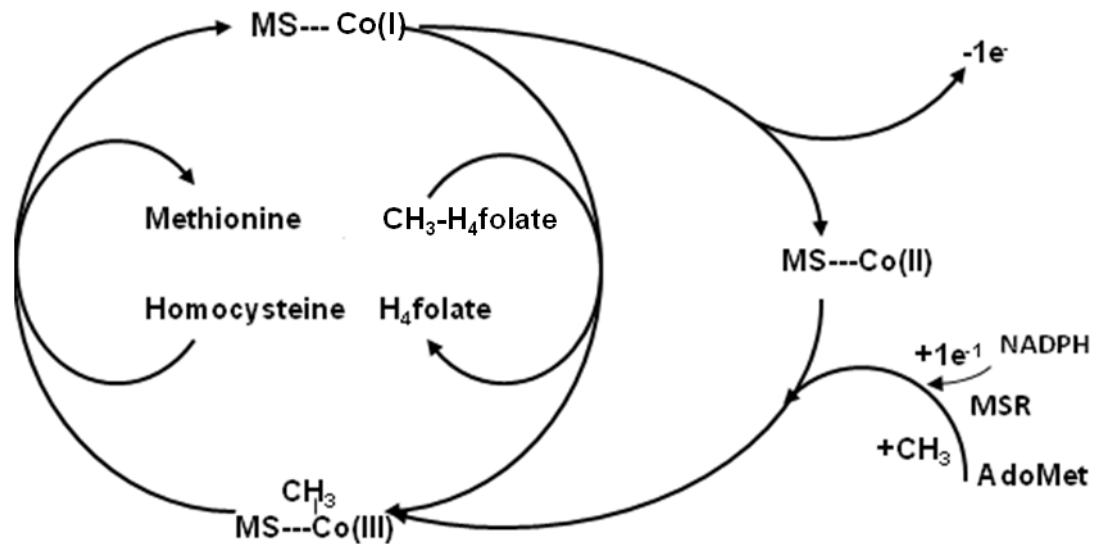
with the midpoint reduction potential data. The observed rate for the electron transfer between the isolated FAD/NADP-binding domain and isolated FMN is about  $9.5 \times 10^4 \text{ M}^{-1}\text{s}^{-1}$  depending on the domain concentration. This result suggests that this reaction is a bimolecular reaction and that the connecting domain plays an important role. The structure and function of CPR shares other common features with another member in this diflavin reductase, MSR.

## **1.4 Methionine synthase reductase**

### **1.4.1 Cloning and mapping of the cDNA of the methionine synthase reductase**

Megaloblastic anaemia, developmental delay, hyperhomocysteinemia [112] and homomethioninemia [113] are serious recessive diseases which threaten human health. Studies have suggested that mutations that might affect the reductive activation of methionine synthase (MS) are the main cause of these diseases. MS catalyzes the methylation of homocysteine to methionine (**Figure 1.8**). In this reaction, methylcobalamin serves as an intermediate methyl carrier but after 200 to 1000 turnovers, MS is rendered inactive owing to the oxidation of cob(I)alamin to cob(II)alamin [1]. The regeneration of the function of MS requires reductive methylation of the cob(II)alamin using S-adenosylmethionine as a methyl donor and using MSR as electron donor. Based on the gene sequence from selected patients deficient in the reactivation process catalysed by MSR and the predicted consensus binding site of FAD, FMN and NADPH, the cDNA of MSR has been cloned and termed MTRR. The gene MTRR is localised at chromosome 5p15.2 -15.3 [1]. One predominant mRNA of 3.6 kb is detected by Northern blot analysis. The deduced protein from this gene contains 698 amino acids with a predicted molecular mass of 77.700 Da. This gene also shares 38% sequence identity with human cytochrome

P450 reductase [114]. The sequence was confirmed by identifying the mutations in cblE patients, including 4-bp frame shift in two affected siblings and 3-bp deletion [115]. The cloning of cDNA was the starting point for biochemical research on human MSR.



**Figure 1.8 Scheme illustrating the catalytic cycle and reactivation of MS.** During the primary catalytic cycle, MS uses enzyme-bound cob(I)alamin to remove a methyl group from methyl tetrahydrofolate to generate tetrahydrofolate and methylcob(III)alamin. Regeneration of MS involves one electron from NADPH catalyzed by MSR and methyl transfer from S-adenosyl methionine.

#### 1.4.2 Molecular and functional properties of human MSR

MSR restores the activity of MS through the reductive methylation of cob (II) alamin using S-adenosylmethionine as a methyl donor. In *E. coli*, this reductive methylation of MS is performed by a two-component flavoprotein system. The NADPH-dependent flavodoxin reductase, a member of the ferredoxin oxidoreductase (FNR) family, transfers reducing equivalents from NADPH to an FMN-containing flavodoxin (FLD); the reduced FLD then donates an electron to MS to complete the reductive methylation. In humans, MSR plays the same role as the

two-component reductase system found in *E. coli*. As discussed above, MSR contains two flavin binding domains: the FMN-binding domain and FAD/NADPH binding domain and it is a member of the diflavin reductase family.

In order to investigate the catalytic and thermodynamic mechanism of MSR, the recombinant human MSR and its component FAD/NADPH-binding domain and FMN-binding domain have been expressed individually in *E. coli* as GST fusion proteins [1]. The GST tags have permitted these proteins to be purified using glutathione affinity chromatography. After cleavage of the GST tag with thrombin and its separation from other GST fusion proteins, full length MSR, the isolated FAD/NADPH binding domain and FMN-binding domain were further purified by anion-exchange chromatography prior to in-depth analysis. The resultant molecular masses of the purified MSR, FAD/NADPH- binding domain and FMN- binding domain were shown to be 78 kDa, 60 kDa and 30 kDa, respectively, in agreement with the values calculated from the amino acid sequences of MSR (77.7 kDa), FAD/NADPH-binding domain (59.4 kDa) and FMN-binding domain (27.1 kDa) [1].

During the purification process, the apparent colour of MSR indicates the redox properties of the FAD and FMN cofactors. The blue colour for the FMN domain at the start of purification shows that FMN is partially reduced at the level of the blue semiquinone. The yellow appearance of the FAD/NADP-binding domain shows that this cofactor is isolated in the fully oxidized state. The green colour of purified full-length MSR at the early stages reflects a mixture of blue semiquinone FMN and yellow semiquinone FAD. The appearance of the purified proteins and inferred redox states are consistent with UV-visible optical spectroscopy analysis of the bound flavin. The absorbance spectra of the fully oxidized full length MSR and the isolated FMN domain show typical flavin absorbance spectra with peaks at 380

nm and 454 nm and a shoulder at 474 nm. The fully oxidized FAD/NADP-binding domain has an absorbance peak at 383 nm and 454 nm [1]. In addition, summation of the component FMN domain and FAD/NADPH domain spectra generates a composite spectrum that is very similar to that measured for full length MSR. This suggests that the domain structure of each domain is retained when expressed as individual FMN- and FAD/NADH-binding domains.

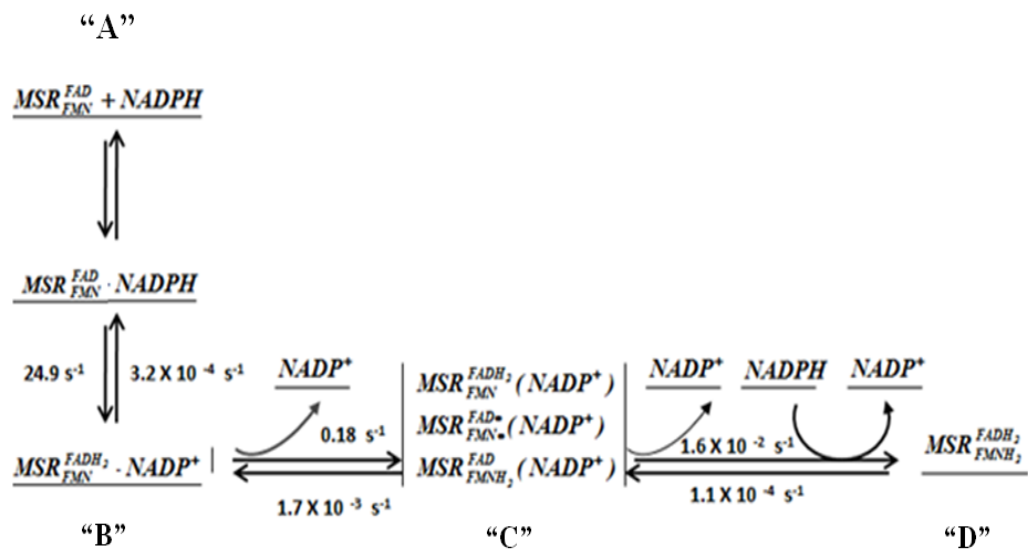
The appearance and absorbance characteristics of full length MSR suggest it is purified in a functionally active form. It has been demonstrated that the full length protein has the ability to catalyze the NADPH-dependent reduction of cytochrome *c* and FeCN [1]. The apparent steady-state turnover rates for MSR are  $0.8 \text{ s}^{-1}$  and  $8.7 \text{ s}^{-1}$  for cytochrome *c* and FeCN reduction, respectively, at  $25 \text{ }^{\circ}\text{C}$ . The apparent  $K_m$  for NADPH with cytochrome *c* as the terminal electron acceptor is  $4.0 \pm 0.3 \text{ }\mu\text{M}$ . These reduction activities are about 25 to 100 times lower than those reported for CPR and NOS using comparable assays. Anaerobic redox titration studies were performed with the isolated FMN-binding domain and full-length MSR. For the FMN-binding domain, the midpoint potentials for the oxidized/semiquinone (ox/sq) couple and semiquinone/hydroquinone (sq/hq) couple are -112 mV and -221 mV, at pH 7.0 and  $25 \text{ }^{\circ}\text{C}$ ; the corresponding couples of the FAD/NADP-binding domain are -222 mV (ox/sq) and -288 mV (sq/hq) [1]. In full length MSR, the values for the FMN couples are -109 mV (ox/sq) and -227 mV (sq/hq) and the values for FAD are -254 mV (ox/sq) and -291 (sq/hq) mV [1]. The similarity of the midpoint potentials of the four couples in full length MSR and the isolated domains confirmed that the separation of MSR does not disturb their dynamic properties. Comparison with the midpoint potential of the other members of diflavin reductase family, such as CPR and NOS, shows that the midpoint potential of MSR are more closely compressed but despite

this, that MSR has a similar electron transfer mechanism with respect to other members in this family.

### 1.4.3 Electron transfer on human MSR

In order to investigate the electron transfer mechanism on MSR, the pre-steady-state kinetic behaviour of the reductive half-reaction of MSR was performed by anaerobic stopped-flow absorbance and fluorescence spectroscopy [60]. Stopped-flow analysis of the NADPH reduction of MSR used a photodiode array to detect the change in flavin spectra of the isolated FAD/NADP-binding domain and full length MSR [60]. The globally analyzed spectra for the FAD/NADP-binding domain were best fitted to a one step reversible kinetic model with two spectral species: the oxidized species A and two- electron reduced species B. The rate constants for the conversion of  $A \rightarrow B$  and  $B \rightarrow A$  were determined as  $20.1 \pm 0.1 \text{ s}^{-1}$  and  $0.017 \pm 0.001 \text{ s}^{-1}$ , respectively [60]. For full length MSR, the spectral data were best fitted to a three-step reversible kinetic model  $A \rightleftharpoons B \rightleftharpoons C \rightleftharpoons D$  with four discrete spectral species. The rate constants for the conversion of  $A \rightleftharpoons B$  were found to be  $24.9 \pm 0.1 \text{ s}^{-1}$  (forward) and  $0.0003 \pm 0.0001 \text{ s}^{-1}$  (reverse); to  $B \rightleftharpoons C$  are  $0.18 \pm 0.01 \text{ s}^{-1}$  (forward) and  $0.002 \pm 0.0001 \text{ s}^{-1}$  (reverse);  $C \rightleftharpoons D$  are  $1.6 \times 10^{-2} \pm 0.001 \text{ s}^{-1}$  (forward) and  $0.0001 \pm 0.00001 \text{ s}^{-1}$  [60]. It should be emphasised that the spectral intermediates, such as A, B, C, are not the discrete enzyme intermediate but are simply spectral intermediates identified from global fitting of spectral data. Based on these results, the electron transfer scheme for MSR was suggested.





**Figure 1.9 Kinetic scheme for the proposed electron transfer mechanism in human MSR [116].**

Under single turnover conditions, the reduction of the FAD- binding domain by NADPH consists of two kinetically resolved steps: a rapid phase ( $120 \text{ s}^{-1}$ ) with the formation of a charge-transfer complex between the oxidised FAD and NADPH followed by the second phase ( $20 \text{ s}^{-1}$ ), which involves flavin reduction [60]. Single-wavelength absorbance measurements at 450 nm and 600 nm demonstrated that the observed rate constants for flavin reduction are hyperbolically dependent on the concentration of NADPH. Work with deuterated NADPH (NADPD) also established a primary kinetic isotope effect of 2.2 and 1.7 [60] for the isolated FAD/NADP-binding domain and full length MSR, respectively. Additionally, hydride transfer in the FAD-binding domain and full length forms of MSR were also analysed by stopped fluorescence analysis, following excitation of residue Trp<sup>697</sup>. This residue is positioned over the isoalloxazine ring of FAD and flips away from the ring to allow binding of NADPH for hydride transfer. The movement of this tryptophan is accompanied by a change in the fluorescence signal associated with this residue. The observed rate constant for the fluorescence change was found to be  $18.0 \text{ s}^{-1}$  [60] for

the isolated FAD/NADP-binding domain, a value that is consistent with the observed rate constant determined from absorbance stopped-flow experiments of hydride transfer. Together, stopped-flow kinetic data and determination of the flavin redox potentials have provided a detailed framework for understanding the mechanism of electron transfer in human MSR.

#### **1.4.4 Complex formation between human MSR and human MS**

MSR is a redox partner of the human methionine synthase (MS) redox system required for methionine synthesis. As discussed, MS is a cobalamin-dependent enzyme, which transfers a methyl group from methyltetrahydrofolate to homocysteine to form methionine and tetrahydrofolate (see **Section 1.5.1**). Human MS is similar to the *E. coli* cobalamin dependent MS [117] (known as Met H) and consists of four discrete functional modules [117]. The C-terminal activation domain (AD) of human MS interacts with human MSR to form a protein complex and it is this complex that facilitates the reaction of MS by electron transfer from MSR (see **Section 1.5.2**).

Complex formation between the AD of MS and the isolated FMN-domain of MSR or full length MSR has been studied to determine the binding affinity between the protein partners. Fluorescence titration assays were performed in which the flavin cofactors in the FMN domain or full length MSR were excited at 450 nm and the change in emission monitored (between 500-600 nm) during titration with AD [118]. The quenched intrinsic flavin fluorescence on adding AD suggested that the flavin is shielded from solvent in the protein complexes. The decrease in the intensity of fluorescence had a hyperbolic dependence on the concentration of AD (dissociation constant  $\sim 15 \mu\text{M}$ ) [118] for the binding of AD to MSR. Analysis of a molecular

model of MSR and the known structure of AD suggested that electrostatic interactions might be important in the formation of this complex. This hypothesis was confirmed by the observation of weaker binding as the ionic strength of the solvent was increased. Additional studies have involved protein chemical cross linking analysis of the complex to identify key residues at the protein interface of the AD—FMN binding domain complex. These studies used the protein chemical cross linkers 1-ethyl-3-[3-(dimethylamino)propyl]carbodiimide (EDC) or sulfo-*N*-hydroxysuccinimide (NHS) [118] to identify the crossed link residues by mass spectrometry. These data suggested that acidic residues on the surface of the FMN-domain interact electrostatically with basic residues found on the surface of the AD of MS. Two lysines (Lysine<sup>987</sup> and Lysine<sup>1071</sup>) were identified as potential basic residues of importance [118]. Changing these residues to threonine caused the dissociation constant to be significantly increased when compared to data obtained for the wild type complex. The importance of electrostatic interactions in protein complex assembly was therefore confirmed.

The thermodynamic features of the binding affinity of full length MSR or the isolated FMN-domain to the AD of MS were also investigated by isothermal titration calorimetry (ITC) [118]. The data suggested that during the interaction conformational changes occur with associated increases in enthalpy ( $\Delta H^\circ$ ) and decreasing entropy ( $\Delta S^\circ$ ). The calculated binding stoichiometry is between 1:1 (FMN domain: AD) and 0.5 (MSR: AD). This suggests the binding model for the MSR-AD complex involves two molecules of AD interacting with one molecule of MSR, or that a conformational subpopulation of MSR interacts with AD, which may exist in a monomer-dimer equilibrium [118]. In addition, measurement of the mid-point redox potentials for the flavin cofactors in these two complexes showed there is a

substantial endergonic barrier for the electron transfer from MSR to MS. This endergonic ‘uphill’ electron transfer is followed by an exothermic methyl transfer reaction, ensuring that the overall reaction chemistry is essentially ‘downhill’.

## 1.5 Methionine Synthase

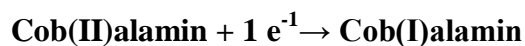
### 1.5.1 The catalytic reaction of *E.coli* MS as a basis for understanding human MS

MS catalyzes the transfer of a methyl groups from methyltetrahydrofolate to homocysteine generating H<sub>4</sub>folate and methionine (see Figure 1.8). Studies of the *E. coli* MS are reasonably well advanced; both mechanistic and partial structural data are available, providing an important knowledge base for studies of the less well characterised human MS. The gene for MetH in *E. coli* encodes a similar cobalamin-dependent MS and this gene has been cloned and sequenced [117]. The gene was expressed and the protein isolated with cobalamin in the active site. The cobalamin was found non-covalently bound to MS and its role is to function as an intermediary in methyl-transfer reactions. In this reaction, MS first catalyses the transfer of a methyl group from enzyme-bound methylcobalamin to homocysteine to generate methionine and cob(I)alamin. The cob(I)alamin is then remethylated by CH<sub>3</sub>-H<sub>4</sub>folate to regenerate methylcobalamin and H<sub>4</sub>folate (**Figure 1.8**). These two half reactions represent the primary turnover cycle of MS. However, the cob(I)alamin in MS is occasionally oxidized to an inactive cob(II)alamin after 100 to 2000 turnovers so it needs to be reactivated in a reductive methylation reaction. In *E. coli*, this methylation reaction requires electron transfer mediated by a flavodoxin and flavodoxin reductase. AdoMet acts as a methyl provider in this reductive chemistry. In humans, MSR substitutes for flavodoxin/flavodoxin reductase and the electron transfer from MSR to MS is the primary function of MSR in the cell.

The kinetic mechanism of the reaction catalyzed by cobalamin-dependent MS has been investigated by both steady-state and pre-steady-state kinetic methods. Steady-state kinetic analysis reveals an ordered sequential mechanism [117], in which two substrates, homocysteine and CH<sub>3</sub>-H<sub>4</sub>folate, bind to the enzyme prior to methyl transfer. The homocysteine then obtains a methyl group from methylcobalamin generating cobalamin and methionine. The cobalamin is then remethylated by methyl group transfer from methyltetrahydrofolate, which is bound to the enzyme. Pre-steady-state kinetic studies have been carried out to determine the rate constants for these reactions. Enzyme bound cob(I)alamin reacts rapidly with methyltetrahydrofolate with an observed rate of catalytic turnover of 19 s<sup>-1</sup>. The rate of product release at 50 s<sup>-1</sup> is probably the rate-limiting step during turnover [117].

### 1.5.2 Mechanism of reductive activation of *E. coli* MS

The mechanism of reductive activation of MS can be illustrated as follows:



The conversion of AdoMet to adenosylhomocysteine is associated with a large free energy decrease to trap the Cob(I)alamin formed by reduction. Because the +1 and +3 states of cobalamin cofactor are diamagnetic [119], electron paramagnetic resonance spectroscopy was used to study this mechanism. UV-visible absorbance spectra and EPR spectra on the isolated inactive MS demonstrated the characteristic features of cob (II) alamin [119]. The oxidation and reduction of the cob(II)alamin were quantified using the dominant EPR signal and the midpoint potential for the enzyme-bound cob(II)alamin/cob(I)alamin and the cob(III)alamin/cob(II)alamin couples were determined to be  $-526 \pm 5$  mV and  $273 \pm 4$  mV versus a standard hydrogen electrode [120]. During the reduction of cob (I)

alamin to form methylcobalamin, the presence of either CH<sub>3</sub>-H<sub>4</sub>folate or AdoMet can change the distribution of the cobalamin species and this result suggests that there is a absolute requirement for AdoMet in this coupled reduction/methylation reaction with a -350 mV potential. At this potential, the equilibrium distribution of cobalamin is in favour of cob(II)alamin species in presence of CH<sub>3</sub>-H<sub>4</sub>folate and of methylated enzyme in the presence of AdoMet[120].

### 1.5.3 Function modules of *E. coli* MS

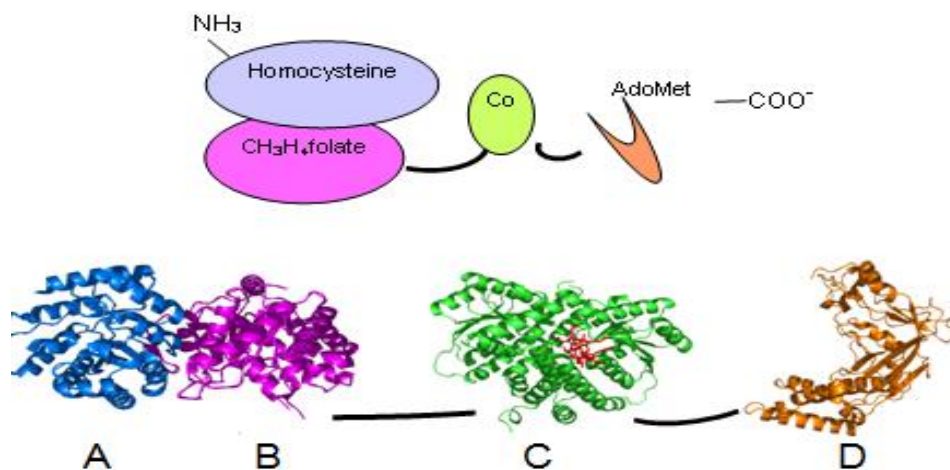
Most of the information on the structural and functional behaviours of MS comes from the research on the MetH in *E coli* [121] and Homo sapiens [30]. Although the whole structure of the full-length MetH has not been determined, the structures of the four divided functional modules have been solved. From the N-terminus to C-terminus, the structure of MetH from *Thermotoga maritima* consist of homocysteine- and CH<sub>3</sub>-H<sub>4</sub>folate-binding domains, cobalamin-binding domain and the AdoMet-binding domain, which is also called the activation domain (AD).

The first two domains, the homocysteine and CH<sub>3</sub>-H<sub>4</sub>folate-binding domains, comprise residues 1 to 354 and have a molecular mass of 38 kDa, consisting of two ( $\beta\alpha$ )<sub>8</sub> barrels [122]. These barrels are packed tightly to each other and have some distinctive distortion to accommodate the metal ion binding sites and substrates. The active sites for homocysteine and folate binding are located near the C terminal ends of the barrel strands and are exposed to solvent. These two barrels stay associated during the catalytic process. As part of the interdomain linker, some residues on the outside of helices and loops of the barrels form an extensive interface [122].

The third functional domain, the cobalamin binding domain, with a conserved structural feature typical of B<sub>12</sub>-dependent enzymes, consists of two parts. One is a

four-helix bundle (also called the cap domain) positioned over the upper ( $\beta$ ) face of the cobalamin; the second part is a Rossmann  $\alpha/\beta$  domain (named cob domain) with a critical histidine residue, which coordinates the cobalt of cobalamin from underneath. In MetH, the dimethylbenzimidazole nucleotide is displaced from the lower face of the cobalamin and is extended into the core of the Rossmann fold. In MS, the Hcy and CH<sub>3</sub>-H<sub>4</sub>folate substrates are bound to their respective barrels and separated by about 50 Å [122]. So to complete the catalytic cycle, the cobalamin-binding domain is believed to travel back and forth between these active sites. The active sites for the Hcy barrel are grouped in metal-(Zn<sup>2+</sup>) and substrate binding sites such as Glu<sup>146</sup>; and the active site for folate barrel includes Asp<sup>390</sup>, Asn<sup>411</sup>, Asp<sup>473</sup> and Asn<sup>508</sup> [122].

The fourth functional module, the activation domain, is comprised of residues from 897 to 1227 with a molecule mass 37 kDa [123]. It consists of C-shaped module with a bent anti parallel sheet which contains the domain core. AdoMet is bound at the centre of the inner surface of the “C” structure in a extended conformation, in which the adenine base is anti to the sugar and the adenine ring is flanked by Tyr<sup>1139</sup> and Tyr<sup>1189</sup> [123].



**Figure 1.10 Structural model of *E. coli* MS.** A. The blue coloured model is the homocysteine-binding domain; B. The pink domain is the  $\text{CH}_3\text{H}_4\text{folate}$ -binding domain; C. The green coloured model is the cobalamin-binding domain. And the red stick molecule is the cobalamin cofactor; D. The golden colour is the activation domain.

#### 1.5.4 A working model for *E. coli* MS

Based on the structure of the MS three different major conformational changes are thought to be required to carry out the  $\text{S}_{\text{N}}2$  methyl transfer reactions [30]. The first conformation of MS is a resting state, in which the  $\alpha$ -helical cap domain of the cobalamin-binding region shields the methyl group of the methylcobalamin and the upper face of the corrin keeps apart the substrate and solvent; the second conformation appears in reductive activation. In this conformation, the cap structure is replaced and the activation domain around the cobalamin allows adenosylmethionine to react with the cobalamin; the third conformation occurs in the reaction with homocysteine and/or methyltetrahydrofolate, in which the substrate binding region in the N-terminal region can contact with cobalamin. According to these conformational changes, the reactivity of cobalamin is dependent on both the properties of the enzyme bound cofactor and its access to a particular substrate. The conformational changes in MS are also controlled by a ‘ligand triad’ which is a set of



hydrogen-bonded residues His<sup>759</sup>-Asp<sup>757</sup>-Ser<sup>810</sup>, that positions and secures the histidine ligand and is in charge of the switching between the catalytic and activation cycles.

### **1.5.5 Human methionine synthase**

Human MS has been cloned and sequenced with a molecule mass of 140 kDa [124]. The sequence of human MS shows about 55% sequence identity with the protein from *E. coli* and 64% sequence identity with the MS from *Caenorhabditis elegans*. The crystallographic structure of the activation domain of human MS has been reported and it is C-shaped with the core comprising mixed  $\alpha$  and  $\beta$ -sheet with a  $\beta$ -meander region [118]. The main features of this structure are similar to the structure of the activation domain of MetH from *E. coli*.

## **1.6 The molecular basis for the autosomal recessive disorders related with MSR**

The physiological function of MSR is to regenerate the inactive MS, which catalyzes the methyl transfer from methyltetrahydrofolate to homocysteine to form methionine. So MSR and MS are key enzymes in homocysteine and folate metabolism [125]. Deficiency of the function of MSR and MS results in hyperhomocysteinemia, homocystinuria [126] and megaloblastic anemia without methylmalonic aciduria [127]. Some hereditary defects have contributed to the functional deficiency and are inherited as autosomal recessive disorders. Those patients with these disorders mainly consist of two complementary groups [128]: one group, cblG is thought to be caused by the defects on MS apoenzyme; another group, cblE is related with the reducing system of MS, MSR. Several mutants on the whole MSR coding region have been identified. The patients containing these polymorphisms on the MSR gene exhibit certain clinical symptoms, such as

development delay, ataxia, cerebral atrophy, neonatal seizures, blindness, thrombosis and arteriosclerotic vascular modification [129, 130]. One mutant A66G substitutes an isoleucine to methionine with an allele frequency of ~0.55 and is a genetic determinant of the increased blood homocysteine level; another mutant S175L has also been identified [125]; other mutants such as L576S, C405R, G487R and G554R are associated with these diseases [131]. The residue L576S, a conserved residue on  $\beta$ -sheet 9 of the NADPH-binding domain of MSR; the G554R, which locates within the  $\alpha$ -helix 9, is believed to disrupt the secondary structure of MSR; the G487R, which is near the pyrophosphate moiety of FAD, decreases the binding affinity of FAD because of the volume of arginine; another mutant C405R, which is near the surface of the protein and close to Pro<sup>243</sup> in the extended linker, is suggested to trigger some clashes in the secondary structure. These mutants cause structural change and affect the function of MSR as well as affecting the function of MS and folate and methionine mechanisms in the human body.

In summary, the broad aim of this thesis is to expand the understanding on the structure and function of MSR and further elucidate the relationship between MS and MSR. A variety of technologies: purification, crystallization, spectroscopic, kinetic and Potentiometric techniques have been applied to this research project. The research results are illustrated in these six chapters of this thesis.

Chapter two contains all the details of the materials, equipments, experimental protocols and conditions, data treatment methods with the equations and software used in this thesis.

Chapter three describes the research on the FAD/NADPH-binding domain of MSR. The experiments include the purification, crystallization, X-ray diffraction,

steady-state and stopped-flow pre-steady-state kinetics and the crystal structure building.

Chapter four illustrates the research on some variants of MSR, namely the D652A, D652R and D652N of the FAD/NADPH-binding domain of MSR and D652A, D652R, D652N, W697A and W697H of the full length MSR. The research results obtained from purification, steady-state, pre-steady-state and redox potential studies are shown and compared with the data obtained with the wild-type protein.

Chapter five details the research on the dynamic properties of wild type full-length MSR. EPR, ENDOR, ESEEM and ELDOR are used to check the conformational changes occurring on MSR at different redox potentials and in different complexes.

Chapter six shows two experimental results. The first experiment is the construction of two expression plasmids of full-length MSR: one expression plasmid contains GST and (His)<sub>6</sub> two tags to be expressed in *E. coli* and another plasmid with pPICZ vector to be expressed in *Pichia pastoris* Yeast system; the second experiment is the purification and crystallization of the activation domain of MS.

Chapter seven is a discussion of the data in this thesis and a suggestion for the further research on the MSR and the MSR-MS complex.

In general, the special aim of this PhD study is to apply biochemical and biophysical research methods to investigate the relations of the structure and function of MSR. For example, protein purification, crystallization and model building methods were used to illustrate the structure of MSR; the kinetics methods, including steady state kinetics and pre-steady state stopped flow, were designed to check the electron transfer catalytic ability and substrate specificity of MSR; the EPR, ENDOR, ESEEM and ELDOR were applied to uncover the dynamic features

of MSR. All of these research results will deep the understanding of the structure, catalytic mechanism and electron transfer ability of MSR. Further, this research will provide a good background for the invention of new medicine, which is purposely designed to cure some patients with the rare autosomal recessive disorders such as megaloblastic anemia, hyperhomocysteinemia and hopomethioninema. These diseases have believed related with the deficiency of MSR in human body.

**CHAPTER TWO**

**MATERIALS AND METHODS**

## **2.1 Materials**

All chemicals used in this project were Analar grade or equivalent purity. Glycerol, sodium chloride, potassium chloride, calcium chloride, potassium dihydrogen orthophosphate and dipotassium hydrogen orthophosphate were from Fisher Chemicals. Restriction enzymes and the plasmid pGEX-4-T1 were from Amersham Pharmacia Biotech. Genelute<sup>TM</sup> miniprep and midiprep kits were from Sigma-Aldrich. *PfuTurbo*<sup>TM</sup> DNA polymerase was purchased from Stratagene. Complete EDTA-free protease inhibitor tablets were from Roche. NADPH, 2', 5'-diphosphate, NADH, isopropyl- $\beta$ -D-thiogalactopyranoside (IPTG) were from Melford.

EPR tubes (cat.no.W706-PQ-9) from Wilmad-Labglass were ordered from Fluorochem Ltd.

## **2.2. Media**

Luria-Bertani (LB) medium was made up using 4 g tryptone, 4 g sodium chloride, and 2 g yeast extract with 400 mL ddH<sub>2</sub>O and autoclaved at 121°C for 20 minutes; the LB agar medium was prepared by adding an additional extra 5 g agar. Terrific Broth included 20 g yeast extract, 10 g bactotryptone, 4 mL glycerol, 4.33 g Na<sub>2</sub>HPO<sub>4</sub> and 2.65 g KH<sub>2</sub>PO<sub>4</sub> with 1 litre ddH<sub>2</sub>O. SOC medium consists of 20 g Bacto-tryptone, 5 g Bacto-yeast extract, and 2.5 mL 1 M KCL with 1 litre ddH<sub>2</sub>O.

## **2.3. Recombinant DNA techniques**

### **2.3.1. Isolation of plasmid DNA**

In the mini-preparation of plasmid DNA, a single transformed colony of *Escherichia coli* (*E. coli*), containing the target plasmid, was picked from an agar

plate and inoculated into 5 mL of LB medium with 50 µg/mL ampicillin. This culture was grown with shaking at 200 rpm, at 37 °C for 12 hours. Next, the target DNA plasmids were extracted from the culture using the supplied reagents from the Sigma Genelute™ miniprep kit. For a midi-preparation of plasmid DNA, 5 mL of cells were used to inoculate to 50 mL LB medium containing 50 µg/mL ampicillin at 37 °C for 12 hours, and harvested and manipulated with the midiprep kit reagents according to the manufacturer's instructions. The concentration of the target plasmid was estimated by comparing its band intensity with that of marker bands of known concentration in a 1% agarose gel.

### **2.3.2. Transformation of *E. coli* cells**

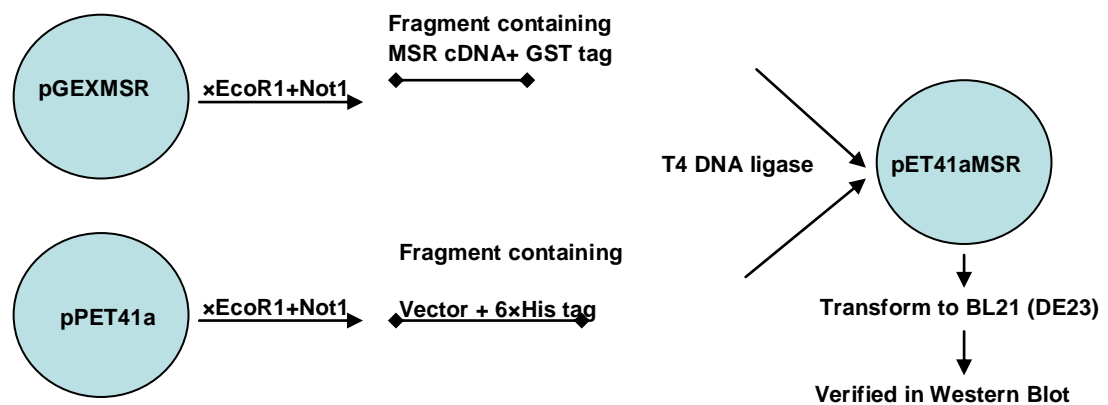
*E. coli* JM109 strain was chosen as the competent cells for transformation with plasmid DNA. The transformation experiment was begun by thawing the JM109 cells on ice. Frozen competent cells were obtained from Promega. Then 2 µL plasmid DNA (the lowest concentration used was 10 ng/µL) was mixed with 50 µL JM109 cells and kept on ice for 30 minutes. A heat shock at 42°C for 45 seconds was performed and the mixture was cooled on ice for 2 minutes. After adding 200 µL SOC medium, which was at room temperature, and gently shaking at 37 °C for 1 hour, the mixture was plated onto LB agar plates, containing 50 µg/mL ampicillin, and incubated inverted at 37 °C for 12 hours.

Competent cells of *E. coli* BL21 (DE3) and BL21 (DE3) pLysS were used for transformations to generate expression hosts for recombinant proteins because of their ability to express recombinant DNA from T7 promoter systems. First, the competent cells were thawed on ice. Then in a pre-chilled 1.5 mL polypropylene micro centrifuge tube, 20 µL competent cells were added to 1 µL of DNA plasmid

(the lowest concentration used was 10 ng/μg) and gently mixed. After 5 minutes, the cell mixture was placed in a water bath at 42 °C for 30 seconds and cooled on ice for 2 minutes. After adding 250 μL SOC medium, at room temperature, the cell mixture was shaken at 250 rpm, at 37 °C for one hour. Then the mixture was spread on an LB plate containing 50 μg/mL ampicillin. Finally, the plates were incubated in inverted position at 37 °C for 12 hours.

### 2.3.3 Construction of MSR expression plasmids

#### 2.3.3.1 Construction of plasmid pET41aMSR containing cDNA encoding the MSR gene with a GST tag and a (His)<sub>6</sub> tag.



**Figure 2.1 Construction of plasmid pET41aMSR**

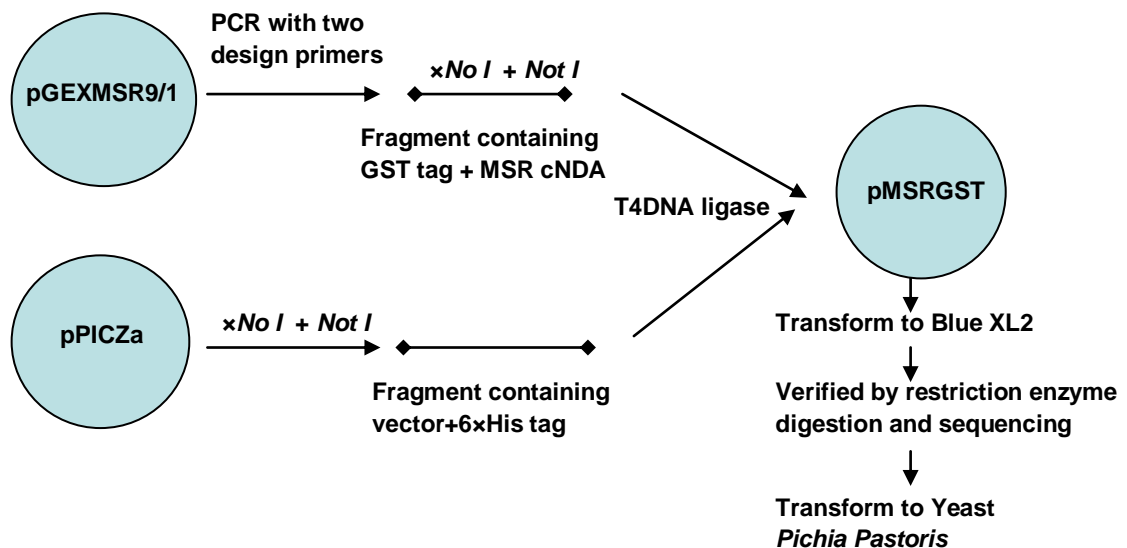
General methods to construct expression clones for human MSR are described in following sections. To overcome some difficulties, such as proteolysis of the MSR protein, the expression plasmid, pPET41aMSR, was constructed (Figure 2.1). This plasmid contains the cDNA that encodes the MSR protein with a GST tag and a (His)<sub>6</sub> tag. The plasmid pGEXMSR, which contains the MSR cDNA and an N-terminal GST tag that was previously constructed by Dr Kirsten Wolthers in the Scrutton laboratory [1]. The plasmid was digested with the restriction enzymes



*EcoRI* and *NotI* to release the gene encoding MSR. A second plasmid (pET41a) that contains a (His)<sub>6</sub> tag was also digested using the same two restriction enzymes. The products of the restriction of plasmid pGEXMSR were run on a 1% agarose gel. The DNA pieces corresponding to the MSR cDNA with the GST tag were isolated from the gel and purified using the QIAquick Gel Purification Kit (QIAGEN). Similarly, the DNA from the pET41a digest was purified using the QIAquick PCR Purification Kit. Next, the MSR cDNA was cloned into the pET41a vector by combining 200 ng of insert with 60 ng vector to achieve a 3:1 (insert: vector) ratio. The ligation reaction was incubated at 16 °C for 16 hours. The reaction (10 µL) was transformed to *E. coli* XL1 Blue and BL21 (DE3) competent cells by the heat shock method. The transformed colonies were grown in 5 mL LB medium containing 30 µg/mL kanamycin and incubated overnight at 37 °C. The plasmids, extracted from the growth culture, were digested by the restriction enzyme *EcoR I*, *Not I* and *Avr I* to screen for the correct construct. In addition, Western Blot analysis using an XCell II™ Blot Module from Invitrogen Life Technologies was used to test for the expression of MSR protein in the recombinant *E. coli* strain. Mouse primary antibodies against the His tag region of the protein were used to identify the protein and a nitrocellulose membrane was used for transblotting. Western blot methods used were essentially as described by the manufacturer. Prior to electrophoresis, sample preparation involved several steps including: (i) IPTG induction of recombinant *E. coli* strains during the exponential growth phase of the culture. Induction of recombinant protein was at different final concentration (0 mM, 0.1 mM, 0.5 mM and 1 mM) and cells were collected 1 hour, 3 hour and 16 hour after induction; (ii) cell lysates were prepared by the addition of BugBuster; (iii) SDS-PAGE electrophoresis; (iv) transfer protein to the nitrocellulose membrane; (v)

blocking and immune-detection followed by exposure to X-ray film. The general component methods used in Western blotting are described in more detail below.

### 2.3.3.2 Construction of a plasmid containing MSR cDNA encoding the MSR fused to a GST tag for expression in *Pichia pastoris*.



**Figure 2.2 Construction of plasmid pMSRGST**

The yeast expression system combines some of the advantages of both the prokaryotic and eukaryotic expression systems. For example, the methylotrophic yeast *Pichia pastoris* produces a high yield of recombinant proteins from cells grown to a high cell density on minimal media and offers a cost-effective method for example of making  $^{15}\text{N}$  or  $^{13}\text{C}$ -labelled proteins for NMR structural analyses [132]. In addition, the expression of a gene in *Pichia pastoris* can be easily controlled and tightly regulated using the alcohol oxidase1 (AOX1) promoter. With this efficient expression and control in mind, the plasmid pMSRGST was constructed to express human MSR in *Pichia pastoris*. First, a PCR reaction was performed with a pair of

primers (sequences shown in Table 2.2) which were synthesised by MWG Biotech Company. These PCR primers were designed to contain *Nco I* and *Not I* restriction sites. PCR reactions used plasmid pGEXMSR9/1 as PCR template. The PCR product is a 2.8 kb DNA fragment which contains MSR cDNA and an N-terminal GST tag. The PCR product was purified using the QIAquick PCR Purification Kit, and then digested with the restriction enzymes *Nco I* and *Not I*. The product was ligated to *Nco I* and *Not I* cut pPICZa using T4 DNA ligase. The ligation reaction was transformed to XL1-Blue competent cells and transformants were selected for on low salt LB (10 g tryptone, 5 g yeast extract, 10 g NaCl, per litre) plates containing 25 µg/mL Zeocin<sup>TM</sup>. The plasmid was subsequently extracted from an overnight culture of the recombinant host and digested using *Not I* and *Nco I* or *Not I* alone. The digests were electrophoresed on a 1 % agarose gel to confirm that the clone size is correct. Containing MSR cDNA and a GST tag and a (His)<sub>6</sub> tag at the C-terminus, this new plasmid, named pMSRGST, was sequenced commercially by the company MWG to confirm the correct construction of this plasmid.

#### **2.3.4. Agarose gel electrophoresis**

A 1 % (w/v) agarose gel was prepared for use in electrophoresis by dissolving 0.5 g agarose in 50 mL 1x TBE buffer, which had been diluted from a stock 10x TBE buffer ( 10x TBE buffer consists of 324 g Tris base, 165 g boric acid and 27.9 g EDTA with 2 litre dd H<sub>2</sub>O). After heating in a microwave oven for 50 seconds and following the addition of 2 µL ethidium bromide solution (0.5 µg/µL), the gel was cooled to 40 °C and poured into the gel former and a Teflon comb was inserted. Once the gel was completely set, it was covered with 1x TBE buffer and the comb was removed to form the sample wells. Wells were filled with individual samples, each of which was prepared using 30 µL DNA and 20 µL loading buffer, which was

made up of 60 % v/v glycerol, 0.25 % w/v bromophenol blue, 0.25 % w/v xylene cyanol [133].

### **2.3.5. Polymerase Chain Reaction (PCR)**

Polymerases chain reaction (PCR) is a modern technology that had an enormous impact in the development of the biological sciences. PCR is a molecular genetics technique for making multiple copies of small pieces of DNA. Under controlled conditions, small segments of DNA are produced by the enzyme, DNA polymerase, with the coupling of deoxynucleotides (dNTPs) to the target DNA, which is called 'template' DNA. Some small pieces of DNA, called 'primers' are required as the starting point for the reaction. During a typical PCR reaction, the template DNA is heated and separated to single strands; in the next annealing process, the primers bind to the template to begin the synthesis of DNA; then the extension step is required to extend the synthesis of the DNA strand until completion of the reaction. Conceptually and experimentally, PCR technology can produce microgram quantities of defined sequences of DNA ranging from 100 bp to 10 kb, in a couple hours.

In this project, PCR was applied in two experiments. The first use was in the cloning of the gene coding full-length MSR which also contained a GST tag and a (His)<sub>6</sub> tag; The second use was in the site-directed mutagenesis of the gene encoding the MSR protein. The products of this site-directed mutagenesis reaction include the variants D652A, D652R and D652N of the FAD/NADPH binding domain of MSR and the D652A, D652R, D652N, W697H and W697A of variants of the full-length MSR.

The PCR experiments were performed using a Techne TC-512 thermo cycler, which was programmed to carry out the initial denaturation, annealing and extension steps of the PCR reaction. All of the DNA primers were synthesised commercially by MWG. The following principles were used in the design of the primers: (1) The length of the primers was between 25 to 45 bases, with a melting temperature  $T_m \geq 78$  °C; (2) Melting temperatures were calculated using the following equation [QuikChange Instruction manual]:

$$T_m = 81.5 + 0.41 (\% \text{ GC}) - 675/N$$

**Equation 2.1**

Where N is the length of the primers; % GC is GC content of each DNA primer.

(3) The primers were designed to have a minimum GC content of 40 % and to terminate in one or more C or G bases. The primers in this project are listed in **Table2.2**

name	Forward primer	Reverse primer
pMSRGST	5'-cat gcc atg gcc cct ata cta ggt tat tg-3'	5'-acg atg cgg ccg cac ttg acc aaa tat cct g-3'
D652A	5'-cca tat tta tgt gtg tgg agc tgc aaa gaa tat ggc caa g-3'	5'-ctt ggc cat att ctt tgc agc tcc aca cac ata aat atg g-3'
D652R	5'-cca tat tta tgt gtg tgg acg tgc aaa gaa tat ggc caa g-3'	5'-ctt ggc cat att ctt tgc acg tcc aca cac ata aat atg g-3'
D652N	5'-cca tat tta tgt gtg tgg aaa tgc aaa gaa tat ggc caa-3'	5'-ctt ggc cat att ctt tgc att tcc aca cac ata aat atg g-3'
Full D652A	5'-cca tat tta tgt gtg tgg agc tgc aaa gaa tat ggc caa g-3'	5'-ctt ggc cat att ctt tgc agc tcc aca cac ata aat atg g-3'
Full D652R	5'-cca tat tta tgt gtg tgg acgtgc aaa gaa tat ggc caa g-3'	5'-ctt ggc cat att ctt tgc acg tcc aca cac ata aat atg g-3'
Full D652N	5'-cca tat tta tgt gtg tgg aaa tgc aaa gag tat ggc caa g-3'	5'-ctt ggc cat att ctt tgc att tcc aca cac ata aat atg g-3'
Full W697A	5'-gct acc ttc agg ata ttg cgt cat agc ggc cgc atc gtg ac-3'	5'-gtc acg atg cgg ccg cta tga cgc aat atc ctg aag gta ac-3'
Full W697H	5'-gct acc ttc agg ata ttc act cat aaa acc aga aat taa	5'-ctt taa ttt ctg gtt tta tga gtg aat atc ctg aag gta gc

**Table2.2.**The DNA primers used in PCR experiments. The yellow highlighted colour indicates alterations in DNA sequence compared with the template DNA sequence.

All PCR reactions performed in this project included 1  $\mu$ L template DNA (see Section 2.3.6), 5  $\mu$ L 10x Pfu Turbo DNA polymerase buffer, 1.25  $\mu$ L of 25  $\mu$ M forward primer, 1.25  $\mu$ L of 25  $\mu$ M reverse primer, 1  $\mu$ L of 10 mM of each of the four kinds of dNTPs, and 40  $\mu$ L of sterile dd H<sub>2</sub>O. PCR reaction conditions were determined according to the different primers and template DNA used.

	<b>Initial reaction</b>	<b>Cycle reaction</b>	<b>Last cycle</b>
<b>GST+MSR construction</b>	1 cycle 94 °C, 2 mins	36 cycles 94 °C, 2mins; 59 °C, 1 mins; 72 , °C, 7 mins.	1 cycle 4 °C, 24 hour
<b>PCR reactions for site-directed mutagenesis to generate variant forms of MSR</b>	1 cycle 95 °C, 2 mins	18 cycles 94 °C, 45 seconds; 55 °C, 1 mins; 72 °C, 10 mins	1 cycle 4 °C, 24 hour

**Table 2.3 PCR reaction conditions used in this project.**

Details of the mutagenesis methods used are given in **Section 2.3.7**.

### **2.3.6. Sources of DNA**

The plasmids encoding wild-type MSR, the FAD/NADPH binding domain of MSR [1] and the activation domain of MS [118] were all constructed by Dr Kirsten Wolthers and have been described previously.

### **2.3.7. Site-directed mutagenesis**

The aim of these mutagenesis reactions was to substitute one aspartic acid residue (Asp<sup>652</sup>) in MSR to alanine, arginine and asparagine and one tryptophan residue (Trp<sup>697</sup>) in MSR to asparagine and histidine, respectively. The Quikchange site-directed mutagenesis kit from Stratagene was used in all these mutagenesis reactions.

For each mutagenesis reaction, one forward and one reverse direction primer, which contained the code of the target amino acid to be changed, were designed and then synthesised by MWG Biotech. Each PCR reaction consisted of 5µL of 10 x PCR reaction buffer, 1.25 µL (125 ng) of each of the forward and reverse direction primers, 50 ng ds DNA template, 1 µL *Pfu* Turbo DNA polymerase (2.5 unit/µL), 1 µl dNTP mix (10 mM dNTPs stocks) with dd H<sub>2</sub>O to a final volume of 50 µL. The PCR reaction cycling parameters are shown in Table 2.2. When the cycling reaction finished, 1 µL *Dpn1* (20 units/µL) was added at 37°C for 1 hour to digest the DNA template.

The product of the PCR experiment was identified by electrophoresis on the basis of size in a 1 % agarose gel by comparison with the standard DNA ladder marker and then transformed in to *E. coli* JM109 competent cells to amplify the DNA. After growing at 37 °C over night in 5 mL LB medium with 5 µg/µL ampicillin, the cells were treated with the QIAGEN plasmid purification kit to extract the plasmid DNA. Some of the extracted plasmids were digested with specific restriction enzymes and sequenced to confirm the target mutants. After confirmation, the plasmids were transformed to competent *E. coli* BL21 (DE3) cells to express target mutant proteins.

## **2.4. Protein expression and purification**

### **2.4.1. Protein analysis**

#### **2.4.1.1 Protein concentration**

The concentration of the wild-type and variant proteins of full-length MSR and the FAD/NADPH binding domain of MSR were calculated using the absorbance of the flavin cofactors and the Beer-Lambert relationship [134].

$$A = \epsilon \cdot c \cdot l$$

### **Equation 2.2**

Where A is absorbance, c is the concentration of the protein sample, l is the path length in cm, and  $\epsilon$  is the molar extinction coefficient. At 454 nm the molar extinction coefficient for MSR and the FAD/NADPH binding domain are 21,600 M<sup>-1</sup>cm<sup>-1</sup> and, 11,300 M<sup>-1</sup>cm<sup>-1</sup>, respectively.

#### **2.4.1.2 SDS-PAGE electrophoresis**

SDS-PAGE electrophoresis was performed to separate and characterise mixed protein samples. It was also used as a routine method to determine the purity of the proteins. A Biorad mini-protean assembly was used with a 15 % running gel, which consists of 5 mL 30 % acrylamide, 2.3 mL ddH<sub>2</sub>O, 2.5 mL 1.5 M Tris-HCl pH 8.8, 100  $\mu$ L 10 % APS and 10  $\mu$ L TEMED. After the running gel formed, the stacking gel, which comprised of 2.1 mL ddH<sub>2</sub>O, 0.5mL 30 % acrylamide, 0.38 mL 1 M Tris-HCl pH 6.8, 30  $\mu$ L 10 % SDS, 50  $\mu$ L 10 % APS and 3  $\mu$ L TEMED, was poured on the top of the running gel and a Teflon comb inserted. When the gels were completely cooled and set, samples were added.

Protein samples were mixed with an equal volume of loading buffer, which contains 0.25M Tris-HCl, 1% SDS, 10% glycerol, 2-mercaptoethanol (v/v) and 0.2% bromophenol blue and boiled for 5 minutes. Then the mixture was added to the well on the gel which was left by removing the comb from the gel. The gel was



submerged in SDS-PAGE running buffer, which consisted of 25 mM Tris base, 192 mM glycine, and 3.5 mM SDS. Once the sample was loaded, it was run under a constant voltage of 160 V. It took about 1 hour for the dye front to travel to the bottom of the gel. Then, the gel was unpacked and stained in Coomassie Brilliant Blue R250 buffer, which comprised 50 % v/v methanol, 10 % v/v acetic acid, 0.25 % w/v Coomassie Brilliant Blue R250, for 30 minutes with gentle shaking. Finally the SDS-PAGE gel was destained in a solution including 40 % v/v methanol, 10 % v/v acetic acid for at least 30 minutes.

#### **2.4.2.Expression of wild-type MSR, MSR mutant proteins, and MS activation domain**

All of the protein samples used in this thesis including the wild-type full-length MSR, its FAD/NADPH binding domain, mutants of these proteins and the activation domain of MS, were expressed in *E. coli*. The *E. coli* strain BL21 (DE3) which harboured the target expression plasmids, was grown in 5 mL LB medium containing ampicillin (100 µg/mL) at 37 °C overnight. Then 0.2 mL of the overnight culture was used to inoculate 200 mL LB medium containing ampicillin (100 µg/mL) at 37 °C overnight for use as a seed culture. 10 mL of the seed culture was used to inoculate 500 mL modified Terrific Broth medium (TB) with ampicillin (100 µg/mL). This TB medium culture was grown at 28 °C whilst checking the optical density (OD) at 600 nm after 5 or 6 hours. When the OD<sub>600nm</sub> reached about 1.0, IPTG was added to a final concentration 0.1 mM to induce expression of the target protein. The culture was grown further at 25°C overnight. Finally, the overnight culture was centrifuged at 5000 g for 20 minutes to harvest the cells. The cells were stored at -80 °C for further purification.

### **2.4.3. Purification of MSR and MS**

#### **2.4.3.1. Purification of wild-type FAD/NADPH binding domain of MSR and mutant proteins**

Purification of the wild-type FAD/NADPH binding domain of MSR was essentially as described previously [1]. In the purification process, cells which had been stored at -80 °C were thawed on ice and suspended in 1x GST binding buffer (4.3 mM Na<sub>2</sub>HPO<sub>4</sub>, 147 mM KH<sub>2</sub>PO<sub>4</sub>, 137 mM NaCl, 2.7 mM KCl, 0.5 mM EDTA, pH7.2) containing a Complete<sup>TM</sup> protease inhibitor tablet (Roche) (~ 2 per 200 mL cell pellet volume) and lysozyme at a final concentration of 200 unit/mL. Then, after 20 minutes of gentle mixing of the suspended cells, the cells were sonicated in a Misonix XL2020 sonicator (Misonix Inc) using the following parameters: 20 seconds burst, 3 minutes pause intervals for 40 minutes in position 7. Then the sonicated cells were immediately centrifuged at 15000 g for 60 minutes.

After adding one volume of ice cold 1 x GST binding buffer to adjust the pH and to decrease the ionic concentration, the supernatant from the centrifugation mixture was loaded on to a Glutathione-Sepharose 4B (Glutathionine Superflow Resin, Fisher Scientific) column (75 x 39 mm), which had been equilibrated with 1 x GST binding buffer. The washing speed is an important factor which affects the protein binding to this column, and it was discovered that protein bound more efficiently when applied at a slow rate 20 mL/min. After loading, 1 litre GST binding buffer was applied to the column to wash off any non-specifically bound protein. After the washing step, the bound protein was eluted from the column in 50 mM Tris-HCl buffer pH8.0 containing 10 mM reduced glutathionine, 0.5 mM EDTA and 1 mM DTT.

After concentrating to a small volume of about 10 mL, the elution mixture, (the target enzyme protein containing a GST tag,) was incubated with Thrombin protease (Thrombin Protease, 500 units, Amersham Biosciences No. 27-0846-0) to separate the GST tag and the target protein. The solution was dialysed against 50 mM Tris-HCl buffer, pH 8.0 containing 0.5 mM EDTA and 1 mM DTT at 4 °C overnight. Then the dialysis mixture was applied to a small Glutathione-Sepharose 4B column (54 x 30 mm), which had been equilibrated with 1x GST binding buffer to completely separate the target protein from the GST tag. Finally, the target protein was collected and concentrated by ultracentrifugation at 145,421g (maximum 193,357g) for 1 hour for further purification.

After purification on the GST affinity column, the target protein was purified further by anion exchange chromatography. A Q-Sepharose high-performance column (145 x 25 mm) was used, which was equilibrated in 50 mM NaCl in 50 mM Tris-HCl buffer, pH 7.5 containing 50 mM NaCl. After loading the sample and washing to remove weakly bound proteins, the target protein was eluted using a linear gradient (50 mM to 500 mM NaCl) at a flow rate of 4 mL/min. The eluted fractions, containing the target protein, were identified by the absorbance spectrum at 454 nm and 280 nm and the protein identity was confirmed by electrophoresis in a 10 % SDS-PAGE gel by comparison with a standard protein marker ladder. After concentration and dialysis against 50 mM Tris-HCl buffer, pH 7.5, 20 % glycerol was added to the target protein, (wild-type FAD/NADPH binding domain of MSR or its corresponding variants) and proteins were frozen in liquid nitrogen and stored at -80 °C for further crystallography and kinetic studies.

#### **2.4.3.2. Purification of wild-type full-length MSR and its mutant forms**

The procedure for the purification of the wild-type full-length MSR and mutant proteins consists of two phases. The first phase of purification is identical to the purification procedures used for the FAD/NADPH binding domain of MSR, which is described in **section 2.4.3.1**. In the second phase of the purification, the MSR protein, which had undergone GST affinity chromatography and Q-Sepharose anion exchange chromatography, was loaded onto a Superdex 200 gel filtration column (volume 180 cm<sup>3</sup>), which had been equilibrated with 50 mM Tris-HCl buffer, pH 7.5 containing 0.3 M NaCl. The protein was eluted in the same buffer at a flow rate of 0.3 mL/min. The MSR fraction in the elution profile was indicated by its absorbance at 280 nm and 454 nm and the protein identity was confirmed by SDS-PAGE electrophoresis. Protein samples of interest were pooled and concentrated by ultracentrifugation at 145,421 g (maximum 193,357 g) for 1 hour and 20 % glycerol was added to the purified MSR and the solution prior to freezing in liquid nitrogen and storage at -80 °C for further kinetic studies.

#### **2.4.3.3. Purification of the activation domain of MS**

The protocol for the purification of the activation domain of MS comprises sonication, centrifugation, and affinity and anion exchange chromatography procedures. First, the frozen *E. coli* BL21 (DE3) cell pellet, which had been stored at -80°C and contained the over expressed protein, was thawed on ice and suspended in cold 50 mM potassium phosphate buffer, pH 7.4, also containing 1 mM EDTA. Complete protease inhibitor tablets (~ 2 tables per 200 mL cell pellet volume, Roche) and lysozyme 200 µg/mL were also contained in the buffer. The cell suspension was sonicated 10 times using a High Intensity Ultrasonic Liquid Processor (Sonics, Sonics & Materials, Inc) in 20 second bursts with 50 second cooling intervals on ice. After sonication, the mixture was centrifuged at 15000 g, 4

°C for 1 hour. The supernatant from the centrifugation was then mixed with Ni-NTA resin (Ni-NTA His·Bind Resin, Novagen 70666-4) concentrated in 0.5 M sodium chloride, 20 mM imidazole and 50 mM potassium phosphate buffer, pH 7.4, for 1 hour. Then, the Ni-NTA resin was centrifuged at 3000 g, 15 minutes, 4 °C and packed in a column (54 x 30 mm) for purification by affinity chromatography.

The Ni-NTA column, containing the bound activation domain of MS, was washed with 50 mM potassium phosphate buffer, pH 7.4, which also contained 0.5 M NaCl and 60 mM imidazole. Then the target protein was eluted from the column in 50 mM potassium phosphate buffer, pH 7.4, containing 0.5 M NaCl and 0.4 M Imidazole. The eluted fractions were dialyzed against 2 litres ddH<sub>2</sub>O at 4°C for 2 hours and 50 mM Tris-HCl buffer, pH 7.5, at 4 °C for 16 hours. The dialysed protein was loaded onto a Q-Sepharose column (54 x 30 mm) which had been pre-equilibrated with 50 mM Tris-HCl pH 7.5. The column was then washed with 300 mL 50 mM Tris-HCl buffer, pH 7.5. The column was developed with a linear gradient ranging from 0 mM to 500 mM NaCl in 50 mM Tris-HCl buffer pH 7.5. The fractions containing the activation domain of MS were identified by the absorbance peak at 280 nm and confirmed by 12 % SDS-PAGE electrophoresis. Finally, the purified activation domain of MS was concentrated and stored at -80 °C with 20 % glycerol for further crystallography experiments. Prior to the crystallography experiment, the frozen enzyme samples were thawed and passed over a 10 mL Bio-Rad Econo-Pac 10 DG column, which had been equilibrated with 10 mM Tris/HCl buffer, pH 8.0 containing 0.5 mM DTT, 1 mM EDTA, and 0.05 % NaN<sub>3</sub>, to remove the glycerol.

## **2.5. Crystallogenesis, X-ray diffraction and model building**

### **2.5.1. Crystallogenesi s of the FAD/NADPH binding domain of MSR**

Crystals of the FAD/NADPH binding domain of MSR were produced using the sitting drop vapour diffusion method. In this process the purified enzyme (10mg/mL) was first dialyzed against 10 mM Tris/HCl buffer, pH 8.0 containing 0.5 mM DTT, 1 mM EDTA, and 0.05 % NaN<sub>3</sub> to desalt. The enzyme then was mixed into different precipitant buffers at 4 °C. Some higher resolution diffraction crystals came from the reservoir solution which contains 0.1 M Tris/HCl buffer, pH 7.5, 0.2 M KBr and 15 % PEG 4000. Some of these crystals were bathed in the mother liquid to which a saturating concentration of NADP<sup>+</sup> was added. These crystals were then soaked in a 50:50 mixture of Paratone and mineral oil (cryoprotectant) at 4 °C before being flash-cooled in liquid nitrogen and prepared for an X-ray diffraction experiment.

### **2.5.2. X-ray diffraction on the FAD/NDAPH binding domain of MSR**

The X-ray diffraction experiment on the FAD/NADPH binding domain of MSR was carried out at the European Synchrotron Radiation Facility (Grenoble, France) on ID14-EH3 using an ADSC Q4 CCD detector. The data sets were collected to 1.9 Å resolution with and without bound NADP<sup>+</sup> and used for model building of the structure of protein. Data collection was performed by Dr David Leys (University of Manchester).

### **2.5.3. Structure determination and refinement of the model for the FAD/NADPH binding domain**

The data from the X-ray diffraction studies of the FAD/NADPH domain of MSR were processed and scaled by the HKL package program DENZO and

SCALEPACK [135]. With the aid of the recorded structure of cytochrome P450 reductase as the research mode (PDB code 1 AMO), the structure was resolved using the molecular replacement method and the program AMoRE [4]. The REFMAC5 program [136] was used to do the positional and B-factor refinement using the restrained and TLS modes; the program TURBO-FRODO [137] and COOT [138] were used for the alternate rounds and manual rebuilding of the model; the program ARP/wARP was used to build the waters and partial rebuilding of the model. Dr Helen Toogood provided assistance with data analysis and model building throughout the crystallographic work presented in this thesis, and this input is gratefully acknowledged.

#### **2.5.4. Crystallogenesi on the activation domain of MS**

The crystals of the activation domain of methionine synthase (MS) were grown using the sitting drop vapour diffusion method at 4 °C and 19 °C respectively. The Mosquito robot from TTP Lab Tech Ltd was used in these experiments. The concentration of the activation domain of MS was 20 mg/mL and it took 3 days until the crystals appeared in reservoir solutions, which comprised 0.1 M tri-sodium citrate buffer, pH 5.5, 0.1 M tri-sodium citrate 10 % w/v PEG 3000, 0.2 M sodium malonate 20 % w/v PEG 3350, respectively. The crystals were picked out and identified by 12 % SDS-PAGE electrophoresis and the SDS-PAGE gel was stained using one Silver Quest<sup>TM</sup> Silver staining Kit (Invitrogen<sup>TM</sup> Life Technology). The crystallogenesi of the activation domain of MS provided useful information for further crystallization trials of the complex formed between MSR and the activation domain of MS (now being pursued by others in the research group).

#### **2.6. Kinetic studies**

### 2.6.1. Steady-state kinetic studies with the FAD/NADPH binding domain of MSR

Steady-state kinetic activities of wild-type FAD/NADPH binding domain of MSR and the mutants D652A, D652R and D652N, were measured using FeCN as an electron acceptor and NADPH as electron provider using a Varian Cary 50 Bio single-beam UV-Visible spectrophotometer with a 1 cm light path. Each 1 mL reaction mixture consisted of 50 mM potassium phosphate buffer, pH 7.0, 1  $\mu$ M FeCN and NADPH, the concentration of which was varied from 0 to 100  $\mu$ M and was measured by the absorbance at 340 nm, ( $\epsilon_{340} = 6,220 \text{ M}^{-1} \text{ cm}^{-1}$ ) and the wild-type FAD/NADPH binding domain of MSR or its mutants. The reaction was started by the addition of the FAD/NADPH binding domain of the MSR enzyme to a final concentration of 0.0126  $\mu$ M at 25°C and data were recorded over 1 minute. The initial velocities were determined by the change in the absorbance at 420 nm using the extinction coefficient for FeCN at 420 nm ( $\epsilon_{420} = 1020 \text{ M}^{-1} \text{ cm}^{-1}$ ). The initial velocity obtained under the varied NADPH concentration from 0.5 to 100  $\mu$ M were analysed using the Michaelis-Menten equation to obtain the apparent values for  $V_{max}$  and apparent  $K_m$  [139]. Origin (version 6.0) software was used to finish the non-linear least-squares regression analysis on the data. After several iterations reasonable estimates, the final data was repeat at least 30 times, allowing the  $V_{max}$  and  $K_m$  values to vary in the final fitting sessions.

$$v = \frac{V_m[S]}{K_m + [S]}$$

**Equation 2.3**



### **2.6.2. Steady-state kinetic studies with the wild-type full-length MSR and its mutant forms**

The methodology and equipment employed for the measurement of the steady-state activities of wild-type full-length MSR and some of the mutant forms (W697A, W697H and W697) were similar to that used for analysis of the FAD/NADPH-binding domain of MSR, but with some changes to the substrate and enzyme quantities. Cytochrome *c* was chosen as the electron acceptor and NADPH as an electron provider. The rate of the reduction of cytochrome *c* was monitored at 550 nm using the extinction coefficient  $\epsilon_{550} = 21,100 \text{ M}^{-1}\text{cm}^{-1}$  after the addition of 1 to 2  $\mu\text{g}$  MSR to start the reaction. Finally, the initial velocity was obtained by varying concentrations of electron donor and acceptor and data were analysed using the Michaelis-Menten equation to obtain the apparent values for  $V_{max}$  and the apparent  $K_m$  (see **Equation 2.3**). Origin (version 6.0) software was used to finish the non-linear least-squares regression analysis on the data. After several iterations reasonable estimates, the final data was repeat at least 30 times, allowing the  $V_{max}$  and  $K_m$  values to vary in the final fitting sessions.

### **2.6.3. Steady-state inhibition studies with wild-type and the mutant forms of the FAD/NADPH- binding domain of MSR**

Steady-state inhibition studies were carried out in a 1.0 mL mixture at 25 °C in a 1 cm path length cuvette. The mixture contained 50 mM Tris/HCl, pH7.5, 8  $\mu\text{M}$  FeCN for the mutants of the NADPH/FAD binding domain (or 8  $\mu\text{M}$  cytochrome  $c^{3+}$  for the full length MSR mutants), a variable concentration of NADPH, and a variable concentration of the inhibitors  $\text{NADP}^+$  and 2'5' ADP. The reaction was initiated by the addition of the enzyme, one of the NADP/FAD binding domain mutants or the

full length MSR mutants. The absorbance change at 420 nm for FeCN,  $\epsilon_{420\text{nm}} = 1,100 \text{ M}^{-1}\text{cm}^{-1}$ , was used to monitor the reaction and data fit with the nonlinear least-squares analysis to the equation for competitive inhibition [140]. Origin (version 6.0) software was used to finish the non-linear least-squares regression analysis on the data. After several iterations reasonable estimates, the final data was repeat at least 30 times, allowing the  $V_{\text{max}}$ ,  $K_{\text{m}}$  and  $K_{\text{i}}$  values to vary in the final fitting sessions

$$v = \frac{V_m A}{K_M \left( 1 + \frac{I}{K_i} \right) + A}$$

**Equation 2.4**

In **Equation2.4**,  $v$  is the initial velocity;  $V_m$  is the maximal velocity;  $A$  is the varied substrates concentration;  $K_M$  is the apparent Michaels constant;  $I$  is the inhibitor concentration and  $K_i$  is the inhibition constant.

#### **2.6.4.Pre-steady-state kinetic studies on the wild-type FAD/NADPH binding domain of MSR and mutants.**

Pre-steady-state turnover studies with the FAD/NADPH binding domain of MSR were performed using an Applied Photophysics SX1.7 MV stopped-flow spectrophotometer. The following conditions were used for these experiments: reaction buffer, 50 mM potassium phosphate buffer pH 7.0 at 25 °C; enzymes concentration, 4 $\mu$ M for single-wavelength studies and 20  $\mu$ M for photodiode array experiments. To avoid any undesired oxidation, experiments were carried out under

anaerobic conditions using a stopped-flow device maintained in a Belle Technology anaerobic glove box. The buffer was made oxygen-free by evacuation and extensive bubbling with nitrogen before being placed in the glove box overnight. Before starting the experiment in the glove box, the enzyme sample was treated with potassium ferricyanide to ensure that it was fully oxidized and then passed through an Econo-Pac 10 DG column (Bio-Rad) equilibrated with anaerobic 50 mM potassium phosphate buffer pH 7.0, to remove excess ferricyanide. In addition, the NADPH was prepared in the glove box and the concentration was calculated using  $\epsilon_{340} = 6,220 \text{ M}^{-1}\text{cm}^{-1}$ . These experimental conditions were used for both the multiple wavelength absorbance studies and single-wave length absorbance studies.

The stopped-flow multiple wavelength absorbance studies were carried out using a photodiode array (PDA) detector and X-SCAN software (Applied Photophysics Ltd). Under the single turnover condition, the FAD/NADPH- binding domain of MSR was mixed with NADPH (20-fold excess over MSR to ensure pseudo-first order conditions). The reduction of the FAD/NADPH binding domain of MSR was detected by the bleaching of the absorbance maxima at 454 nm. The resulting spectra were interpreted using global analysis and numeral integration methods (PROKIN software, Applied Photophysics Ltd). The resulting stopped-flow traces were fitted to a single-exponential expression equation [113]. Origin (version 6.0) software was used to finish the non-linear least-squares regression analysis on the data. After several iterations reasonable estimates, the final data was repeat at least 30 times, allowing the  $k_{\text{obs}}$  values to vary in the final fitting sessions :

$$A = C_1 e^{-k_{\text{obs}}t} + b$$

**Equation 2.5**

Where  $k_{\text{obs}}$  is the observed rate constant,  $t$  is time,  $C_1$  is the amplitude change and  $b$  is the offset value corresponding to the non-zero baseline value. This method was also used in the stopped-flow studies with the mutant forms of the FAD/NADPH binding domain of MSR (F652A, F652R and F652N) and wild-type of full-length MSR and its mutants (F652A, F652R and F652N, W697A, W697H). However, for full length MSR rate constants ( $k_{\text{obs1}}$  and  $k_{\text{obs2}}$ ) for successive hydride transfers were obtained by fitting to a double exponential function. Origin (version 6.0) software was used to finish the non-linear least-squares regression analysis on the data. After several iterations reasonable estimates, the final data was repeat at least 30 times, allowing the values to vary  $k_{\text{obs1}}$  and  $k_{\text{obs2}}$  in the final fitting sessions:

$$A = C_1 e^{-k_{\text{obs1}}t} + C_2 e^{-k_{\text{obs2}}t} + b$$

**Equation 2.6**

Where  $k_{\text{obs1}}$  and  $k_{\text{obs2}}$  are the observed rate constants and  $C_1$  and  $C_2$  are their relative amplitude and  $b$  is the final absorbance.

### **2.6.5.Redox titrations of the flavin cofactors in FAD/NADPH binding domain of MSR**

As with the stopped flow experiments, redox titration experiments with the FAD/NADPH binding domain of MSR were carried out in a Belle Technology glove box under a nitrogen atmosphere (oxygen concentration < 5 ppm) at 25 °C. The enzyme sample was put into the glove box and oxidized with added potassium ferricyanide to ensure full oxidation and, then applied to the 10 mL Bio-Rad Econo-

Pac 10DG column(15 x 60 mm). This column had been equilibrated with 100 mM potassium phosphate pH 7.0, which had been extensively bubbled with argon and stored in the glove box. After adding three kinds of redox mediators [i.e. benzyl viologen (final concentration 1  $\mu$ M), methylviologen (final concentration 0.5  $\mu$ M), 2-hydroxy-1, 4-naphoquinone (final concentration 5  $\mu$ M)], the enzyme sample was initially titrated to the reduced state by adding sodium dithionite, then reoxidized by adding potassium ferricyanide. The absorbance spectra from 280 nm to 800 nm were recorded by a fibre optic absorption probe (Varian) linked to a Varian Cary 50 probe UV-visible spectrophotometer. After the addition of the reductant or oxidant, the electrochemical potential was measured with a Hanna instruments pH21 pH/voltmeter coupled with Pt/calomel electrode (Thermo Russell Ltd). The Fe(II)/Fe(III)-EDTA couple (+108 mV) was used as a standard to calibrate the instrument. Because every observed potential needed to be normalized to the standard hydrogen electrode, it was necessary to add 244 mV to every potential value. Finally, the absorbance data for the FAD cofactor at 600 nm of the enzyme sample was plotted to the determined redox potential and the data were fitted to **equation 2.7** [113]:

$$A = \frac{a10^{(E-E_1)/59} + b + c10^{(E_1-E)/59}}{1 + 10^{(E-E_1)/59} + 10^{(E_1-E)/59}}$$

**Equation2.7**

This equation is derived from the Beer- Lambert Law and Nernst equation to describe a two electron reduction process. In this equation,  $A$  is the total absorbance, and  $a$ ,  $b$ ,  $c$  are the component absorbance values contributed by one flavin in the

oxidized, semiquinone and hydroquinone state.  $E$  is the observed potential;  $E_1'$ ,  $E_2'$  are the midpoint potential for the ox/sq and sq/hq couples. The absorbance of the enzyme sample versus potential was illustrated by non-linear least-squares regression analysis using Origin software (version 6.0) according to these equations. After several iterations reasonable estimate, the final data was repeated at least 30 times, allowing the values to vary  $E_1$  and  $E_2$  in the final fitting sessions. The midpoint potential for the ox/sq and sq/hq can be calculated from this treatment.

Analysis of redox titration experiments for mutants of the FAD/NADPH binding domain of MSR, D652A, D652R and D652N were performed using similar procedures.

## **2.7. Fluorescence studies on the wild-type MSR and mutants**

Fluorescence is one of the most useful tools in flavoprotein research. It can be employed to investigate the structure integrity, kinetic properties and other aspects of flavoproteins. The basic theory of fluorescence is that the sample molecules can absorb a photon of energy at a defined wavelength. The absorbed energy promotes electrons from a low state to higher energy state with return to the ground state accompanied by the loss of energy and emission of photons. In flavoproteins, two types of groups can emit fluorescence. One is flavin, which has absorption maxima at 369 nm to 390 nm and 440 nm to 470 nm. The other comprises the amino acids tryptophan (the indole group of which absorbs with a  $\lambda_{\text{max}} = 280$  nm with the extinction coefficient,  $\epsilon = 5050 \text{ M}^{-1} \text{ cm}^{-1}$  and fluorescence emission maxima between 320 nm to 360 nm); there are also smaller contributions from the fluorescence emission of tyrosine and phenylalanine [141].

Tryptophan fluorescence was used in stopped-flow fluorescence studies of electron transfer of wild type full-length MSR and the mutant W697A full length MSR protein. These studies were used to report on local dynamic changes associated with residue W697 located in the NADPH binding pocket. In stopped-flow studies the emission wavelength 340 nm and excitation 295 nm was selected using an appropriate band-pass filter. Time dependent fluorescence data were analysed by fitting to a standard monophasic equation. Corresponding static (i.e. not time resolved) fluorescence studies were performed using a Cary Eclipse fluorimeter (excitation wavelength of 295 nm and an emission wavelength of 340 nm was selected with an appropriate band-pass filter).

## **2.8. Electron spin echo (ESE) studies on the wild-type full-length MSR**

### **2.8.1 Sample preparation for ESE**

The enzyme samples for ESE experiments on the wild-type full-length MSR were prepared within the Belle Technology glove box under anaerobic conditions ( $O_2 < 5$  ppm). The fully oxidized enzyme was reduced by adding sodium dithionite to generate the semiquinone or hydroquinone state of the cofactor FAD. The concentration of the sample was determined using the extinction coefficient  $\epsilon_{454}$  of  $25,600 \text{ M}^{-1} \text{ cm}^{-1}$ . While titrating with sodium dithionite, the absorbance of the sample was monitored. When the spectral feature of semiquinone or hydroquinone were identified, 100  $\mu\text{L}$  aliquots of 400  $\mu\text{M}$  protein samples were transferred into four EPR tubes and mixed with either 100  $\mu\text{L}$  800  $\mu\text{M}$  NADP, 100  $\mu\text{L}$  800  $\mu\text{M}$ , 2,5-ADP or 100  $\mu\text{L}$  800  $\mu\text{M}$  activation domain of MS, respectively. The final 200  $\mu\text{L}$  protein sample which contains 200  $\mu\text{M}$  protein were immediately sealed in EPR tubes by

using parafilm and flashed-frozen in liquid nitrogen and stored in liquid nitrogen for subsequent analysis by EPR, ENDOR, ESEEM and ELDOR spectroscopy.

## **2.8.2 EPR**

### **2.8.2.1. Theory of EPR**

Paramagnetic centres refer to the sites in molecules and atoms with free unpaired electrons. Under the absence of an external magnetic field, the unpaired electron spins in a random way; when the external magnetic field is applied, the unpaired electron spins around an axis in either +1/2 or -1/2 spin state. Under the external magnetic field, the unpaired electrons are divided into two groups: one group spins parallel to magnetic field orientation with decreasing energy level; another group spins anti-parallel to the magnetic field orientation with increasing energy level. EPR can detect these spin state transitions.

Sample are placed into a strong homogenous magnetic field and simultaneously exposed to an electromagnetic radiation with a frequency  $\nu$ , which is equal to the difference between the two electron levels [142].

$$h \nu = g \beta H$$

#### **Equation 2.8**

Where  $h$  stands for the Plank constant;  $\nu$  is the electromagnetic radiation frequency;  $g$  is a constant ( $g$  factor);  $\beta$  is the Bohr magneton, a unit that expresses the magnetic moment of the electrons.

The radiation energy will cause the odd electron, which is located on the low energy level, to jump to higher level with a simultaneous change in the spin direction



and energy absorption. When the upper level electrons pass onto the lower level, radiation of a quantum of electromagnetic energy occurs. This kind of change of spin direction at the resonance conditions is related with net absorption energy from the applied electromagnetic radiation, which can be detected by a spectrometer to produce an EPR signal. Among the main parameters of EPR spectrum, such as the integral intensity, line width, and saturation effect, the g-factor is the most important parameter g-factor characterises the resonance point position and is determined by the field value giving rise to the resonance. The g-factor of a free electron B is 2.0023 [143]. Now EPR spectroscopy is a routine method to provide reliable and detailed information on the formation of flavin semiquinone in the flavoprotein.

#### **2.8.2.2. EPR experiments and conditions**

All EPR spectra were obtained using a Bruker ELEXSYS E500/E580 spectrometer operating at X-band. Temperature control was achieved using an Oxford Instruments ESR900, for continuous wave EPR, or ESR935, for pulsed measurements, cryostat connected to an ITC503 temperature controller. Continuous wave spectra were obtained at 80K using the parameters given in the figure caption.

#### **2.8.3. ENDOR**

##### **2.8.3.1. Theory of ENDOR**

Electron Nuclear double Resonance, ENDOR, is a double resonance technique which combines the high resolution and nuclear selectivity of an NMR experiment with the sensitivity of an EPR experiment. An ENDOR experiment is performed by monitoring the EPR signal intensity while sweeping a RF (Radio Frequency) signal to drive the NMR transitions. Double resonance experiments such as ENDOR

require more effort than EPR or NMR experiments, but provide greater insight into the structure, dynamics, and electronic structure of the sample.

In biochemical research on flavoproteins, ENDOR spectroscopy provides improved spectral resolution and information on the molecular structure and electronic distribution on model flavin and flavin radicals. Usually, ENDOR focuses to detect the strong hyperfine coupling aroused by 8-CH<sub>3</sub> and 6-CH<sub>3</sub> proton in anionic and neutral semiquinone and the change of the electron density distribution on the flavin ring. ENDOR spectra of flavin semiquinones are essentially symmetrical about the central ‘matrix’ feature which occurs at the proton Larmor frequency which is ~14.7 MHz in the spectrometer used. The symmetrical pairs of lines are separated by the hyperfine coupling constant, A, of the proton in question. Anisotropy (asymmetry) in the hyperfine coupling constant is manifested as asymmetry in the ENDOR lines.

### **2.8.3.2 ENDOR experiments and conditions**

The sample preparation, equipments and conditions for ENDOR are the same as those employed for EPR. The Davies pulsed ENDOR methodology was used to acquire the spectra. The pulse sequence was  $\pi$ -T- $\pi/2$ - $\tau$ - $\pi$ - $\tau$ -acquire with  $\pi = 200$  ns,  $\tau = 1200$  ns and T = 12  $\mu$ s with a 10  $\mu$ s radiofrequency (NMR) pulse applied 1  $\mu$ s after the initial  $\pi$  pulse.

### **2.8.4 ESEEM**

#### **2.8.4.1 Theory of ESEEM**

Electron spin echo envelope modulation, ESEEM, is a pulsed EPR method, which is used to detect weak hyperfine interaction between the paramagnetic centers

and quadrupolar nuclei such as  $^{14}\text{N}$ ,  $^2\text{H}$ . The electron spin echoes in ESEEM are induced by the application of two or more resonant microwave-pulses and the amplitude of the echo modulates with a periodic variation as a function of the interval between the pulses and coupling of the unpaired electron to ‘magnetic’ nuclei. Fourier transformation of the modulation pattern indicates the resonant frequencies of the nuclei coupled to the paramagnetic center. These frequencies can be used to determine the hyperfine and electric quadrupole couplings of nuclei within the sample.

#### **2.8.4.2 Sample preparation and equipment**

The sample preparation and equipment for ESEEM are the same as that for the EPR experiment. The ESEEM spectra were recorded using a  $\pi/2$ - $\tau$ - $\pi$ - $\tau$ -acquire sequence with  $\tau$  increasing from 200 ns to 4296 ns in 4 ns steps. The echo decay obtained contained the nuclear modulation information. The decay function, essentially  $T_M$ , was fitted as an exponential and subtracted. The remaining modulation pattern was apodized using a Hamming window function and then Fourier transformed.

#### **2.8.5. ELDOR**

##### **2.8.5.1 Theory of ELDOR**

Electron-electron double resonance, ELDOR, is an EPR technique in which two microwave frequencies are applied to a sample. One frequency, called the observe frequency, is applied to monitor a specific region of the EPR spectrum and a second frequency, called the pump frequency, is applied to other regions of the EPR spectrum. An ELDOR response is any pump frequency dependent change in the EPR spectrum. Principally, ELDOR measurement is a way to study a variety dynamic

processes that control relaxations between the pumped and observed spins. Since pulsed ELDOR can generate electron spin echo modulation via dipolar coupling, it is possible to determine the distance between the FAD and FMN centres in the wild-type MSR. The dipole-dipole coupling between the two electronic magnetic centers is related to the distance between them, and can be calculated by **equation 2.9** [115].

$$v_{\text{DD}}(\theta, r) = \frac{g_1 g_2 \mu_0 \mu_B^2}{4\pi h} \frac{1}{r} (3 \cos^2 \theta - 1)$$

**Equation 2.9**

Where  $g_1$  and  $g_2$  are the  $g$  values of the two spins,  $r$  is the distance between them, and  $\theta$  is the angle between the inter-spin vector and the applied magnetic field. Therefore, determination of the dipole-dipole coupling between the two flavosemiquinone of MSR provides a means of quantitating differences in inter-flavin distance brought about by ligand binding. The four pulse ELDOR experiment provides a means of determining such dipole-dipole couplings.

### 2.8.5.2 Sample preparation and equipment

The sample preparation, equipment and conditions for ELDOR are exactly the same as that for EPR. Some changes on the parameters are mentioned. Four pulse ELDOR spectra were recorded using a  $\pi/2$ -T- $\pi$ -T+ $\tau$ - $\pi$ - $\tau$ -acquire sequence with T = 200 ns and  $\tau$  = 1280 ns. The  $\pi$  pulse was 32 ns. The ‘fourth’ pulse was a  $\pi$  pulse applied at the pump frequency 300 ns after the beginning of the sequence. The position of this pulse within the sequence was incremented by 16 ns during the T+ $\tau$  period. All pulse experiments were recorded at 80K and at a repetition frequency of 200 Hz due to the long electron spin lattice relaxation time of the flavosemiquinone

radical. Inter-electron dipolar couplings were determined using Fourier transform of the baseline corrected four pulse ELDOR data to produce dipolar spectra [144].

Some materials, purification and kinetic research protocols in this chapter have applications in the further structure and kinetics studies on the FAD/NADPH binding domain.

## **CHAPTER THREE**

# **STRUCTURAL STUDIES ON THE WILD-TYPE FAD/NADPH BINDING DOMAIN OF MSR**

### 3.1. Introduction

Human MSR, one member of the diflavin reductase family, is known to comprise two structural domains: a N-terminal FMN-binding domain and a C-terminal FAD/NADPH-binding domain. The FAD/NADPH binding domain contains 536 amino acids, which range from residue 163 to residue 698. In previous work this domain has been fused genetically to a GST tag in plasmid pGEX-4-T1 and expressed in *E. coli*, to enable rapid purification of the domain [1]. This domain is an essential part of MSR and is involved in the binding of NADPH and the electron transfer from NADPH to cofactor FAD.

In this chapter, the expression of the FAD/NADPH-binding domain of MSR in *E. coli* BL21 cells is described. Further, the extraction by sonification and centrifugation methods and the purification by affinity chromatography and ion-exchange chromatography procedures are also described. The purified FAD/NADPH-binding domain was then studied using steady-state and pre-steady-state kinetic analysis, and crystallogenesis experiments were performed to enable structure determination of the domain. Diffraction quality crystals of the FAD/NADPH-binding domain were obtained and employed in X-ray diffraction experiments. Data obtained from the X-ray diffraction studies were used to build the crystal structure of the FAD/NADPH domain.

X-ray diffraction crystallography is a method used to determine the protein structure at atomic level, in which a beam of X-rays is applied to a protein crystal which subsequently diffracts into many specific directions. Based on the angle and intensity of these diffracted beams, a three dimensional picture of electron density within the crystal can be produced. From such an electron density map, the positions

of the atoms and chemical bonds of the protein are determined. Being the only method used for investigating protein structure at the atomic level, X-ray crystallography is still the main and most effective method for the study of protein structure. X-ray diffraction techniques originated in the 1950s and studies were focused on the measurement of a single protein structure [145]. In the 1960s and 1970s, this method was developed to illustrate the structure of protein complexes such as the enzyme-substrate complex [146], enzyme-inhibitor complexes [147], antibody-antigen complexes [148], and DNA-protein complexes [149]. The complexity of protein structures being determined by this method is increasing. Now, the structure of macromolecular assemblies such as microtubules and flagella are the targets of structure determination and there are additional new technological developments enabling research on dynamic crystal structures [150], conformational changes within the crystal as a function of time [151] and cryogenic X-ray crystal structure analysis [116].

X-ray crystallography has been employed in studies of the diflavin reductase family of enzymes. The crystal structures of rat CPR (free enzyme and in complex with ligands) have been solved [51], as well as the crystal structure of neuronal NOS reductase [52]. In this chapter, the crystal of the FAD/NADPH-binding domain of MSR was determined by the sitting drop vapour diffusion method [152]. The structure was solved using the DENZO [135] and AMoRE software [4] via molecular replacement. Structures for free FAD/NADPH-binding domain of MSR and the FAD/NADPH-binding domain combined with  $\text{NADP}^+$  are reported.

## **3.2. Results**

### **3.2.1. Expression of the FAD/NADPH binding domain of MSR**

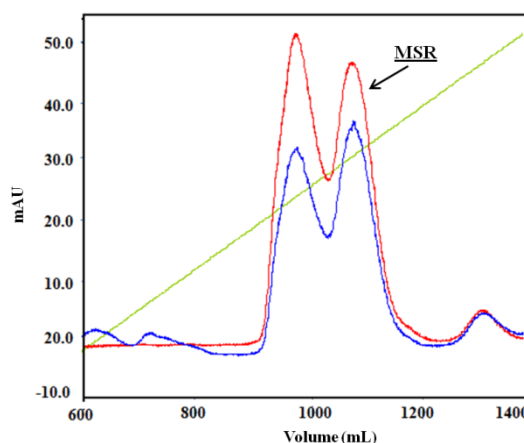


The FAD/NADPH-binding domain of MSR was available cloned in plasmid pGEXFADH (residues 163-698) [52]. This plasmid was transformed into *E. coli* BL21 (DE3) competent cells. The product of the transformation was plated onto the selective LB agar containing ampicillin added at a final concentration of 100 µg/ mL and incubated overnight at 37 °C. A single colony was picked from the plate and inoculated in 5 mL liquid LB medium with 100 µg/mL ampicillin. Following 12 hours incubation at 37 °C, 0.2 mL was used to inoculate 200 mL LB containing 100 mg/mL ampicillin and grown for a further 12 hours at 37 °C. 5 mL of the 200 mL LB product culture was transferred to 500 mL TB containing 100 µg/ mL ampicillin. This TB culture was grown at 28 °C for about 4 hours. When the optical density at 600 nm reached 1.0 OD unit, IPTG was added to the culture in a final concentration of 0.1 mM. This culture was then grown for a further 12 hours at 25 °C. Finally, the cells containing the expressed FAD/NADPH-binding domain of MSR were harvested using centrifugation at 5000 g for 25 minutes at 4 °C. Cells were then stored at -80 °C for further purification.

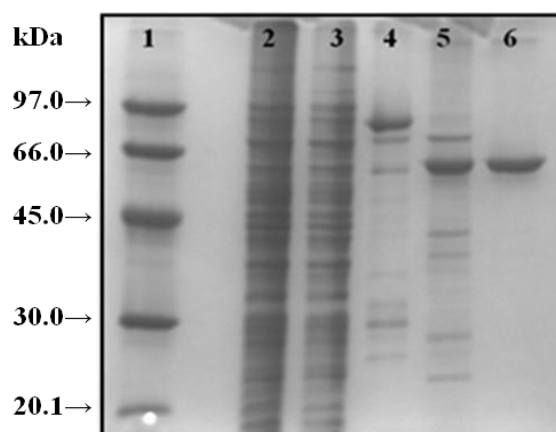
### **3.2.2. Purification of the FAD/NADPH-binding domain of MSR.**

The purification of the FAD/NADPH-binding domain was carried out in the same manner as described in chapter two, which exploits the use of GST affinity chromatography and Q-Sepharose chromatography. A typical elution profile from the Q-Sepharose chromatography is shown (**Figure 3.1**) and an analysis of fractions throughout the purification process was achieved using SDS-PAGE electrophoresis (**Figure 3.2**). Following purification, the enzyme sample was analysed using 12 % SDS PAGE electrophoresis which revealed a single band corresponding to a molecular mass of ~ 60 kDa. This was in agreement with the theoretically calculated mass of 60 kDa determined from the amino acid sequence of the FAD/NADPH-

binding domain. The purified protein was further analysed by UV/VIS spectroscopy and revealed two peaks at 382 nm and 454 nm, which are the two characteristic absorbance peaks for the FAD cofactor. These data confirmed the FAD/NADPH-binding domain of MSR had been purified successfully. The protein sample was then stored at -80 °C for crystallization experiments.



**Figure 3.1 Q-Sepharose anion-exchange chromatography of the FAD/NADPH-binding domain of MSR.** The plot shows the traces of signal intensity from the UV light detectors analysing the elution from a Q-Sepharose anion-exchange column after the application of FAD/NADPH binding domain. The Y-axis represents the intensity of the signal from each respective detector. The X-axis indicates the volume of buffer eluted from the column. The protein of the FAD/NADPH-binding domain of MSR is eluted from 1050 mL to 1250 mL. The blue line indicates the absorbance intensity at 280 nm; the red line represents the absorbance intensity of 454 nm; the green line indicates the anion gradient of the buffer.



**Figure 3.2: Analysis by SDS/PAGE electrophoresis of the purification procedure for the NADPH/FAD-domain of MSR.** Lane 1 is the low molecular weight marker (97.0, 66.0, 45.0, 30.0 and 20.1 kDa), lanes 2 and 3 are the whole cell protein samples from BL21 (DE2) cells which contain the FAD/NADPH-binding domain expression plasmids, lane 4 is the elution fraction from the GST glutathione affinity column, lane 5 is the mixture of the digestion of thrombin, lane 6 is the elution protein from the anion-exchange column.

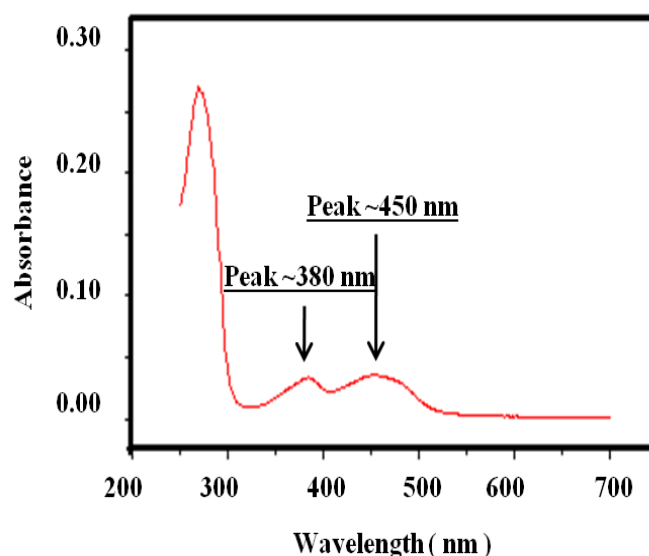
Typically, the FAD/NADP-binding domain was pure following GST affinity chromatography, but a final ‘polishing’ chromatography step was sometimes used using Q-Sepharose chromatography prior to attempts to grow protein crystals. In some cases, this chromatography step was successful in removing additional contaminants from the protein sample (**Figure 3.1**)

### **3.2.3. Kinetic studies on the FAD/NADPH binding domain of MSR**

Prior to performing crystallisation studies with the purified FAD/NADPH-binding domain it was considered important to characterise the protein both spectroscopically and kinetically to ensure that the protein was functionally active and that it was behaving in a manner expected. Consequently, a series of steady-state and stopped-flow studies with the isolated domain were performed to be sure that the protein was functionally active. These studies are described in the following sections.

#### **3.2.3.1. Spectral properties of the FAD/NADPH-binding domain of MSR**

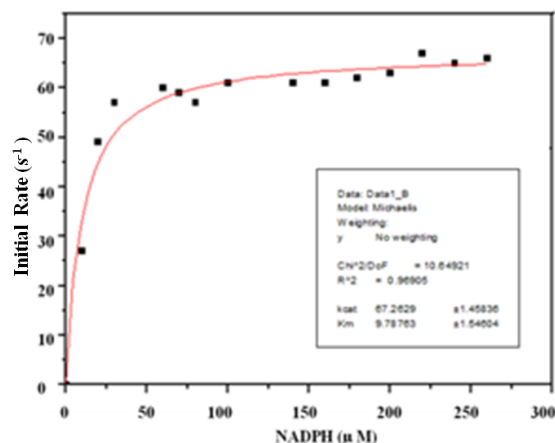
The absorbance spectrum of fully oxidized wild-type FAD/NADPH-binding domain of MSR was found to have two absorbance peaks at 382 nm and 454 nm (**Figure 3.3**). These two absorbance peaks are characteristic of flavoproteins and confirmed that FAD was indeed bound to the purified enzyme sample. The ratio of absorbance at 280 nm and 450 nm was  $\sim 6.75$  [153], similar to published values and indicates that the FAD cofactor was stoichiometrically assembled with the protein.



**Figure 3.3** The absorbance spectra of the oxidized FAD/NADPH-binding domain of MSR. The protein was contained in 50 mM Tris HCl buffer, pH 7.5, 20 % glycerol. Protein concentration was approximately 3.5  $\mu\text{M}$ .

### 3.2.3.2. Steady-state reduction properties of the FAD/NADPH binding domain of MSR

The FAD/NADPH-binding domain of MSR was evaluated using the steady-state experiment described in chapter two (**section 2.6.1**). The result of this experiment shows that the initial velocity was hyperbolically dependent on NADPH concentration. The Michaelis-Menten equation was used to calculate the  $k_{\text{cat}}$  ( $67.26 \pm 1.4 \text{ s}^{-1}$  for FeCN reduction at 25 °C) and the apparent  $K_m$  for NADPH ( $9.788 \pm 1.5 \mu\text{M}$ ) for the steady-state reduction of FeCN by NADPH.



**Figure 3.4** The apparent steady-state turnover rates of the FAD/NADPH-binding domain of MSR with variable NADPH concentration and using ferricyanide as artificial electron acceptor. Fitting to the Michaelis-Menten equation gave values for apparent  $k_{\text{cat}}$  of  $67.26 \pm 1.45 \text{ s}^{-1}$  and  $K_{\text{m}}$  of  $9.78 \pm 1.64 \text{ }\mu\text{M}$ .

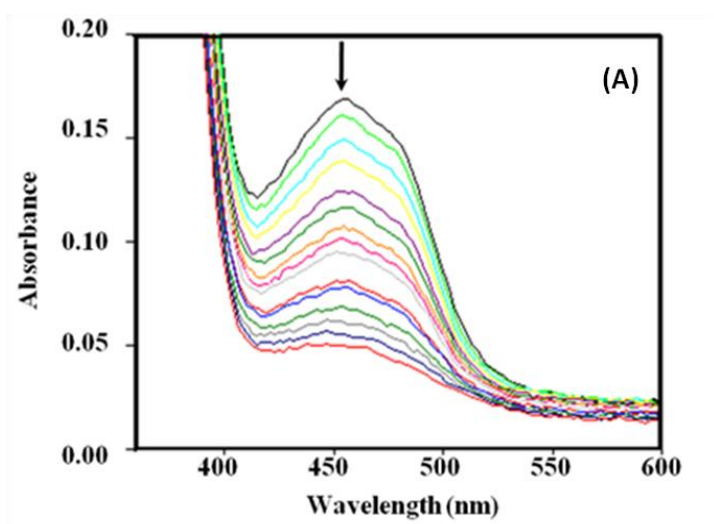
### 3.2.3.3 Pre-steady-state reduction properties of the FAD/NADPH binding domain

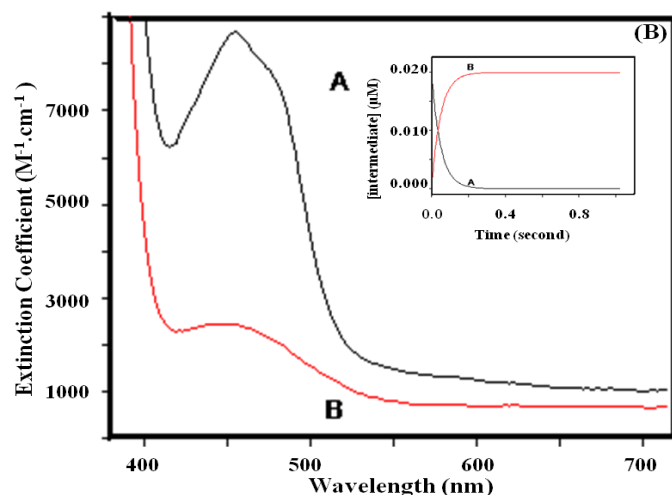
Two pre-steady-state stopped-flow kinetic studies on the FAD/NADPH-binding domain were carried out based on the methods described in chapter two (section 2.6). The first study involved a reduction of the FAD cofactor by mixing with NADPH and following flavin reduction using photodiode array spectroscopy. The second study was a similar analysis for flavin reduction, but with the reduction process being monitored at 450 nm. Given the second experiment was performed using a photomultiplier tube rather than a photodiode array detector, the data are less noisy and rate constants can be extracted from these data with a high degree of confidence.

#### 3.2.3.3.1. Photodiode array spectroscopy analysis of reduction of the FAD/NADPH binding domain by NADPH

Flavin reduction reactions were performed under a pseudo first order single turnover condition (i.e. where the NADPH concentration is 20-fold excess over

enzyme concentration). The FAD/NADPH-binding domain of MSR was mixed with NADPH under anaerobic conditions at 25 °C. The reduction of the FAD/NADPH binding domain of MSR was detected by the bleaching of the maximal flavin absorbance at 454 nm over 1 second. The spectral data (**Figure 3.5(A)**) were collected using a photodiode array detector and X-SCAN software (Applied Photophysics Ltd., Surrey, UK) and spectral deconvolution was performed by the singular-value decomposition (SVD) method using PROKIN software (Applied Photophysics Ltd.). A one-step reversible kinetic model with two species (A, oxidised enzyme; B, two electron-reduced reduced enzyme) adequately described the kinetic process (**Figure 3.5(B)**). The calculated rate constant from the fitting of the spectral data were as follows: for the reduction of the enzyme by NADPH ( $A \rightarrow B$ ;  $20.1 \pm 0.001\text{s}^{-1}$ ) and for the reverse reaction ( $B \rightarrow A$ ;  $0.0017 \pm 0.001\text{s}^{-1}$ ). The calculated concentration profiles of the enzyme species shown as a function of time are depicted in **Figure 3.5 (B)**.

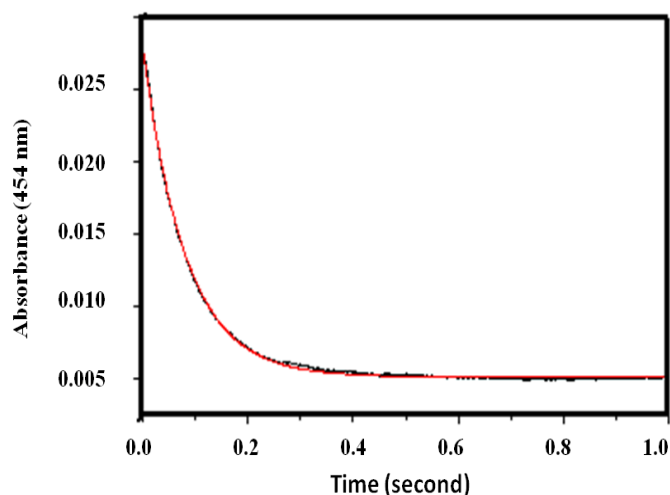




**Figure 3.5 Reaction of the FAD/NADPH-binding domain of MSR with NADPH followed by stopped-flow photodiode array spectroscopy.** (A) Time-dependent spectral changes (recorded over 1 second) shown after rapid mixing the FAD/NADPH-binding domain and NADPH. (B) Deconvoluted spectra of the intermediates generated by global SVD analysis of the reaction depicted with spectra in panel (A). The data in (A) were fitted globally to a reversible one step  $A \rightleftharpoons B$  model. The insert plot in (B) is the calculated concentration profile of intermediates in the reaction of the FAD/NADPH-binding domain with NADPH.

### 3.2.3.3.2 Single-wavelength analysis on FAD/NADPH binding domain of MSR

Under pseudo-first-order conditions, the rate constants for the reduction by NADPH to FAD/NADPH binding domain of MSR were monitored using single-wavelength absorbance spectroscopy at 454 nm. Following mixing of NADPH with the FAD/NADPH-binding domain of MSR, a monophasic absorbance change was observed which could be fitted using **Equation 2.5**. The resulting rate constant is similar to the rate constant obtained from the species  $A \rightarrow B$  in the SVD analysis, suggesting that the minimal kinetic model used in SVD analysis is adequate in describing this reaction.



**Figure 3.6 Single-wavelength absorption (454 nm) transient for the reaction of the FAD/NADPH-binding domain of MSR with NADPH.** The condition used was: 50 mM potassium phosphate buffer (pH 7.0) at 25 °C, [FAD/NADPH-binding domain] = 10  $\mu\text{M}$ , and [NADPH] = 1000  $\mu\text{M}$ . A monophasic absorption trace for the reduction of FAD/NADPH binding domain. The reaction is best described by a monophasic absorption change at 454 nm, consistent with the simple reversible model used in SVD analysis of diode array spectral data.

The kinetic data collected for the isolated FAD/NADPH-binding domain of MSR is similar with that published previously by Wolthers *et al* [60] (**Table 3.1**). This provides confidence that the samples purified in this thesis are suitable for use in crystallisation trials with the aim of determining the molecular structure of the domain. These studies are described in the following sections.

	Results from this work	Published results by Wolthers.[60]
$k_{\text{cat}}$	$67.3 \pm 1.4 \text{ s}^{-1}$	Not determined
$K_{\text{m}}$	$9.8 \pm 1.5 \mu\text{M}$	Not determined
$k_{+1}$	$20.1 \pm 0.001 \text{ s}^{-1}$	$20.1 \pm 0.01 \text{ s}^{-1}$
$k_{-1}$	$0.017 \pm 0.001 \text{ s}^{-1}$	$0.018 \pm 0.001 \text{ s}^{-1}$

**Table 3.1. Comparison of the kinetic data of the FAD/NADPH binding domain of MSR**

### 3.2.4. Crystallization, X-ray diffraction, structure elucidation and molecular modelling



A Mosquito robot was used to carry out a crystal growth experiments with the FAD/NADPH-binding domain of MSR using the sitting drop method and QIAGEN screening kits. The enzyme samples were desalted and centrifuged prior to crystallization trials. The desalting process was accomplished by dialysing the protein sample against 5 litres 50 mM Tris/HCl buffer pH 7.2 overnight at 4 °C. After dialysis the protein sample was centrifuged to remove particulates. Generally, one drop of enzyme sample (1 µL) was mixed with 1 µL mother liquor and incubated with 98 µL mother liquor in a reservoir at 4° C and 19 °C, respectively. Crystals were allowed to form for about 4 days under one of four conditions: 0.1 M Tris/HCl, pH 7.5, 0.2 M KBr or PEG4000; 0.2 M KBr 8 % PEG 20 K+8 % PEG 550, MME pH 8.5 at 4 °C; 0.2 M sodium citrate with 25 % PEG 1500 pH 5.0 or 0.2 M ammonium citrate 25 % PEG 2K MME pH 5.0 at 19 °C.



**Figure 3.8 Crystals of the FAD/NADPH binding domain of MSR.** The conditions used to produce this crystal are: one drop of enzyme sample (1 µL, 10 mg/mL) was mixed with 1 µL mother liquor (0.1 M Tris/HCl, pH 7.5, 0.2 M KBr), and incubated with 98 µL the same mother liquor in a reservoir at 19 °C. Crystals formed after about 4 days.

Crystals of the FAD/NADPH binding domain of MSR were grown in mother liquor (0.2 M sodium citrate pH 5.0 containing 25 % PEG 1500) at 19 °C for 4 days. Some crystals were soaked in mother liquor containing saturating levels of NADP<sup>+</sup>. The soaked crystals were immersed in cryoprotectant (50:50 Paratone: mineral oil)

and the excess mother liquor was removed. Crystals were flash frozen in liquid nitrogen. Some of the crystals were bathed in saturated NADP<sup>+</sup> before cryo-protection and transfer to the synchrotron at the European Synchrotron Radiation Facility Grenoble. X-ray diffraction data collection and structure calculations were performed mainly by Dr Helen Toogood and Professor David Leys (University of Manchester). The statistics presented below are from these studies and are presented to indicate the overall quality of the structures for the NADP<sup>+</sup>-bound protein and the protein in the absence of bound ligand. Since this aspect of the work was performed by Dr Toogood and Professor Leys, detailed discussion of these data is not presented herein. A more detailed discussion of the diffraction data can be found in Wolthers et al [3]. X-ray diffraction data were collected to 1.9 Å resolution and the related data are shown in **Table 3.2**. The structure of the FAD/NADPH-binding domain of MSR was solved by the molecular replacement method using a truncated structure of CPR as the search model (PDB code 1 AMO). CPR is the most widely researched member of the diflavin reductase family and was used as the initial model.

	NADP <sup>+</sup> -free structure	NADP <sup>+</sup> -bound structure
	<b>Data collection</b>	
<b>Resolution limits(Å)</b>	20-1.9 (1.95-1.90)	20-1.9 (1.95-1.90)
<b>Space group</b>	P2 <sub>1</sub>	P2 <sub>1</sub>
<b>Unit cell(Å)</b>	a=52.6 b=67.3, c=78.8	a=51.8 b=67.2 c=78.6
<b>Total reflections</b>	593861	644500
<b>Unique reflections</b>	39892	39791
<b>Redundancy</b>	3.5	3.6
<b>Completeness (%)</b>	100.0 (100.0)	100.0 (100.0)
<b>I/σI</b>	25.3 (3.1)	23.6 (3.3)
<b>R<sub>merge</sub> (%)</b>	4.0 (26.1)	5.2 (30.4)
<b>Solvent Content (%)</b>	45	44
	<b>Refinement</b>	
<b>No. of residues</b>	448	447
<b>No. of water molecules</b>	498	359
<b>R<sub>fac</sub>/R<sub>free</sub> (%)</b>	18.4/23.2 (22.9/35.8)	17.6/21.2 (19.7/26.5)

<b>RMSD bond lengths(Å)</b>	0.016	0.014
<b>RMSD bond angles (°)</b>	1.527	1.493
<b>Average B factor(Å<sup>2</sup>)</b>	31.2	29.3
	<b>Ramachandran plot</b>	
<b>Most favoured region(%)</b>	98.9	99.1
<b>Additionally allowed regions</b>	0.9	0.7
<b>Outliers</b>	0.2(Gly <sup>544</sup> )	0.2(Gly <sup>544</sup> )

**Table 3.2 The final crystallographic and refinement values for the FAD/NADPH binding domain of human MSR with and without NADP<sup>+</sup> bound.** Data were analysed by Dr Helen Toogood and Prof David Leys and a full description is given in Wolthers et al [3].

In the following sections a description of the overall structure of the FAD/NADPH-binding domain is given and the complex formed with NADP<sup>+</sup>. These structures form an important part of the hypothesis tested in chapter four and the basis of solution and mutagenesis work described in the same chapter.

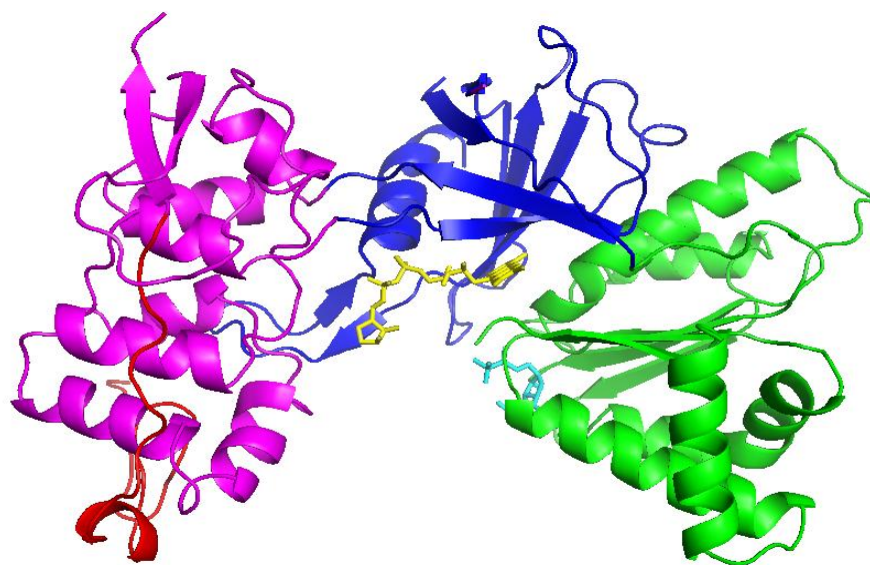
### **3.2.5. Description and analysis of the structural model of the FAD/NADPH-binding domain of MSR**

#### **3.2.5.1. Overall domain structure of the FAD/NADPH-binding domain of MSR**

The whole structure of the FAD/NADPH binding domain consists of 448 visible residues extending from residue Ser<sup>217</sup> to Ser<sup>698</sup>. The first 54 residues of this domain are disordered suggesting a high degree of flexibility in this region of the protein. There are also additional flexible regions, notably Leu<sup>258</sup>-Asp<sup>271</sup>, Gln<sup>502</sup>-Ala<sup>515</sup>, and Val<sup>615</sup>-Ala<sup>620</sup>, as indicated by the poor electron density observed for these residues. The flexibility of the N-terminal region is consistent with the idea that in full length MSR the FMN-binding domain “toggles” between MS and the FAD/NADPH binding domain of MSR during the electron transfer process.

The domain structure of the FAD/NADP-binding domain comprises from the N- to C- terminus a hinge region, a connecting domain region, an FAD-binding region and NADPH-region domain (**Figure 3.9**). The hinge and the connecting

region are mainly made up of  $\alpha$ -helices. The FAD-binding region consists of six  $\beta$ -strands to form a flattened anti parallel  $\beta$ -barrel and the NADPH binding region has five-stranded parallel  $\beta$ -sheets sandwiched between six  $\alpha$ -helices to form an  $\alpha\beta\alpha$  structural motif. A more detailed analysis of the structural properties within the individual domains/regions is given below.



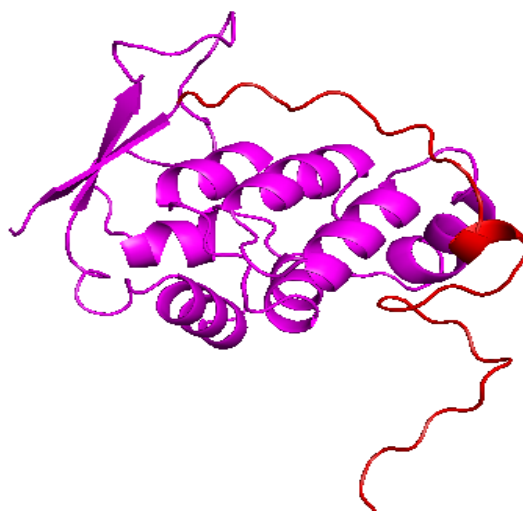
**Figure 3.9 A cartoon representation of the human MSR FAD/NADPH-binding domain.** The extended hinge region is in red, and the connecting domain, FAD-domain, and NADPH-binding domain are in pink, blue, and green, respectively. The FAD (yellow) and the NADP<sup>+</sup> (cyan) are shown in stick format. The figure was produced using PyMOL software: (<http://pymol.sourceforge.net/>).

### 3.2.5.2. The hinge region and connecting domain

The hinge region is positioned between the FMN-domain and the connecting region in full length MSR and consists of 82 amino acids, of which only 31 residues are visible (Ser<sup>217</sup> to Pro<sup>247</sup>) in the X-ray electron density map. Because of their interaction with a symmetry-related molecule, the initial seven visible residues (Ser<sup>217</sup> to Asp<sup>223</sup>) probably adopt a non physiological structure. This is likely due to

truncation of the protein (i.e. in making the isolated FAD/NADP-binding domain) and/or crystal packing. The region from Ser<sup>227</sup> to Pro<sup>247</sup> forms a random coil at the surface on the axis of three short helices. The analysis of the interface between the hinge region and other parts of the connecting domains shows that 41 hydrogen bonds and salt bridges have formed. The other part of this region is thought to be folded behind the connecting domain to position the FMN-domain at the binding interface of the FAD-binding domain and the NADPH binding domain.

The connecting domain mainly contains  $\alpha$ -helices and is structurally integrated with the FAD-domain region with three  $\beta$ -strands of the FAD-domain mixed into the connecting domain. The domain is globular and reasonably compact (**Figure 3.10**).

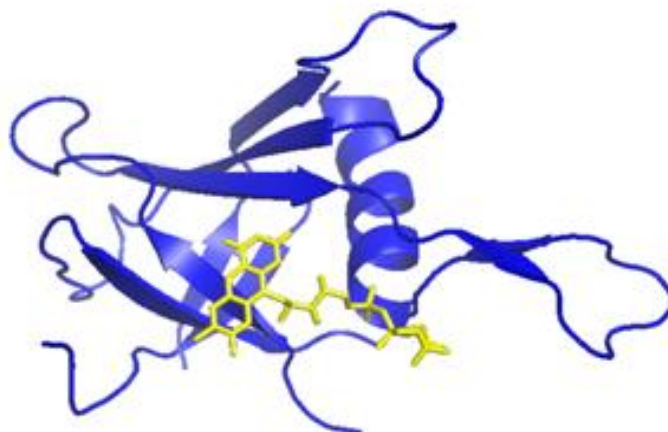


**Figure 3.10** A cartoon representation of the connecting region of the FAD/NADPH-binding domain of MSR. The red part indicates the extended hinge region visible in X-ray studies. The purple region represents the connecting domain. The figure was created using PyMOL software (<http://pymol.sourceforge.net/>).

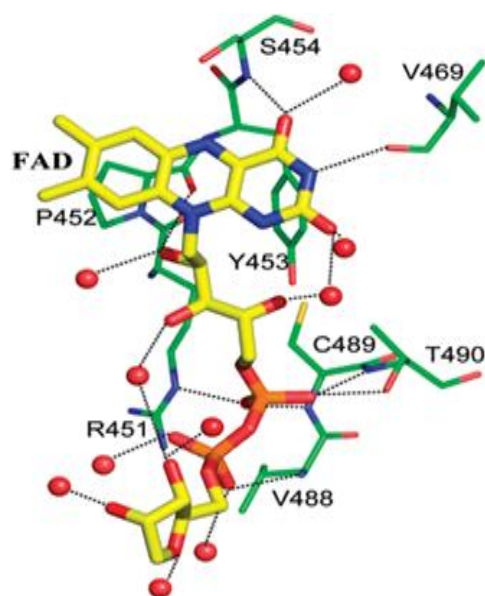
### 3.2.5.3. The FAD binding region and FAD binding site

The FAD-binding region consists of six  $\beta$ -strands which form a flattened anti parallel  $\beta$ -barrel (**Figure 3.11**). This region is bound to the FAD cofactor which adopts an extended conformation. The FAD cofactor is made up of two parts: the

riboflavin moiety and an ADP molecule. The isoalloxazine ring in the riboflavin is located at the interface between the FAD-binding domain and the NADPH-binding domain and it is stabilized via hydrophobic interaction and several hydrogen bonds. The O2 atom of the isoalloxazine ring forms hydrogen bonds with the main chain atom Ser<sup>454</sup> (amide nitrogen) and the water molecule. The N3 atom in the isoalloxazine ring interacts with Val<sup>469</sup> (carbonyl oxygen) through hydrogen bonds, and the N5 and O4 atoms in the isoalloxazine ring are in contact with single water molecules via hydrogen bonds. The pyrophosphate group of ADP in the FAD cofactor interacts with water molecules, the amide nitrogen and the hydroxyl group of Thr<sup>490</sup>, the side chains of Arg<sup>451</sup> and the peptide backbone of the Cys<sup>489</sup> and Val<sup>488</sup> (**Figure 3.12**). The electron density of the ribose group in the ADP part shows that it has more than one position in the structure and the oxidization of nearby Cys<sup>421</sup> to cysteinic acid is related to the mobility of the ribose group.



**Figure 3.11** A cartoon representation of the FAD-binding region of the FAD/NADPH-binding domain of MSR. The yellow stick represents the FAD. The figure was produced using PyMOL software.



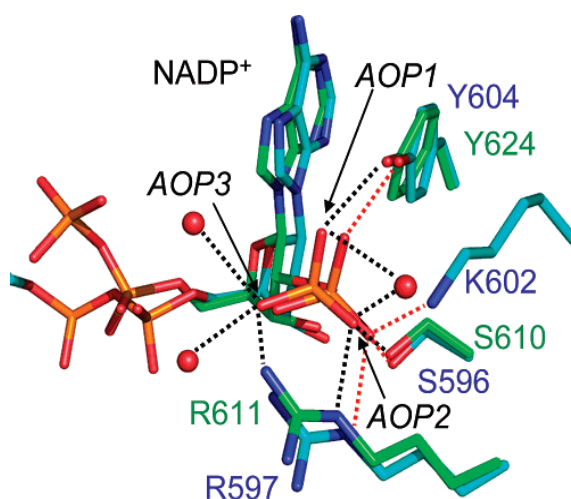
**Figure 3.12 Structure of the FAD-binding domain in MSR in the region of the FAD cofactor.** FAD and residues are shown as atom-coloured sticks and lines, respectively. Water molecules are denoted by red spheres. Interactions are shown as dotted lines. The image was created using PyMOL software (<http://pymol.sourceforge.net/>).

#### 3.2.5.4. The NADPH-binding domain and NADPH binding sites

The NADPH-binding domain contains six  $\alpha$ -helices sandwiched with five stranded parallel  $\beta$ -sheet to form an  $\alpha\beta\alpha$  structural motif. NADPH is bound at one end of the  $\beta$ -sheet (**Figure 3.13**). The NADPH molecule comprises of a ribitylnicotinamide ring and a 2'-phosphoryl-AMP moiety. However, the solvent-exposed ribitylnicotinamide ring is disordered and only the 2'-phosphoryl-AMP group can be observed. The oxygen atom (AOP2) of the 2'-phosphate forms several hydrogen bonds with a water molecule and the hydroxyl group of Ser<sup>610</sup>, Arg<sup>611</sup> and Tyr<sup>624</sup>. In addition, three well ordered water molecules form hydrogen bonds with the 2'-phosphate. This network of residues stabilizes the 2'-phosphate of the nicotinamide and presumably accounts for the substrate specificity of MSR in its preference for NADPH over NADH (**Figure 3.14**).



**Figure 3.13** A cartoon representation of the NADPH-binding region of the FAD/NADPH binding domain of MSR. The coenzyme NADP<sup>+</sup> is shown in cyan. Image created using PyMOL software (<http://pymol.sourceforge.net/>).



**Figure 3.14** Superposition of the MSR and rat CPR 2'-phosphate binding sites. The colour scheme is: oxygen, red; nitrogen, blue; carbon of CPR, cyan; carbon of MSR, green; phosphorus, orange. Residue numbers for MSR are written in green, and those are named in italics. Hydrogen bond contacts in MSR and CPR are denoted by black and red dashed lines, respectively, and water molecules are red spheres. The structure of CPR is from the PDB file: 1JA1.

The structure of the FAD/NADPH-binding domain provides some useful information from which to design new kinetic and mutagenesis studies of the enzyme.

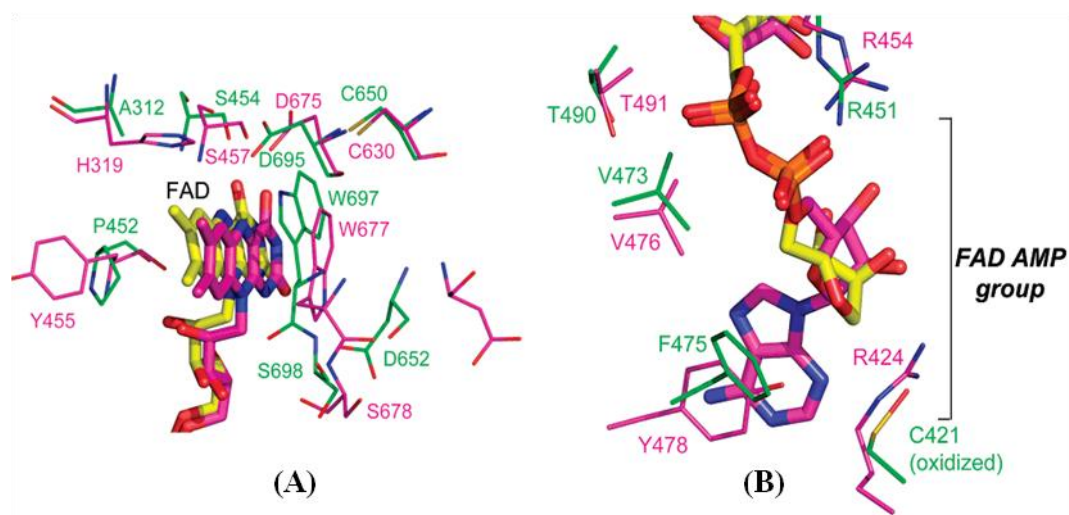


### 3.3. Discussion

In mammalian systems, MSR belongs to the diflavin reductase family which also include CPR, NOS and NR1. When comparing the structure of these four reductases, some similarities and differences in the structure were found. The overall inferred structure of full length MSR, from N- terminus to C-terminus, consists of the FMN-binding domain, the connecting domain and the FAD domain and the NADPH-binding domain. The structures of NOS and CPR are similar and are constructed in the same modular fashion as MSR. However, the analysis presented in this chapter shows that the connecting domain of MSR, which contains 82 residues, is much longer than the connecting domain of CPR (14 residues) and NOS (24 residues). It is considered that the long connecting domain of MSR facilitates the electron transfer between the cofactor FAD of MSR to the cobalamin cofactor of MS through a large-scale movement of the FMN-binding domain of MSR.

Comparison of the FAD-binding sites of the diflavin family shows that the FAD-binding domain of CPR binds the FAD in an extended conformation. The isoalloxazine ring is positioned at the boundary of the FAD and NADPH binding domains. This structure is similar to that of MSR where the remainder of the FAD molecule lies at the interface of the FAD-binding domain and the connecting domain. The similarity of these two structures indicates that there are conserved residues that form a catalytic triad for hydride transfer in MSR (Cys<sup>650</sup>, Asp<sup>695</sup> and Ser<sup>454</sup>) and in CPR (Cys<sup>630</sup>, Asp<sup>675</sup> and Ser<sup>454</sup>). This similarity suggests that MSR and CPR have the same hydride transfer mechanism. In addition some differences exist in these two structures. One difference is the ribose group of FAD in MSR which is near the partially oxidized Cys<sup>421</sup> and which can adopt difference positions.

Consequently, the orientation of this sugar in MSR is quite different from that of CPR. This dynamic character of the ribose in MSR suggests an increase in mobility of the adenine ring. Another difference is on the structure of Trp<sup>697</sup>. In MSR, Trp<sup>677</sup> is located on the *re*-side face of the FAD ring and Tyr<sup>456</sup> at the *si*-side. The side chain of Tyr<sup>491</sup> and Arg<sup>454</sup> are responsible for the stabilization of the pyrophosphate group. The polypeptide from residues Cys<sup>472</sup> to Tyr<sup>478</sup> is almost parallel to the ribityl-pyrophosphate chain, with the adenosine moiety exposed to the solvent and the phenolic ring of Tyr<sup>478</sup> stacking on the other side of the adenine ring. But in CPR, the corresponding Trp<sup>677</sup> is oriented about 90 ° with only the benzyl moiety stacking against the isoalloxazine ring (**Figure 3.15**). With respect to rat NOS, another member of this family, this protein contains 435 residues in the FAD binding domain with the first 10 amino acids disordered due to flexibility. The cofactor FAD binds the enzyme in an extended conformation and lies between the interface between the FAD binding domain and NADPH binding domains. The pyrophosphate group of FAD hydrogen bonds with Arg<sup>1173</sup> and the isoalloxazine ring of FAD is stabilized by several hydrogen bonds with the pyrimidine side chains and water molecules. The O2 atom of the isoalloxazine ring forms hydrogen bonds between Ala<sup>1193</sup> and Thr<sup>1191</sup>; the N3 atoms form hydrogen bonds with Thr<sup>1191</sup>; the N1 atom combine with the carbonyl oxygen of Ala<sup>1193</sup> and Tyr<sup>1175</sup> attach to the *si*-face of the FAD ring with Phe<sup>1395</sup> on the *re*-face.



**Figure 3.15 Superposition of the MSR and rat CPR FAD binding sites.** (A). Superposition of FAD isoalloxazine-binding sites. FAD and residues are shown as atom-coloured sticks and lines, respectively. MSR and CPR carbons are shown as green and magenta atoms, respectively. (B). Superposition of AMP-binding sites FAD and residues are shown as atom-coloured sticks and lines, respectively. MSR and CPR carbons are shown as green and magenta atoms, respectively. The structure of CPR is from PDB entry: 1AMO

Comparison of the NADPH binding domain and NADPH binding site of this diflavin reductase family shows that the nNOS NADPH binding domain consists of an  $\alpha\beta\alpha$  structural motif with a five-stranded sheet sandwiched between  $\alpha$ -helices. The nicotinamide moiety of the coenzyme NADPH is bound at the surface of the molecule in a bent conformation with the nicotinamide and adenine ring pointing to the same side. A conserved arginine is an important structural feature in the binding of NADPH of nNOS. A salt bridge is formed between the pyrophosphate group of NADPH with Arginine<sup>1010</sup>; Arg<sup>1314</sup> interacts with the 2'-phosphate of AMP moiety and Arg<sup>1284</sup> with phosphate. This motif occurs in the CPR structure, but not in the MSR structure.

These structural variations in the family also affect the binding ability of NADPH. Experimental results have shown that the binding energy of NADPH for MSR is 7 KJ/mol which is slightly greater than that of FNR [3, 168]. Because most of the binding energy of NADPH can be attributed to the 2'-5'-ADP moiety of

NADPH, the origin of the binding affinity for 2'5'-ADP is now the focus of further research (see chapter four). Experimental data suggests that the 2'5'-ADP has a similar binding affinity to CPR and NOS, but it is lower with MSR [3]. The reason for the low affinity for MSR could be related to its lower demand on physiological functions (MSR is only needed to reactivate human MS on an occasional basis), and it may be related to its structure. The crystal structure model of the FAD/NADPH-binding domain shows that the binding pocket around the 2' phosphate group of NADPH carries a similar positive charge in both MSR and CPR, but the binding cavity around the 5'-pyrophosphate group is more negatively charged in MSR compared to CPR. A residue, Asp<sup>652</sup>, located between the 5'-pyrophosphate group of NADPH and the isoalloxazine ring of FAD and exposed to the solvent is assumed to be a determinant on the binding ability of NADPH. The properties of mutant MSR proteins altered at residues of Asp<sup>652</sup> and Asp<sup>697</sup> are described in chapter 4 to probe in detail the roles of these residues in NADPH binding and catalysis.

Further structural variations across family members are likely also to change the mechanism of hydride transfer within members of the diflavin reductase family. In nNOS, the possible hydride transfer mechanism involves the phenyl ring of the Phe<sup>1395</sup>, which covers the re-face of the isoalloxazine ring of FAD and this residue swings away from the FAD on binding the nicotinamide moiety. The change in the monodihedral angle at the pyrophosphate linkage results in a bent conformation for the bound NADPH so that the nicotinamide ring can replace the position of the phenyl side chain of the Phe<sup>1395</sup> and then direct the hydride transfer from NADPH to FAD. In CPR, Trp<sup>677</sup> plays the same role as the Phe<sup>1395</sup> in the nNOS. Similarly, in MSR, Trp<sup>697</sup> is the corresponding residue. The crystal structure of the FAD/NADPH binding domain of MSR has shown that the orientation for the aromatic stacking

residue in MSR and CPR is different. This apparent structural difference for Trp<sup>697</sup> in MSR and Trp<sup>677</sup> in CPR prompts further questions the roles of these residues in hydride transfer. Mutagenesis of this residue in MSR is therefore a route to explore the role of this residue in catalysis, and these studies are described in later chapters.

**CHAPTER FOUR**  
**COMPARISON OF WILD TYPE AND VARIANTS OF**  
**MSR PROTEINS**

## 4.1 Introduction

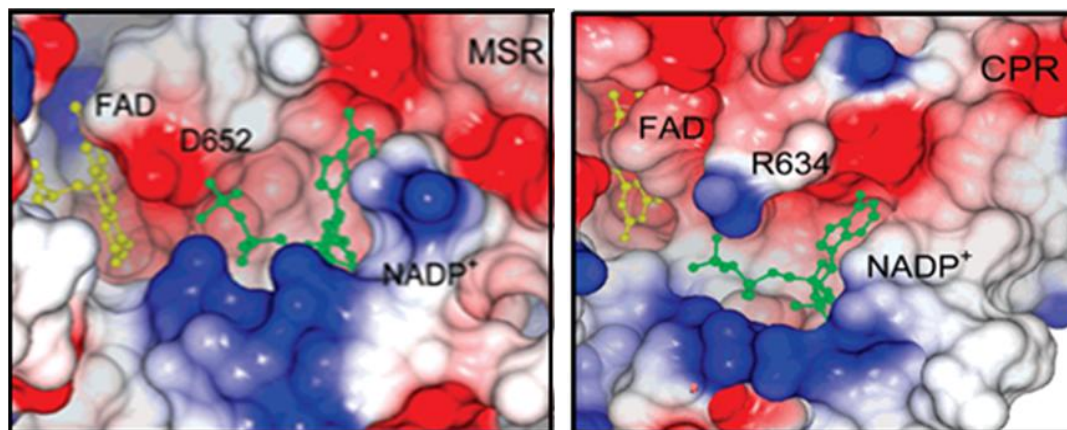
MSR is a 78 kDa flavoprotein that is a member of the diflavin reductase family which includes MSR, NOS, CPR and NR1. Alignment of the primary sequences of these four members shows that MSR lacks some of the conserved sequences which are related to the binding of NADPH, however, in FNR, several conserved residues such as Ser<sup>234</sup>, Arg<sup>235</sup> and Tyr<sup>246</sup> form a network which makes electrostatic interaction with NADPH [75]. Some of these conserved residues have been confirmed as the determinants of coenzyme specificity by differentiating between NADPH and NADH. A further example, from work on the crystal structure of CPR, concerns two conserved residues, Ser<sup>596</sup> and Tyr<sup>604</sup>, which form a consensus sequence for the binding of the 2' phosphate group of NADPH [90]. MSR shows some structural variation in this consensus sequence motif for the binding of 2'-phosphate, with only three of the four binding determinants, Ser<sup>610</sup>, Arg<sup>611</sup> and Tyr<sup>624</sup> being present and with a six amino acid insert between the Ser<sup>610</sup>/Arg<sup>611</sup>, Tyr<sup>624</sup> to extend the distance between them. In the crystal structure of MSR, the six amino acids are disordered and possibly act as a mobile loop. In addition, there are two other important residues in MSR that are involved with the binding of NADPH, namely Asp<sup>652</sup> and Trp<sup>697</sup>.

The solvent-exposed residue Asp<sup>652</sup> is located between the 5'-pyrophosphate and the isoalloxazine ring of FAD. Comparison of the electrostatic surface of the FAD/NADPH-binding domain of MSR with the corresponding domain of CPR (**Figure 4.1**), shows that both are positively charged around the 2' phosphate group of the FAD isoalloxazine ring; but it is more negatively charged around the 5'-pyrophosphate group in the MSR structure than in CPR. Specifically, Asp<sup>652</sup> also has a large B factor value for its carboxylate side chain and is orientated in a

different direction compared to the corresponding residue Asp<sup>632</sup> in CPR. Research on the mutant W677G of CPR identified a steric clash between the ribose of NADP<sup>+</sup> and the carboxylate group of Asp<sup>632</sup> when the nicotinamide group stacks on the FAD isoalloxazine ring [90]. This result could suggest that the movement of the residue Asp<sup>652</sup> in MSR is involved in the hydride transfer reaction. Although Asp<sup>652</sup> is 4 to 5 Å away from the pyrophosphate, the electrostatic repulsion and/or steric interference may be responsible for the rotation along the dihedral angles of the pyrophosphate bonds as NADPH binds in a productive mode for catalysis. The Asp<sup>652</sup> residue possibly forces the equilibrium distribution of the conformation states towards states that are non-productive binding modes. Another residue, Trp<sup>697</sup>, is related to the destabilization of NADP<sup>+</sup> binding. On the basis of structural analogies with the CPR protein, the indole ring of Trp<sup>697</sup> is positioned over the *re* face of the FAD isoalloxazine ring. When NADPH binds, its nicotinamide ring must stack against the *re* face of the isoalloxazine to lead the C4 atom of NADPH close to the N5 atom of FAD for hydride transfer from NADPH to FAD. To avoid steric clashes with the nicotinamide ring, Trp<sup>697</sup> must flip away from the FAD. The movement of the Trp<sup>697</sup> has been confirmed in stopped-flow fluorescence studies on MSR with a rate constant similar to the rate determined for hydride transfer in MSR [60]. However, the overlap of the Trp<sup>697</sup> with the corresponding residue of CPR indicates a different direction for this tryptophan. The corresponding tryptophan in CPR has an approximately 90° rotation with only the benzyl moiety of it stacking against the isoalloxazine ring. So whilst the additional  $\pi$ - $\pi$  interaction between the isoalloxazine ring and Trp<sup>697</sup> increases the thermodynamic stability of this conformation, it weakens the binding of NADPH. In addition, the crystal structure of the complex of NADP<sup>+</sup> with the FAD/NADPH domain of MSR showed that the binding of NADPH



does not change the orientation of the Trp<sup>697</sup> residue. This result supports the hypothesis. In order to confirm the importance of Asp<sup>652</sup> and Trp<sup>697</sup> on the coenzyme binding affinity, mutagenesis experiments were designed and carried out.




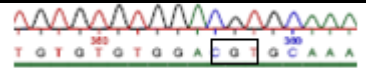
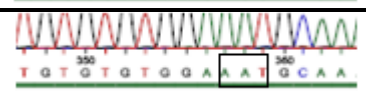
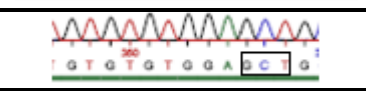

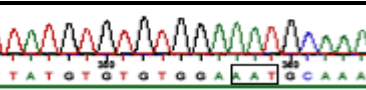
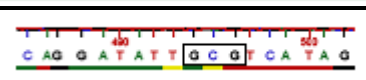
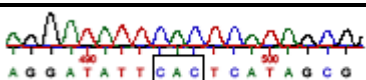
**Figure 4.1** The electrostatic surfaces of the NADP<sup>+</sup> binding pockets in MSR and CPR. NADP<sup>+</sup> and FAD are shown as green and yellow balls and sticks. The Asp<sup>652</sup> of MSR is labelled. The electrostatic surface is shown as blue for a positive potential and red for a negative potential. The CPR is from the PDB entry: 1AMO.

In this chapter, the design and outcome of the site-directed mutagenesis experiments which were undertaken on the two positions Asp<sup>652</sup> and Trp<sup>697</sup> are described. The Asp<sup>652</sup> residue was replaced with asparagine, alanine and arginine. The product mutants D652A, D652R and D652N were cloned and expressed in *E. coli* BL21, a protease deficient host strain, in the FAD/NADPH binding domain of MSR and the full-length MSR. The Trp<sup>697</sup> residue was changed to alanine and histidine. The product mutants W697A and W697H were cloned and expressed in *E. coli* BL21 in full length MSR. The altered proteins were purified by affinity chromatography, followed by anion exchange and gel filtration chromatography. The kinetic properties of these mutant proteins were investigated in steady state turnover, steady state inhibition studies, stopped-flow pre-steady state kinetic and redox potential studies. The study results were compared with data obtained with the wild type MSR protein.

## 4.2. Results

### 4.2.1. Site-directed mutagenesis of the FAD/NADPH binding domain of MSR

All the plasmids of the mutants were confirmed by sequencing and the sequence results are shown in **Table 4.1**. These plasmids were transformed into strain BL21 of *E. coli* and single clones picked from LB plates containing ampicillin (100µg/mL) and grown in TB modicum at 28 °C, 200 rpm/min. After about 4 to 5 hours, when the OD<sub>600nm</sub> of the culture reached approximately 1.0, IPTG was added to give a final concentration of 1 mM. The culture was incubated at 25 °C, 200 rpm/min overnight to allow protein expression. The overnight cells were harvested by centrifugation at 4 °C. Finally, the cells were stored at -80 °C until they were required for purification.

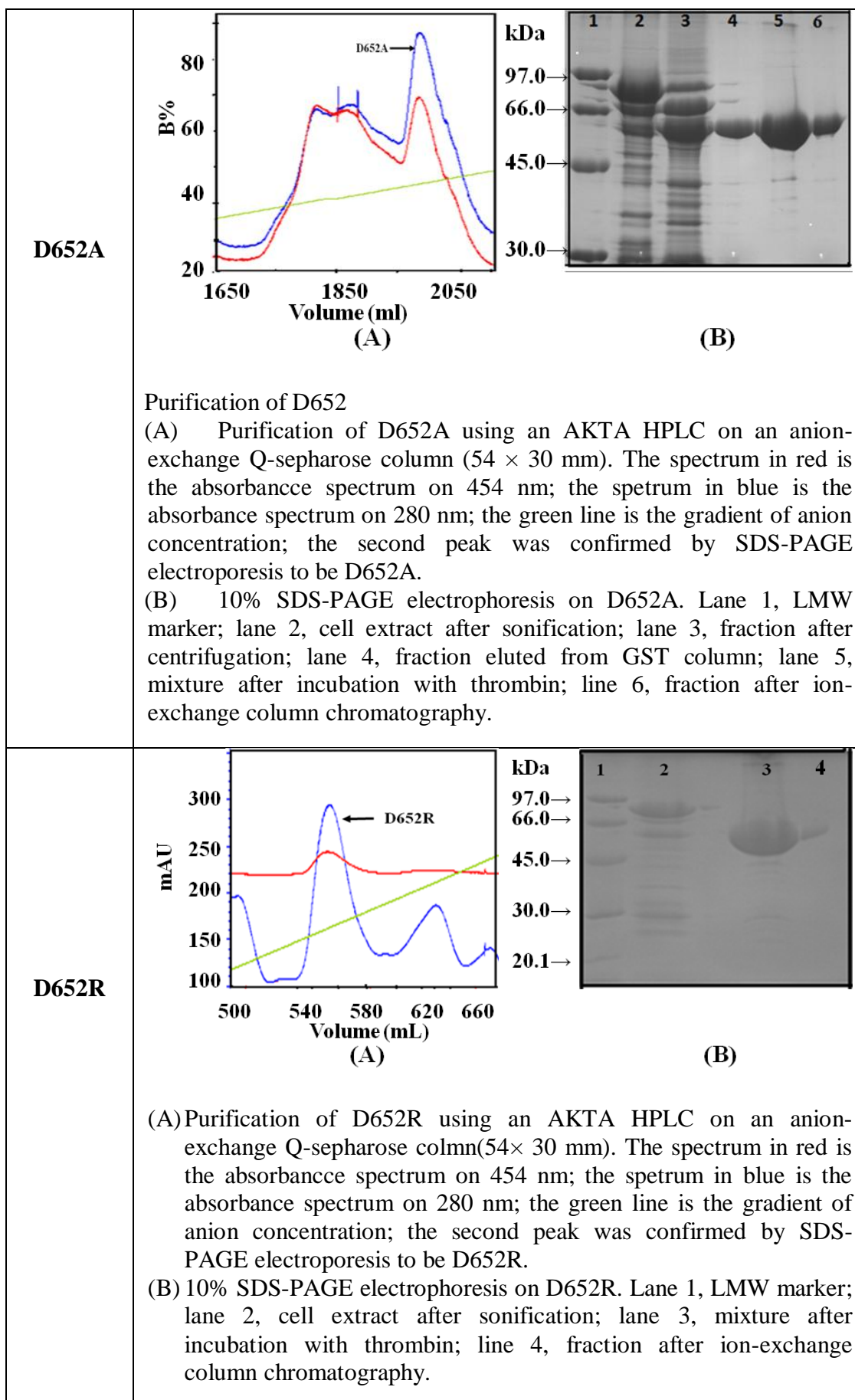
Name of mutant	Mutant site	sequence
D652A	gat→gct	
D652R	gat→cgt	
D652N	gat→aat	
D652A full-length	gat→gct	
D652R full-length	gat→cgt	
D652N full-length	gat→aat	
W697A full-length	tgg→gcg	
W697H full-length	tgg→cac	

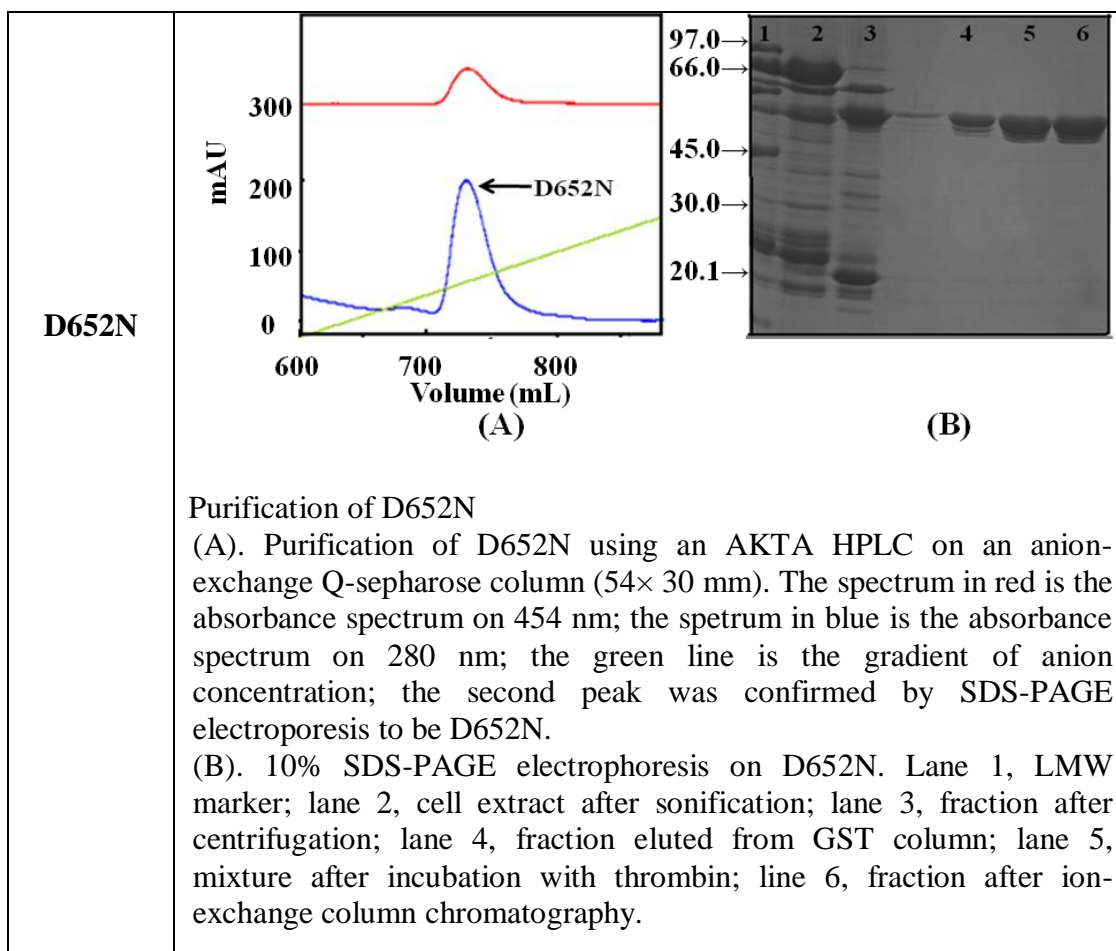
**Table 4.1** Sequence results of plasmids of variants of MSR.

## **4.2.2. Purification of the mutant proteins**

### **4.2.2.1. The purification of the mutants D652A, D652R and D652N of the FAD/NADPH-binding domain of MSR**

Three mutants of the FAD/NADPH binding domain of MSR, D652A, D652R and D652N were purified by the method described in Chapter two (**section 2.4.3**). After purification by affinity chromatography and anion chromatography, the proteins of interest were checked by 10-12% SDS PAGE electrophoresis. All of them exhibited only one major band on SDS-PAGE electrophoresis and were therefore seemed pure. The first purification step employed was an anion exchange Q-Sepharose high-performance column (145 x 25 mm), which was equilibrated in 50 mM NaCl in 50 mM Tris-HCl buffer, pH 7.5 containing 50 mM NaCl. After loading the sample and washing to remove weakly bound proteins, the target protein was eluted using a linear gradient (50 mM to 500 mM NaCl) at a flow rate of 4 mL/min. The eluted fractions of the gradient at 40% to 60%, containing the target protein, were identified by the absorbance spectrum at 454 nm and 280 nm and the protein identity was confirmed by electrophoresis in a 10 % SDS-PAGE gel by comparison with a standard protein marker ladder. The elution profiles from chromatography and photograph of the SDS-PAGE electrophoresis are shown in **Figure 4.2**.



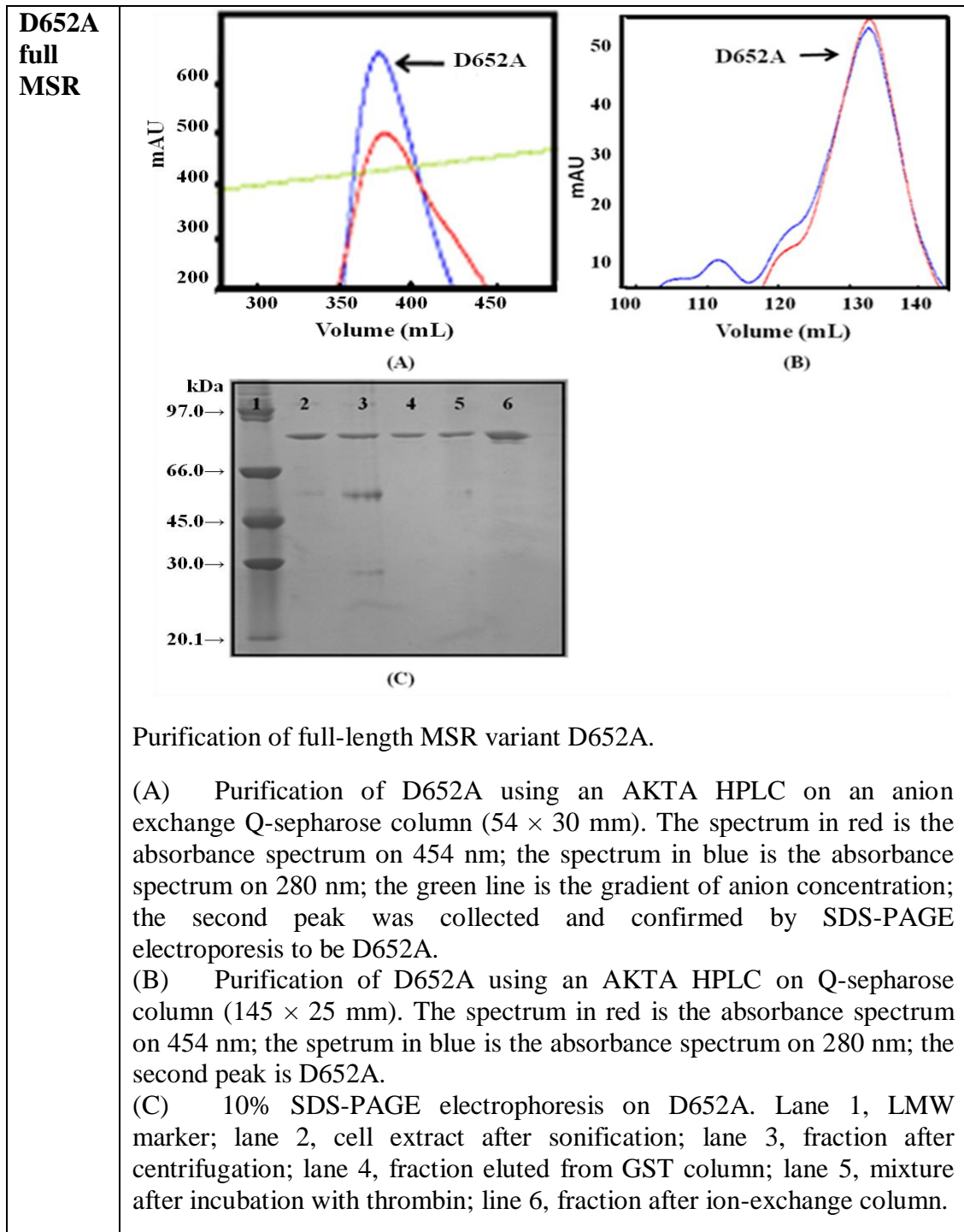


**Figure 4.2 Chromatography elution profiles and SDS PAGE electrophoresis of mutants of the FAD/NADPH binding domain during purification.**

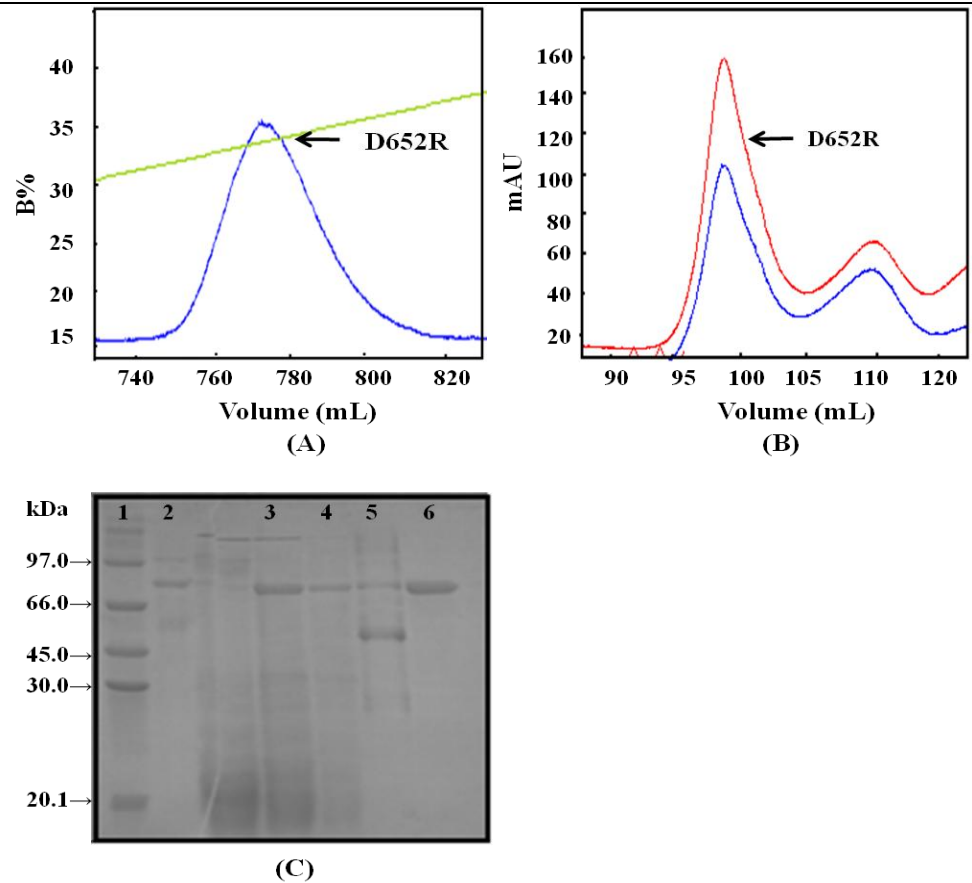
#### **4.2.2.2. Purification of the mutants D652A, D652R, D652N, W679A and W697H of the full-length MSR**

Five full length MSR mutants D652A, D652R, D652N, W697A and W697H were purified by the procedures stated in Chapter two (section 2.4.3). The MSR protein, which had undergone GST affinity chromatography and Q-Sepharose anion exchange chromatography, was loaded onto a Superdex 200 gel filtration column (volume 180 cm<sup>3</sup>), which had been equilibrated with 50 mM Tris-HCl buffer, pH 7.5 containing 0.3 M NaCl. The protein was eluted in the same buffer at a flow rate 0.3 mL/min. The MSR fraction in the elution profile was indicated by its absorbance at 280 nm and 454 nm and the protein identity was confirmed by SDS-PAGE electrophoresis. The proteins of interest were checked by 10-12% SDS PAGE

electrophoresis. All of the proteins purified exhibited a single major band on SDS-PAGE electrophoresis and were considered pure enough for further characterization. The purification plots of the chromatography and photographs of the electrophoresis gels are shown in **Figure 4.3**.



**D652R  
full  
MSR**



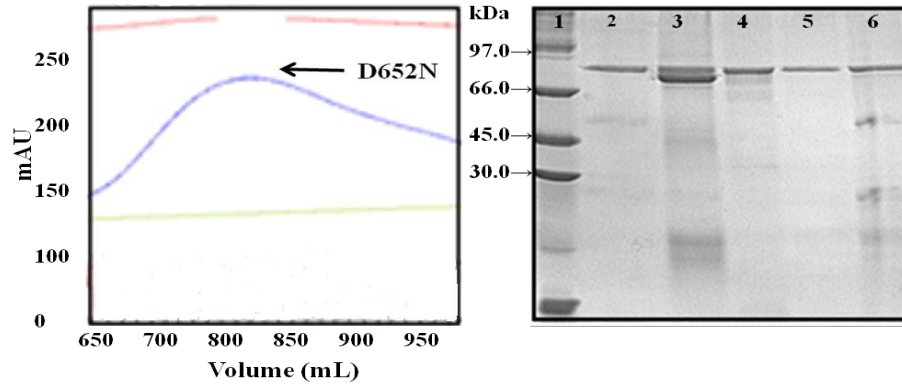
Purification of full-length MSR variant D652R.

(A). Purification of D652R using an AKTA HPLC on an anion exchange Q-sepharose column (54 × 30 mm). The spectrum in red is the absorbance spectrum on 454 nm; the spectrum in blue is the absorbance spectrum on 280 nm; the green line is the gradient of anion concentration; the second peak was collected and confirmed by SDS-PAGE electrophoresis to be D652R.

(B). Purification of D652R using an AKTA HPLC on Q-sepharose column (145 × 25 mm). The spectrum in red is the absorbance spectrum on 454 nm; the spectrum in blue is the absorbance spectrum on 280 nm; the second peak is D652.

(C). 10% SDS-PAGE electrophoresis on D652R. Lane 1, LMW marker; lane 2, cell extract after sonification; lane 3, fraction after centrifugation; lane 4, fraction eluted from GST column; lane 5, mixture after incubation with thrombin; line 6, fraction after ion-exchange column.

**D652N  
full  
MSR**

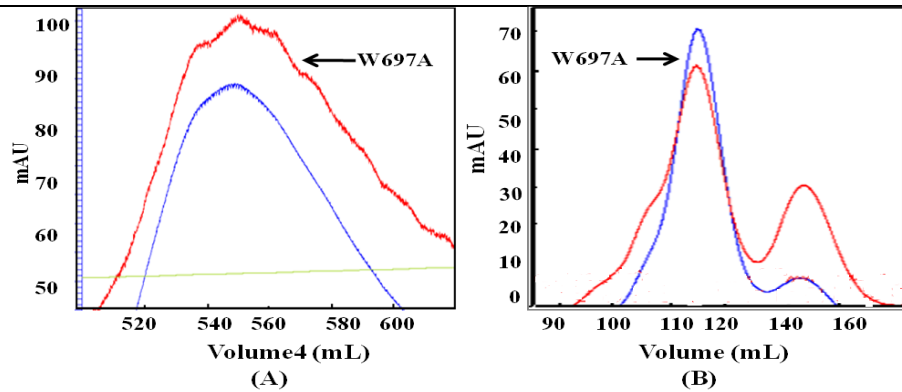


(A)

(B)

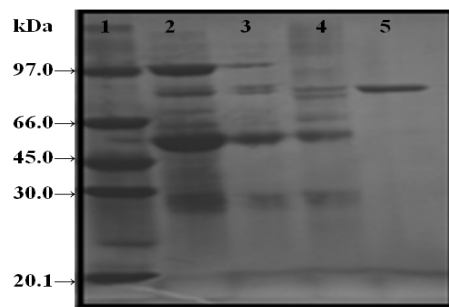
Purification of full-length MSR variant D652R. (A). Purification of D652N using an AKTA HPLC on an anion exchange Q-sepharose column (54 × 30 mm). The spectrum in red is the absorbance spectrum on 454 nm; the spectrum in blue is the absorbance spectrum on 280 nm; the green line is the gradient of anion concentration; the second peak was collected and confirmed by SDS-PAGE electroporesis to be D652N. (B). 10% SDS-PAGE electrophoresis on D652N. Lane 1, LMW marker; lane 2, cell extract after sonification; lane 3, fraction after centrifugation; lane 4, fraction eluted from GST column; lane 5, mixture after incubation with thrombin; line 6, fraction after ion-exchange column.

**W697A  
full  
MSR**



(A)

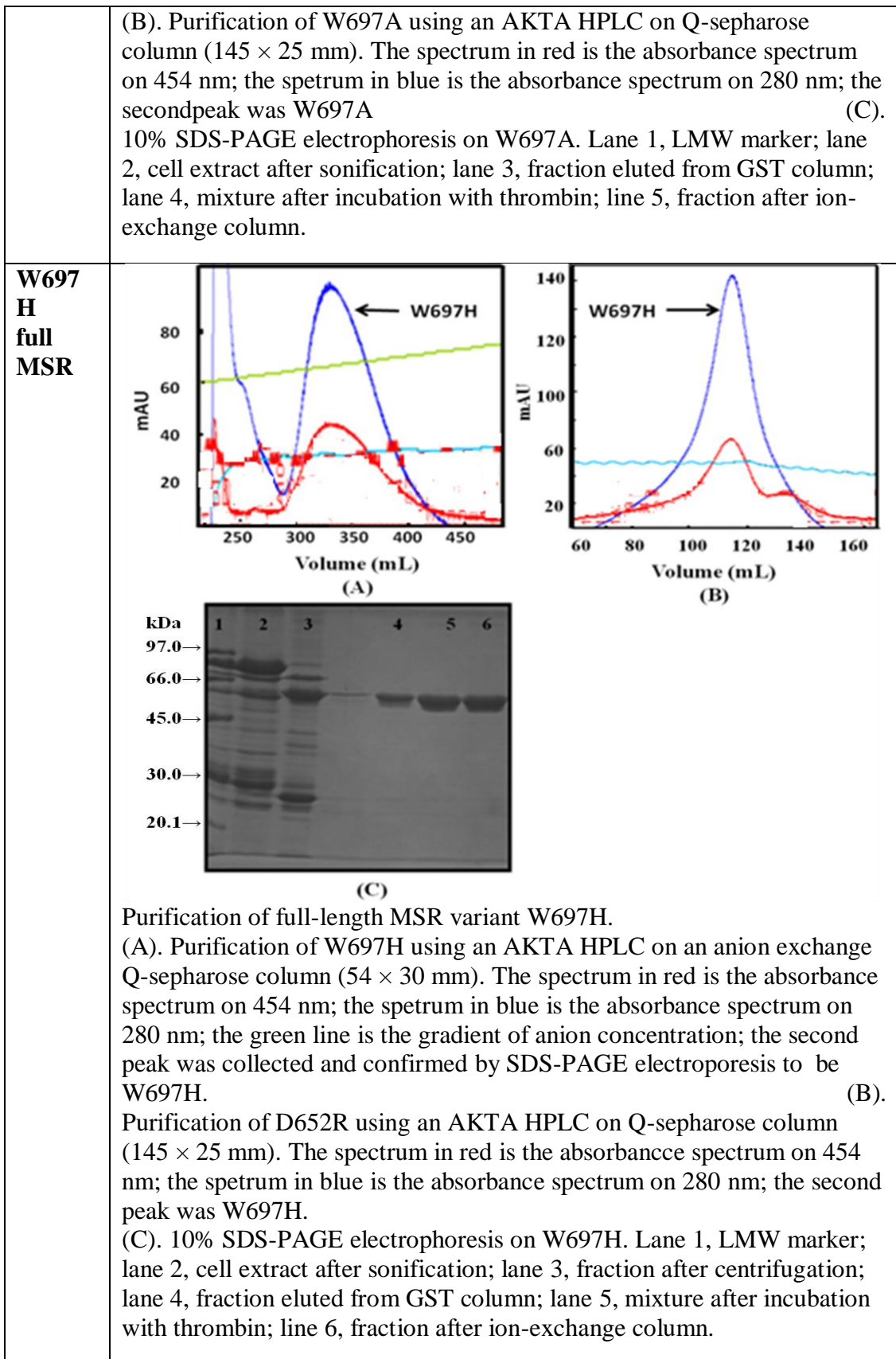
(B)



(C)

(A). Purification of W697A using an AKTA HPLC on an anion exchange Q-sepharose column (54 × 30 mm). The spectrum in red is the absorbance spectrum on 454 nm; the spectrum in blue is the absorbance spectrum on 280 nm; the green line is the gradient of anion concentration; the second peak was collected and confirmed by SDS-PAGE electroporesis to be W697A.





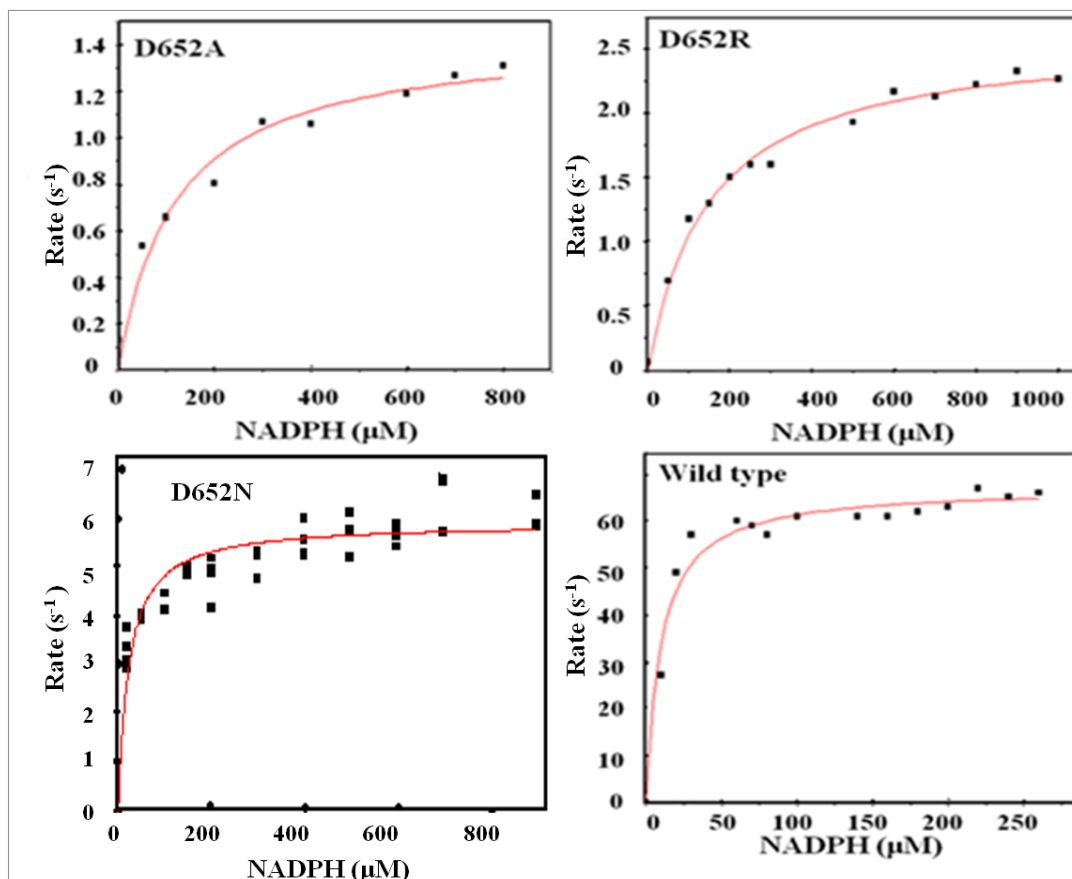
**Figure 4.3 Chromatography elution profiles and SDS PAGE electrophoresis of mutants of the full length MSR mutants**

### **4.2.3. Kinetic studies on the mutants**

#### **4.2.3.1. Kinetic studies on the mutants of the FAD/NADPH binding domain of MSR**

##### **4.2.3.1.1. Steady-state kinetic studies on the FAD/NADPH binding domain mutants D652A, D652R, and D652N**

Similar to the wild type FAD/NADPH binding domain of MSR, the variants of the FAD/NADPH binding domain of MSR, D652A, D652R, and D652N also have the ability to catalyze the NADPH-dependent reduction of FeCN. The apparent steady-state turnover rates for D652A, D652R, and D652N were determined under the conditions described in Chapter two as  $1.4 \text{ s}^{-1}$ ,  $2.6 \text{ s}^{-1}$  and  $3.8 \text{ s}^{-1}$  for FeCN reduction; the apparent  $K_m$  for NADPH binding is  $117 \text{ }\mu\text{M}$ ,  $147 \text{ }\mu\text{M}$  and  $23 \text{ }\mu\text{M}$  for D652A, D652R and D652N, respectively (data are shown in **Figure 4.4** and **Table 4.2**). Compared to the wild type FAD/NADPH binding domain of MSR, the relative catalytic ability is decreased about 560 fold, 239 fold and 25 fold, respectively.



**Figure 4.4** Apparent steady-state turnover rates of the variants of the FAD/NADPH binding domain of MSR with variable NADPH concentration and using ferricyanide as artificial electron acceptor. Fitting to the Michaelis-Menten equation gave values for apparent  $k_{cat}$ ,  $K_m$  (Table 4.2).

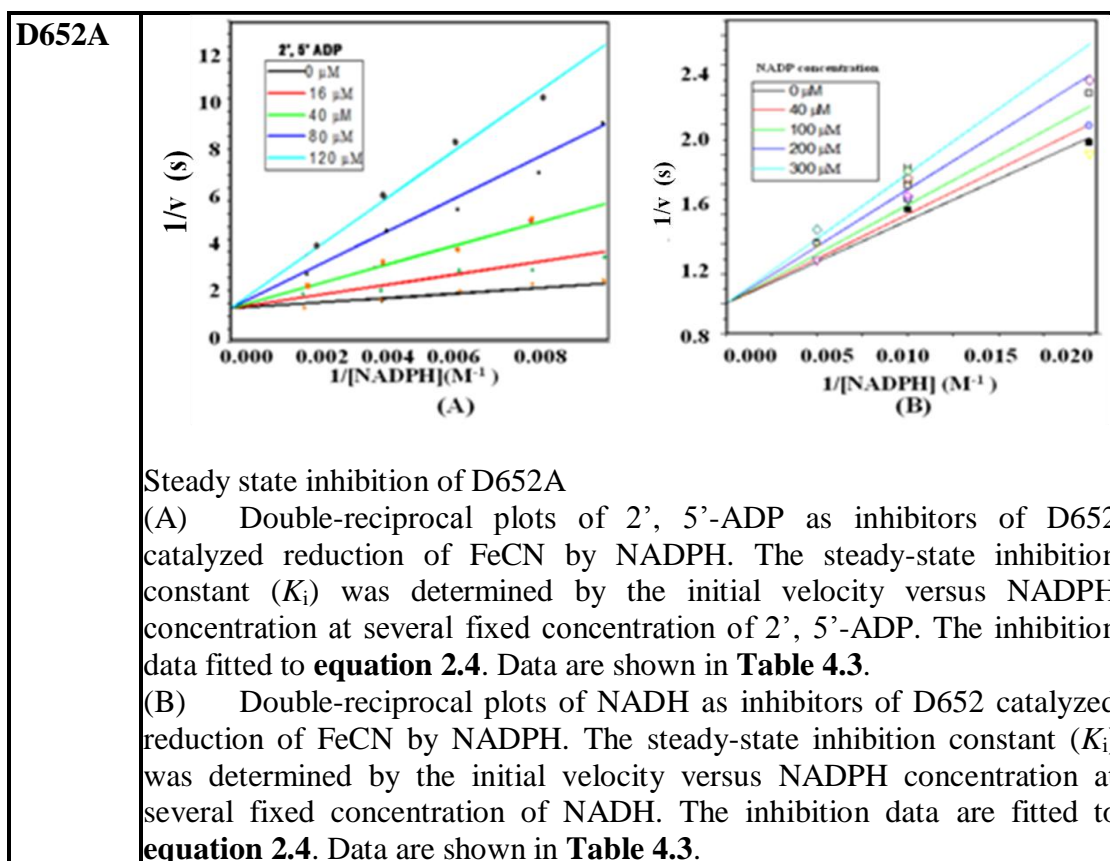
	$k_{cat}$ ( $s^{-1}$ )	$K_m$ ( $\mu M$ )	$k_{cat} / K_m$ ( $\mu M^{-1} \cdot s^{-1}$ )
<b>Wild-type</b>	<b><math>67.3 \pm 0.1</math></b>	<b><math>10 \pm 1</math></b>	<b>6.73</b>
<b>D652A</b>	<b><math>1.4 \pm 0.1</math></b>	<b><math>117 \pm 26</math></b>	<b>0.012</b>
<b>D652R</b>	<b><math>2.6 \pm 0.1</math></b>	<b><math>147 \pm 5</math></b>	<b>0.018</b>
<b>D652N</b>	<b><math>5.8 \pm 0.1</math></b>	<b><math>22.2 \pm 2.0</math></b>	<b>0.26</b>

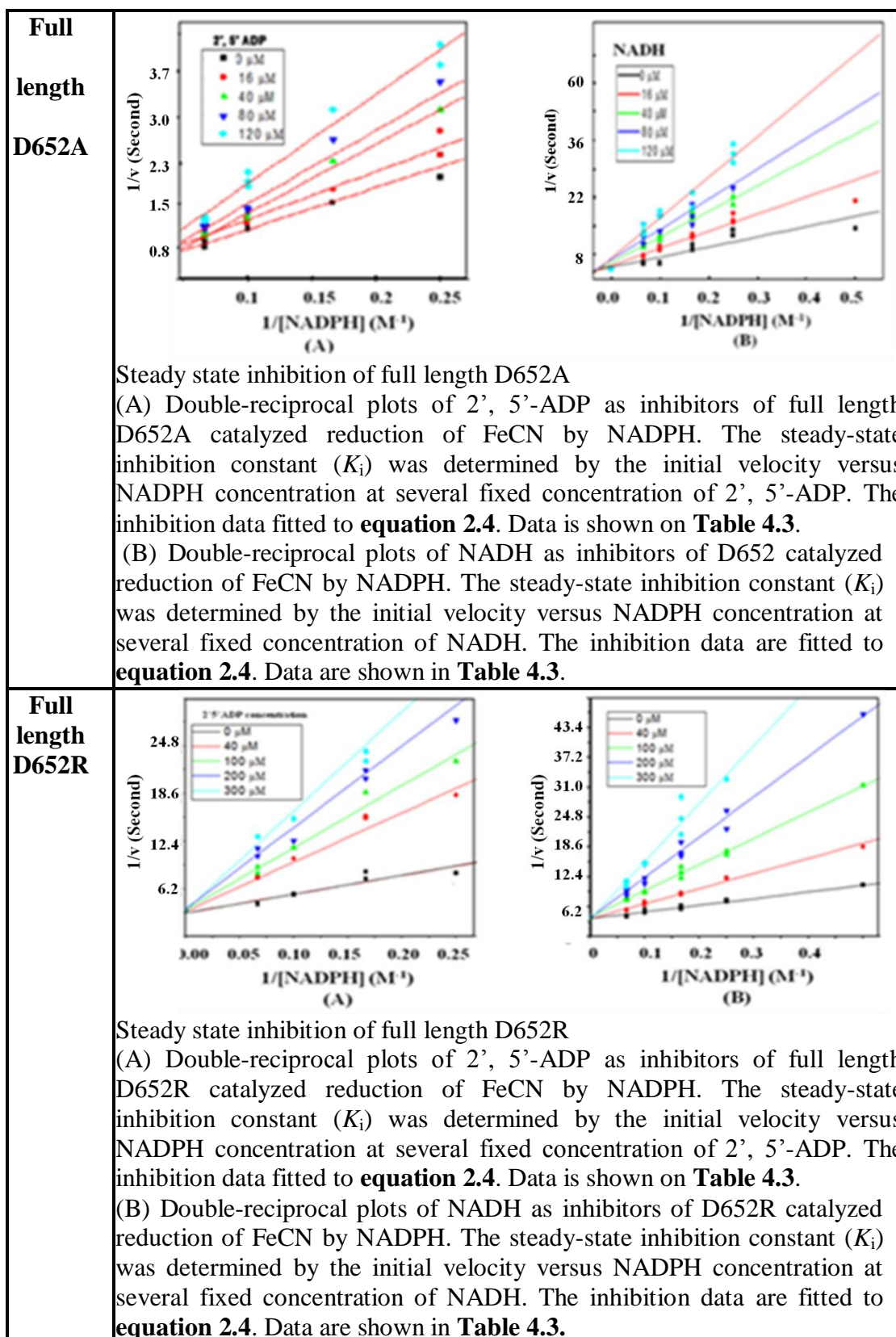
**Table 4.2** Steady-state plots of the variants of the FAD/NADPH binding domain of MSR

#### 4.2.3.1.2 Steady-state inhibition studies on the FAD/NADPH binding domain mutants D652A, D652R, and D652N.

Steady-state inhibition studies were carried out on selected variants of the MSR protein. These included D652A of the FAD/NADPH binding domain and D652A and D652R of the full length MSR. The reaction procedure and conditions

have been described previously in Chapter two (**section 2.6.3**). NADPH, FeCN and cytochrome *c* were the chosen substrates for the reactions. 2', 5'-ADP and NADP<sup>+</sup> were used as inhibitors of the reduction of FeCN and cytochrome *c*, catalyzed by the MSR or the FAD/NADPH binding domain, and used to determine the steady-state inhibition constants. The calculated inhibition constant data is listed in **Table 4.3**. The double-reciprocal plots of the initial velocity versus NADPH concentration with several fixed concentration of NADP<sup>+</sup> or 2', 5'-ADP are shown in **Figure 4.5**. The data indicate that both 2', 5'-ADP and NADP<sup>+</sup> are competitive inhibitors for NADPH. Similar to the wild type of MSR, 2', 5'-ADP is a relatively strong inhibitor for the variants of MSR and NADP<sup>+</sup> is a relatively weak inhibitor. However, compared with the dissociation constants determined from ITC and pre-steady state stopped flow spectrophotometry experiments [3], the dissociation constants for D652A and D652R were lower and higher respectively.





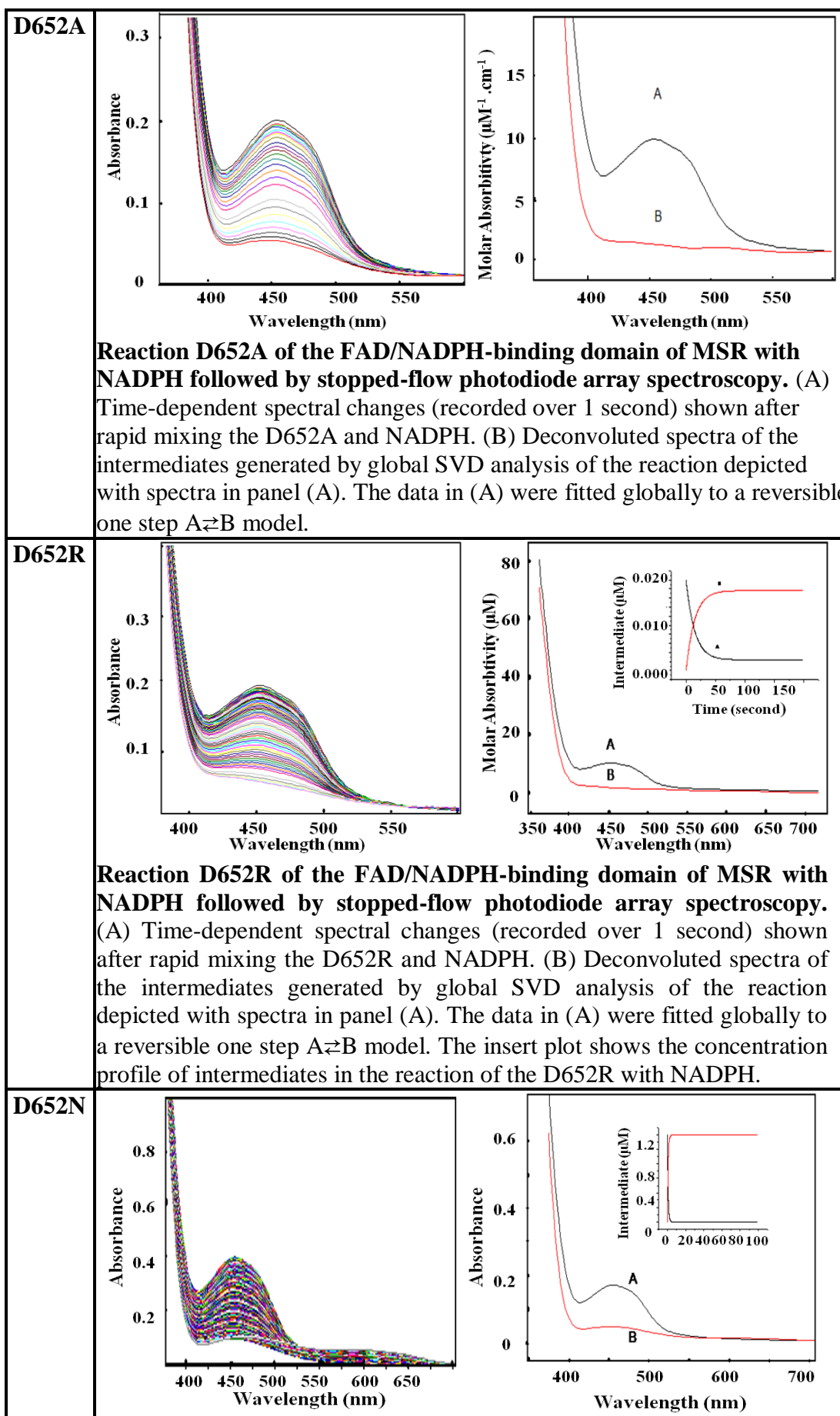
**Figure 4.5** Steady-state inhibition plots of the variants of the FAD/NADPH binding domain of MSR.

	$K_i$ for 2'5'-ADP ( $\mu\text{M}$ )	$K_i$ for NADP <sup>+</sup> ( $\mu\text{M}$ )
<b>D652A</b>	10.34 $\pm$ 0.01	549 $\pm$ 1
<b>D652A full</b>	8.81 $\pm$ 0.01	20.43 $\pm$ 0.01
<b>D652R full</b>	1.13 $\pm$ 0.01	13.95 $\pm$ 0.01
<b>Wild type full</b>	1.44 $\pm$ 0.01	36 $\pm$ 0.01

**Table 4.3 Steady-state inhibition results for the variants of MSR**

#### **4.2.3.1.3 Pre- steady-state kinetic studies on the FAD/NADPH binding domain mutants D652A, D652R, and D652N.**

Studies of the reductive half reaction of the variants of the FAD/NADPH binding domain of MSR were carried out to investigate the pre-steady state kinetics of these proteins. Reactions were performed at 25 °C under pseudo first-order conditions, in a stopped-flow spectrophotometer housed inside a Belle anaerobic cabinet, with a 20 fold excess of NADPH over enzyme. The enzyme sample was mixed with NADPH and the absorbance spectrum change followed for 5 seconds. In this time period, the reduction of the fully oxidized enzyme sample was completed. **Figure 4.6** shows the resulting spectra which demonstrate a characteristic peak at 454 nm. These spectra were globally fitted by SVD analysis to a one step reversible model to obtain the rate constant for electron transfer to the oxidised enzyme. In addition, single wavelength stopped-flow spectrophotometry at 454 nm was performed to determine the rate constant for the spectral intermediate formed in the PDA experiment. Compared with the wild-type FAD/NADPH binding domain of MSR, the variants D652A, D652R, and D652N had the same pattern spectra but with decreased rate constants. The data of the rate constants for these variants are listed in **Figure 4.6** and **Table 4.4**.



**Reaction D652N of the FAD/NADPH-binding domain of MSR with NADPH followed by stopped-flow photodiode array spectroscopy.**  
 (A) Time-dependent spectral changes (recorded over 1 second) shown after rapid mixing the D652N and NADPH. (B) Deconvoluted spectra of the intermediates generated by global SVD analysis of the reaction depicted with spectra in panel (A). The data in (A) were fitted globally to a reversible one step  $A \rightleftharpoons B$  model. The insert plot shows the concentration profile of intermediates in the reaction of the D652N with NADPH.

**Figure 4.6 Stopped-flow spectrophotometry plots of the variants of the FAD/NADPH binding domain of MSR**

		Data (s <sup>-1</sup> )	St. Error
<b>Wild-type</b>	$k_{+1}$	20.01	±0.01
<b>D652A</b>	$k_{+1}$	0.156	±4.562E-03
<b>D652R</b>	$k_{+1}$	0.061	±7.564E-05
<b>D652N</b>	$k_{+1}$	1.344	±3.897E-03

**Table 4.4 The stopped-flow rate of the variants of the FAD/NADPH binding domain of MSR.**

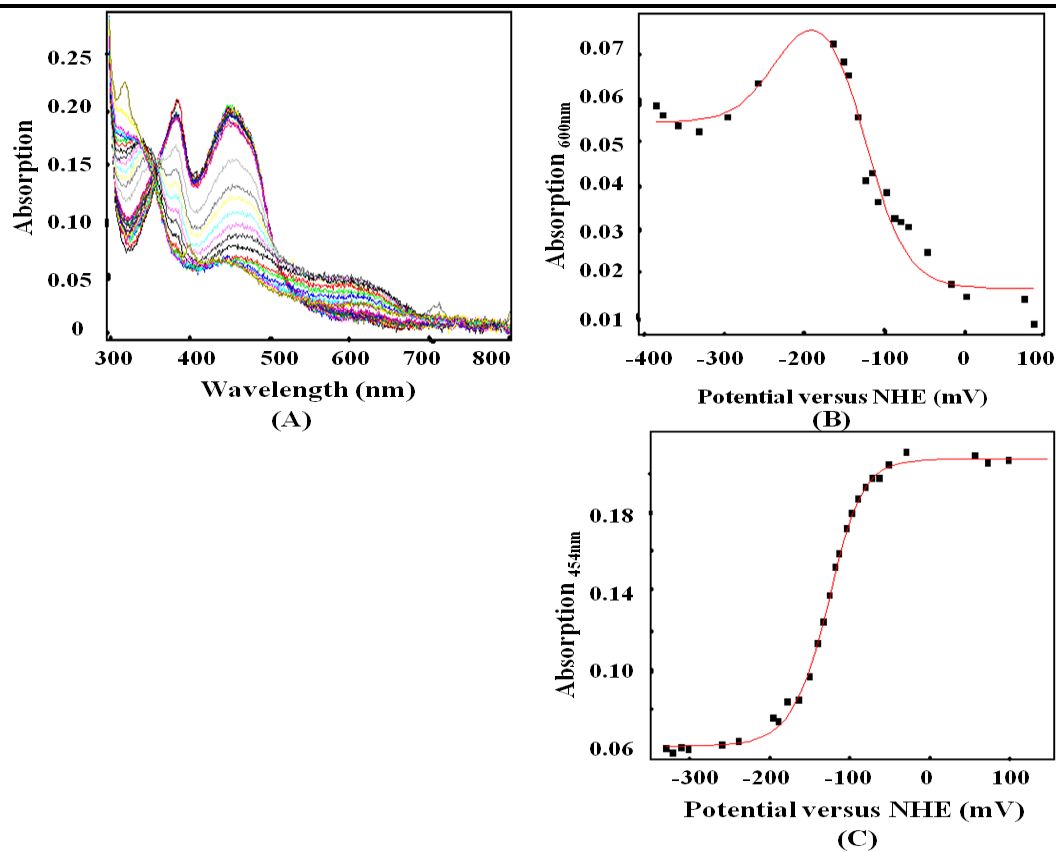
#### **4.2.3.1.4. Redox potential studies on the FAD/NADPH binding domain mutants**

##### **D652A, D652R, and D652N.**

Anaerobic spectroelectrochemical titration experiments were used to determine the midpoint potentials for the cofactor FAD on the variants D652A, D652R, and D652N of the FAD/NADPH binding domain. The reaction protocol and conditions have been described in detail in Chapter two (**section 2.6.5**). During the titration process, the fully oxidized enzyme sample was gradually reduced by the addition of small volumes of sodium dithionite which is freshly prepared in solution just prior to the experiment. To allow the reaction to reach equilibrium before the absorption spectrum was recorded, several minutes were allowed after each addition of the reducing agent until a stable voltage reading was achieved. These procedures were repeated until the half reduction reaction was finished. After changing to potassium ferricyanide, the reduced reaction sample was reoxidized and the experimental process repeated using the same procedure as used for the reductive half reaction. Most of the variants of the FAD/NADPH binding domain of MSR are



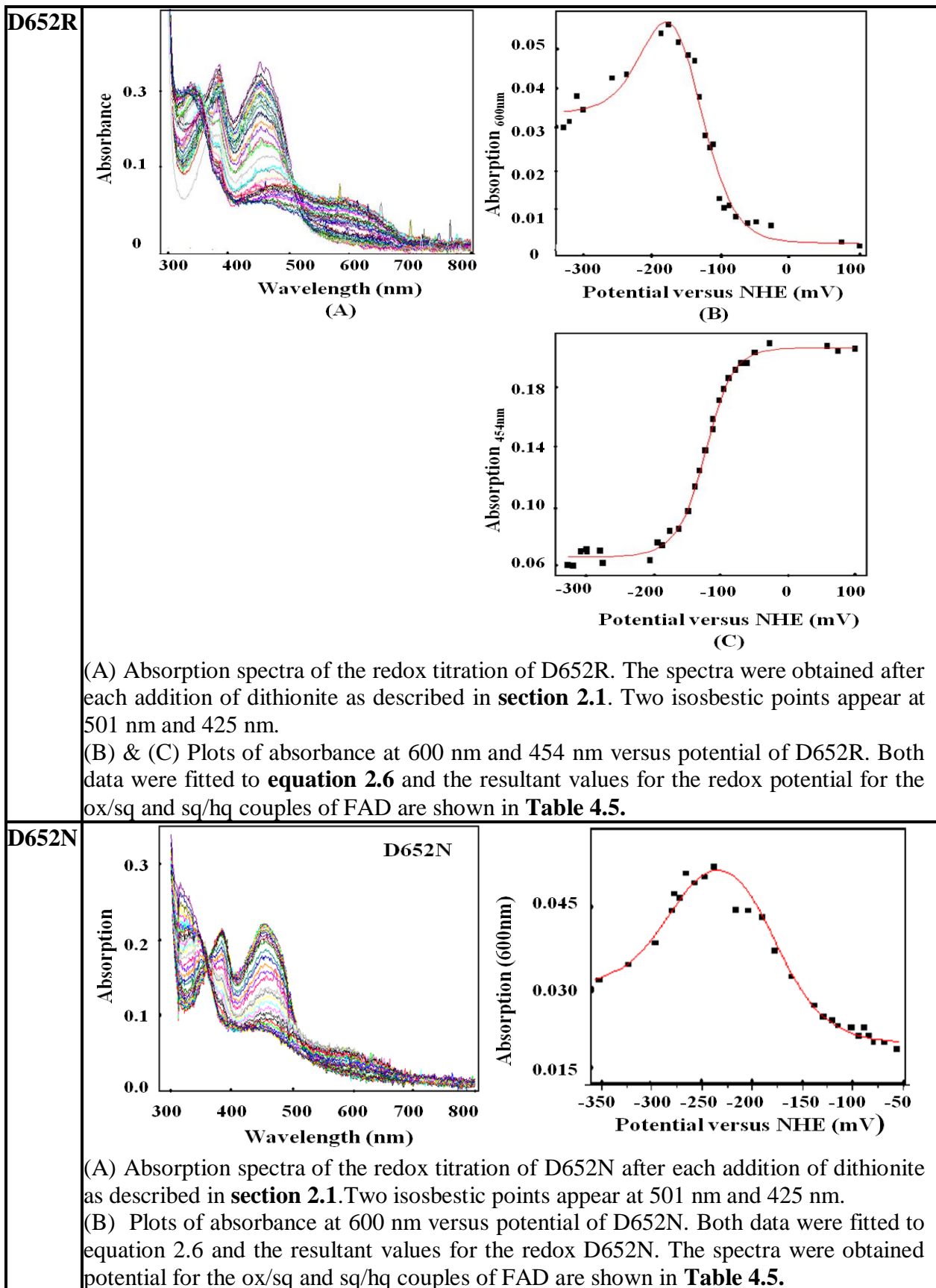
generally stable during the reduction reaction by dithionite. Some minor spectral drifts can be corrected by simple baseline subtraction. The reduction process of the variants D652A, D652R, and D652N consist of two phases as shown in the redox absorption spectra in **Figure 4.7**. The first phase is a result of the blue semiquinone species FADH, which is shown as a broad feature absorbance band near 600 nm. In the second phase, after the addition of more sodium dithionite, the blue semiquinone FADH is gradually reduced to the colourless FADH<sub>2</sub> with the bleaching of the shoulder around 600 nm on the spectrum. Two isosbestic points at 500 nm and 360 nm are visible on the absorbance spectra. The absorbance data obtained at 454nm and 600 nm were plotted versus the redox potential data and are shown in **Table 4.5**. The bell-shape curve at 600 nm indicates the redox potential of two semiquinone species, the high potential FAD<sub>ox</sub>/FAD<sub>sq</sub> in the right-hand region and the low potential FAD<sub>sq</sub>/FAD<sub>hq</sub> at the left side of the curve. Based on **equation 2.6**, the data in these two plots were calculated to obtain the midpoint potentials of the FAD<sub>ox</sub>/FAD<sub>sq</sub>, and FAD<sub>sq</sub>/FAD<sub>hq</sub> redox couples, which are shown in Table 4.4. Compared to the two midpoint potentials of FAD<sub>ox</sub>/FAD<sub>sq</sub>, and FAD<sub>sq</sub>/FAD<sub>hq</sub> of the wild-type FAD/NADPH binding domain (-222 mV and -288 mV), most of the midpoint potentials of the variants D652A (-123 mV, 233 mV), D652R (-124 mV, -306 mV), and D652N (-178 mV, -279 mV) exhibited a positive shift, which is consistent with the decrease in the steady-state turnover numbers for these variant proteins. The catalytic ability of these variants is severely reduced.

**D652A**

Redox potentials of D652A.

(A) Absorption spectra of the redox titration of D652A. The spectra were obtained after each addition of dithionite as described in section (2.1). Two isosbestic points appear at 501 nm and 425 nm.

(B) & (C). Plots of absorbance at 600 nm and 454 nm versus potential of D652A. Both data were fitted to equation 2.6 and the resultant values for the redox potential for the ox/sq and sq/hq couples of FAD are shown in **Table 4.5**.



**Figure 4.7 Redox potentials of the variants of the FAD/NADPH binding domain of MSR**

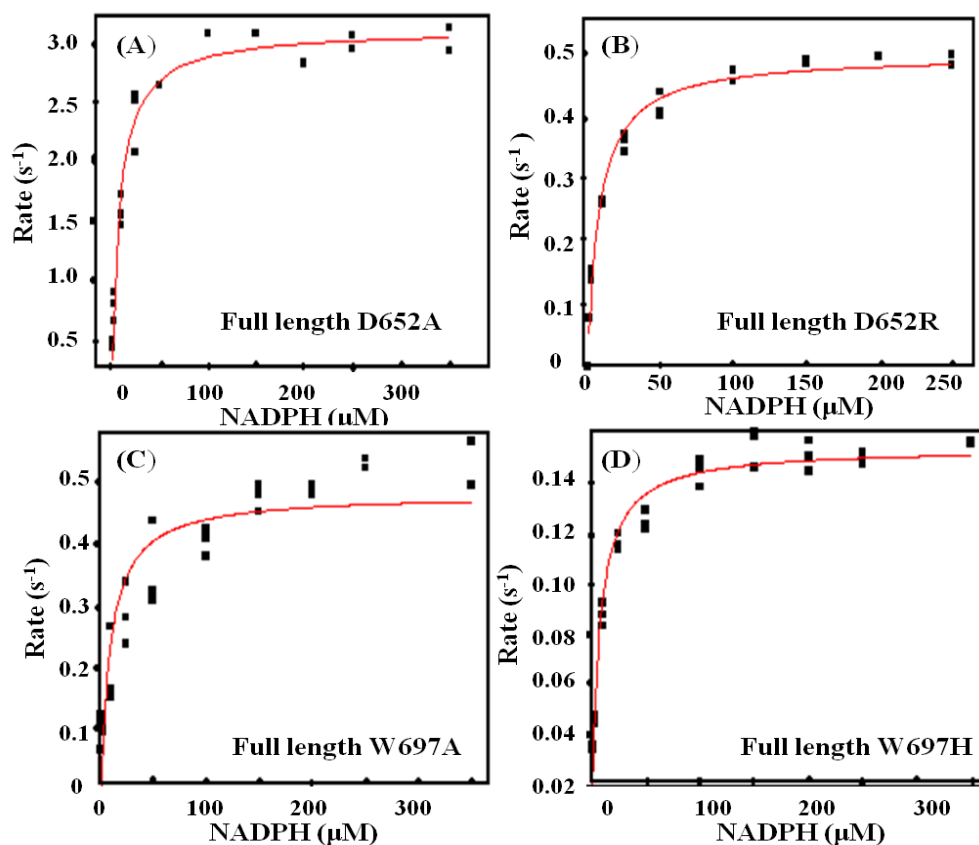
	ox/sq (mV)	sq/hq (mV)
<b>Wild-type</b>	-222 ± 4	-288 ± 7
<b>D652A</b>	-123 ± 7	-233 ± 23
<b>D652R</b>	-124 ± 5	-306 ± 16
<b>D652N</b>	-178 ± 7	-279 ± 10

**Table 4.5 Redox potential data of the variants of the FAD/NADPH binding domain of MSR**

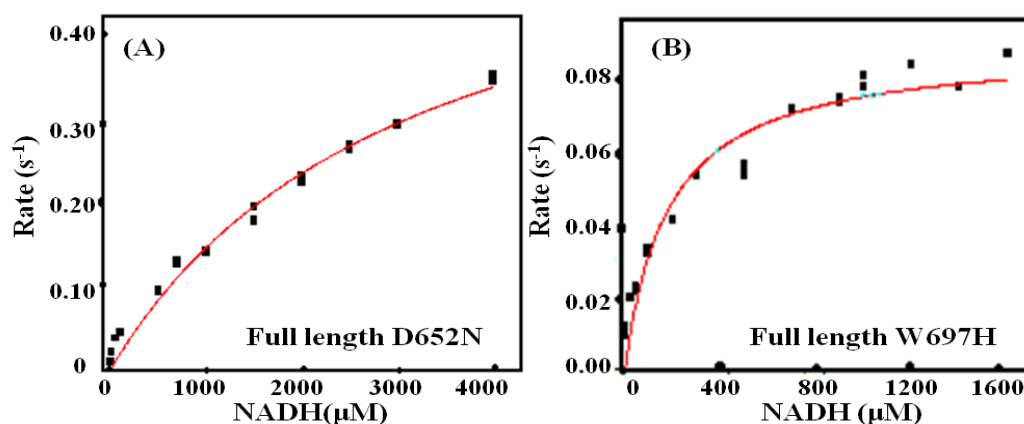
#### **4.2.3.2. Kinetic studies on the full length MSR mutants D652A, D652R, D652N, W697A and W697H**

##### **4.2.3.2.1. Steady-state kinetic studies on the full length MSR mutants D652A, D652R, D652N, W697A and W697H**

As with wild type full length MSR, the variants of full length MSR, D652A, D652R, D652N, W697A and W697H also have the ability to catalyze the NADPH-dependent reduction of cytochrome *c*. The apparent steady-state turnover rates for D652A, D652R, W697A and W697H were determined under the conditions described in chapter two. The  $k_{cat}$  values were  $3.12 \text{ s}^{-1}$ ,  $0.50 \text{ s}^{-1}$ ,  $0.29 \text{ s}^{-1}$  and  $0.154 \text{ s}^{-1}$  for cytochrome *c* reduction and the apparent  $K_m$  values for NADPH are  $8.12 \text{ }\mu\text{M}$ ,  $7.98 \text{ }\mu\text{M}$ ,  $7.75 \text{ }\mu\text{M}$  and  $6.75 \text{ }\mu\text{M}$  for D652A, D652R, W697A and W697H. The  $k_{cat}$  values were  $0.60 \text{ s}^{-1}$  and  $0.09 \text{ s}^{-1}$  and the  $K_m$  values were  $3117 \text{ }\mu\text{M}$ ,  $184.3 \text{ }\mu\text{M}$  for full length and D652N with NADH and cytochrome *c* as substrates. Compared to the data of wild type of full length MSR ( $k_{cat}/K_m$  is  $1.315 \pm 0.088 \text{ s}^{-1}\text{M}^{-1}$  for NADPH and  $6.78 \times 10^{-5} \text{ s}^{-1}\text{M}^{-1}$  for NADH. [3]), the catalytic ability decreased 34.5 fold, 56.6 fold, 2.4 fold and 19.8 fold for W697A, W697H, D652A and D652R with NADPH as electron provider and increased 6 fold and 1.8 fold for W697H and D652N with NADH as electron provider.



**Figure 4.8.** The apparent steady-state turnover rates of the variants of the full length MSR with variable NADPH concentration and using cytochrome *c* as artificial electron acceptor. (A) Full-length D652A. (B). Full length D652R. (C) Full-length W697A. (D) Full length W697H. Fitting to the Michaelis-Menten equation gave values for apparent  $k_{cat}$ ,  $K_m$  (Table 4.6.1)



**Figure 4.9** The steady-state plots of the variants of the full length MSR with variable NADH concentration and using cytochrome *c* as artificial electron acceptor. (A) Full length D652N. (B). Full length W697H. Fitting to the Michaelis-Menten equation gave values for apparent  $k_{cat}$ ,  $K_m$  (Table 4.6.2)

	<b>W697A</b>	<b>W697H</b>	<b>D652A</b>	<b>D652R</b>
$k_{\text{cat}}(\text{s}^{-1})$	$0.29 \pm 0.01$	$0.154 \pm 0.01$	$3.12 \pm 0.06$	$0.50 \pm 0.01$
$K_{\text{m}}(\mu\text{M})$	$7.75 \pm 0.01$	$6.75 \pm 0.66$	$8.12 \pm 0.7$	$7.98 \pm 0.18$
$k_{\text{cat}}/K_{\text{m}}$	0.037	0.0228	0.384	0.063

**Table 4.6.1 Steady state turnover number of W697A, W697H, D652A and D652R with NADPH as substrate.**

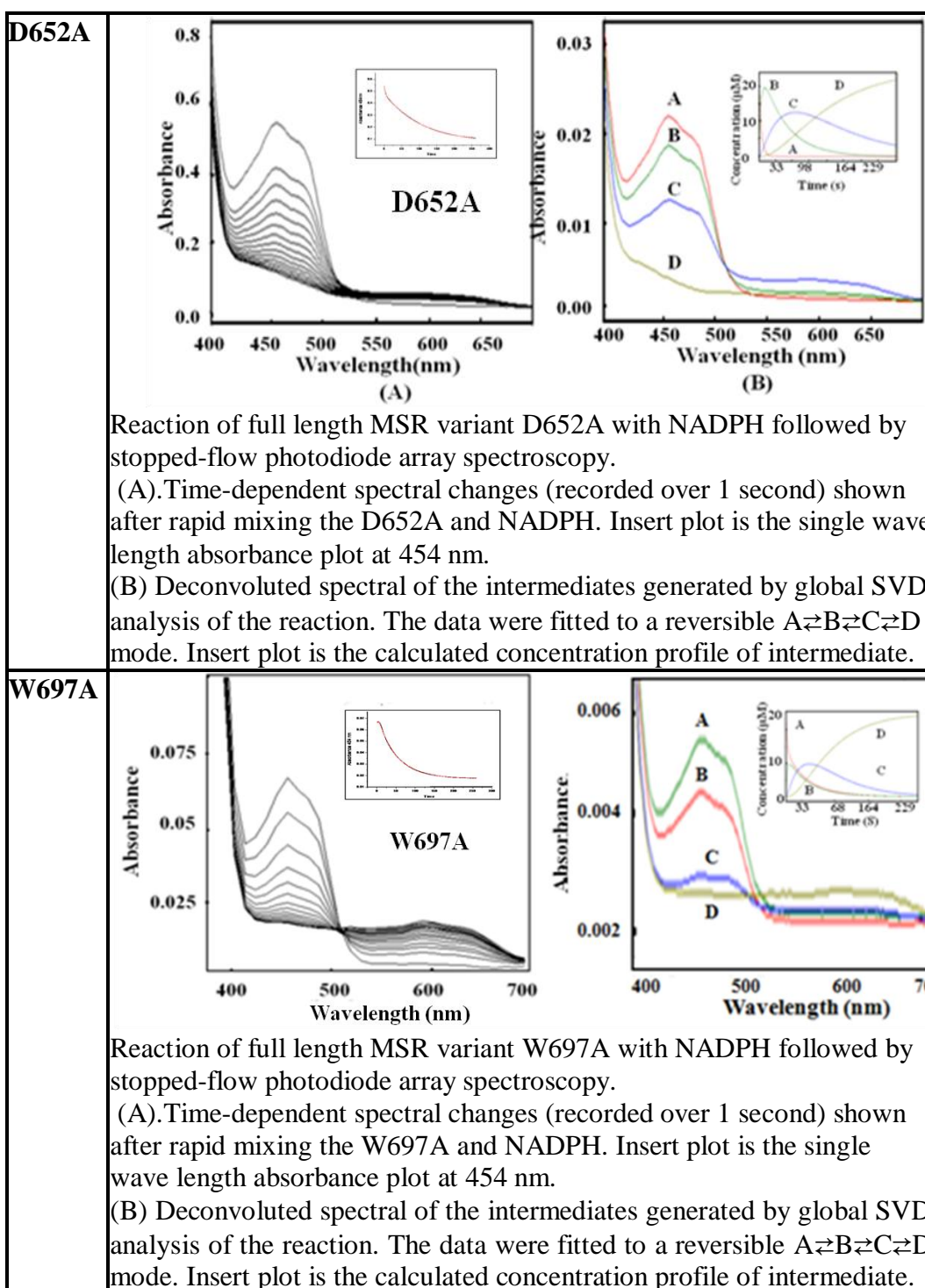
	<b>W697H</b>	<b>D652N</b>	<b>Wild-type</b>
$k_{\text{cat}}(\text{s}^{-1})$	$0.09 \pm 0.01$	$0.60 \pm 0.01$	$0.24 \pm 0.03$
$K_{\text{m}}(\mu\text{M})$	$184.3 \pm 33$	$3117 \pm 460$	$3540 \pm 560$
$k_{\text{cat}}/K_{\text{m}}(\text{s}^{-1}\text{M}^{-1} \times 10^{-3})$	$0.483 \pm 0.0001$	$0.1925 \pm 0.001$	$0.0678 \pm 0.0137$

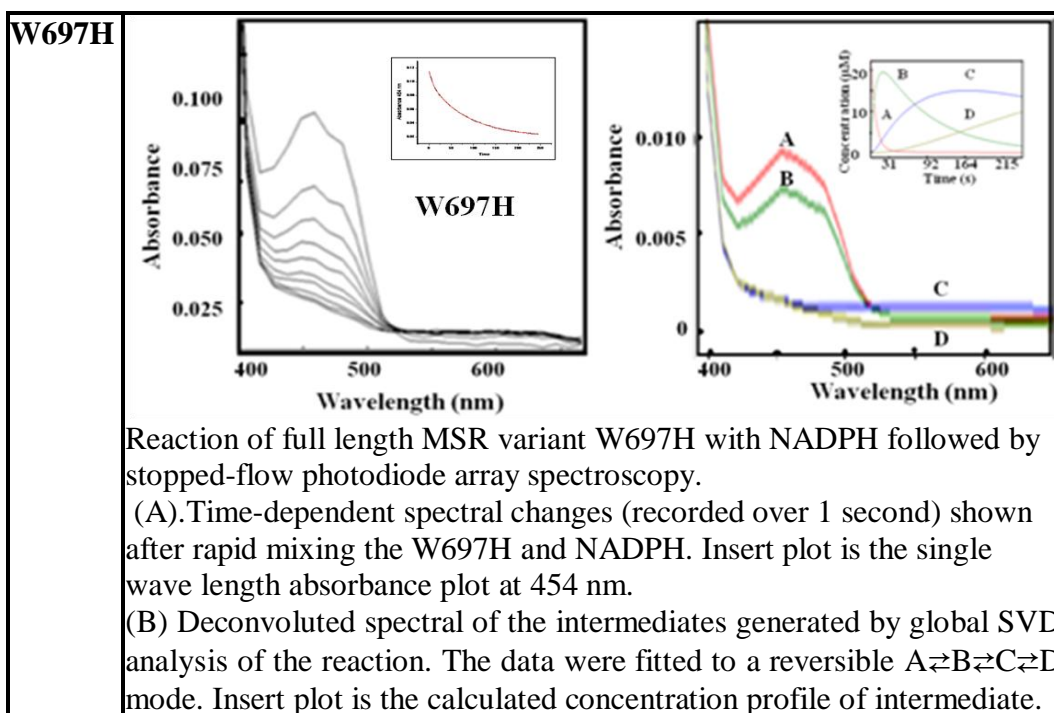
**Table 4.6.2 Steady state turnover number of W697H, D652N with NADH as substrate.**

#### 4.2.3.2.2. Pre-steady-state kinetic studies on the full length MSR mutants D652A, W697A and W697H

Studies of the reductive half reaction of the variants of full length MSR were carried out to investigate the pre-steady state kinetic behaviour of these proteins. Reactions were performed at 25 °C under pseudo first-order conditions, in a stopped-flow spectrophotometer contained inside an anaerobic Belle glove box, using a 20 fold molar excess of NADPH over the enzyme. The enzyme sample was mixed with NADPH and the absorbance spectrum change monitored for 200 seconds during which time the reduction of the fully oxidized enzyme sample was completed. The resulting spectra are shown in **Figure 4.10** with a characteristic peak at 454 nm. This spectrum was globally fitted by SVD analysis to a three step reversible model. Semiquinone can be detected in these spectra. In addition, single wavelength stopped flow spectrophotometric experiments at 454 nm were performed to determine the rate constant for the spectral intermediate formed in the PDA experiment. Compared with the full length wild type MSR, the variants D652A, D652R, D652N, W697A, and W697H had the same spectral features, but with decreased rate constants. The rate constants on the single wavelength 454 nm were fitted with a double electron

transfer model  $A \rightarrow B \rightarrow C$ . The rate constants are listed in **Table 4.7**. The D652A has the fastest rate constant of the three mutants.





**Figure 4.10 Stopped-flow plots of the variants of the full length MSR**

	<b>W697A</b>	<b>W697H</b>	<b>D652A</b>
$k_{+1}$	$0.1400 \pm 0.0007$	$0.1130 \pm 0.004$	$0.3691 \pm 0.022$
$k_{+2}$	$0.0170 \pm 0.0003$	$0.0117 \pm 0.0001$	$0.0095 \pm 0.0001$

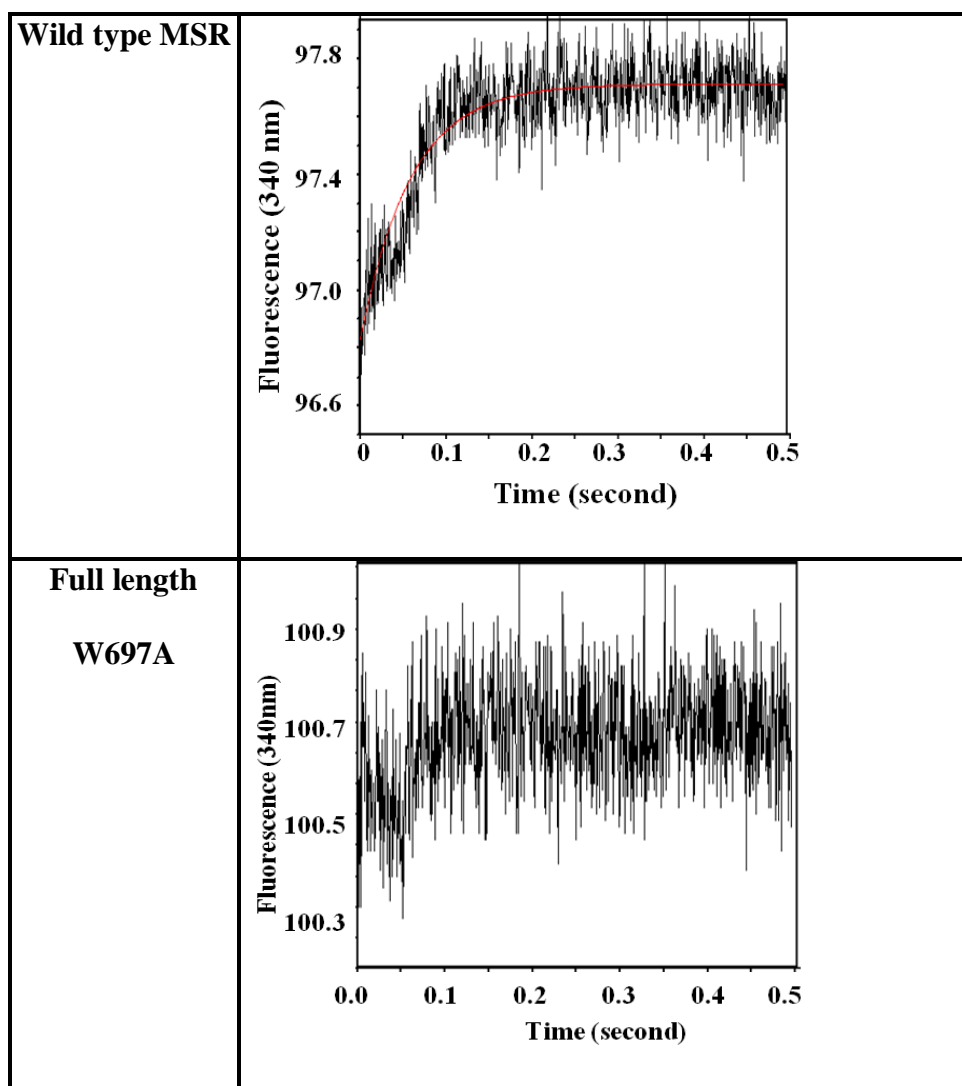
**Table 4.7 Stopped flow experiment data on the variants of full length MSR**

#### 4.2.3.3. Fluorescence studies on the wild-type MSR protein and one variant of full-length MSR

Tryptophan fluorescence-monitored stopped flow spectroscopy was employed to investigate the change in intensity of the fluorescence of the tryptophan in the reaction after mixing wild type full length MSR with NADPH, and the variant W697A of full-length MSR with NADPH (**Figure 4.9.**). The crystal structure of the FAD/NADPH binding domain of MSR confirms that tryptophan<sup>697</sup> covers the re-face of the isoalloxazine ring of the cofactor FAD and moves away when the hydride is transferred from NADPH to FAD. It was thought that the movement of the hydride could be accompanied by a change in the intensity of tryptophan<sup>697</sup> fluorescence. In this experiment, the wild type full length MSR (10  $\mu$ M) was rapidly mixed with a 20 fold excess of NADPH and the tryptophan fluorescence monitored as a monophasic reaction transient. Using the same reaction conditions, after the



rapid mixing of the W697A protein with a 20 fold excess of NADPH, no fluorescence could be detected. This result confirms that tryptophan<sup>697</sup> has been substituted by alanine and that the tryptophan fluorescence signal seen in wild-type MSR is attributed to W697.



**Figure 4.11. Tryptophan fluorescence-monitored stopped flow spectroscopy on wild-type MSR and mutant W697A.** The increase in tryptophan fluorescence (excitation at 295 nm) after rapid mixing of the wild type MSR or W697A (10  $\mu$ M) with NADPH (200  $\mu$ M) was monophasic and was fitted to a single-exponential function.

### 4.3. Discussion

Research on the mutants of MSR focused on two conserved residues, namely Asp<sup>652</sup> and Trp<sup>697</sup>, and included steady state kinetic studies, pre-steady-state kinetic

studies, steady-state substrate inhibition studies, and redox potential studies. The results of these studies demonstrated that these two conserved residues play a key role in coenzyme binding, the electron transfer mechanism and in maintaining the integrity of the environment around the FAD cofactor.

Steady-state kinetic data indicated that the kinetic parameters  $k_{\text{cat}}$  and  $k_{\text{cat}}/K_m$  for the mutants D652A, D652N, and D652R were decreased while the  $K_m$  values obtained were increased compared with the wild type FAD/NADPH binding domain of MSR. This result illustrates that the change on the electrostatic charge and space volume on Asp<sup>652</sup>, substantially affects the binding affinity of NADPH and furthermore lowers the rate of the hydride transfer from NADPH to FAD. The variants obtained by changing another residue, namely Trp<sup>697</sup> which is stacked on the *re*-face of the isoalloxazine ring of FAD, also exhibit a decreased  $k_{\text{cat}}$  and  $k_{\text{cat}}/K_m$  and increased  $K_m$  with respect to the data determined with wild type full length MSR. This result confirms that the binding efficiency of NADPH with the enzyme was decreased. Additionally, although Asp<sup>652</sup> and Trp<sup>697</sup> do not directly form the binding site for the 2'-phosphate of NADPH, these residues have the potential to influence discrimination between NADPH and NADH. The observed preference for NADH binding by the mutant containing the Asp<sup>652</sup> substitution is consistent with this hypothesis. For example, on study of the mutant D652N of the full-length MSR was not able to bind NADPH and only NADH could be used as a suitable electron donor. The  $K_i$  for 2'5'-ADP determined from steady state inhibition studies with the D625A mutant on the FAD/NADPH binding domain was increased compared to that measured with the wild type MSR. These data are consistent with the decreased  $k_{\text{cat}}$  and the increased  $K_m$ . This phenomenon can be explained by a decrease in the ability of the mutant to identify the 2'-phosphate of NADPH. This recognition controls the

binding affinity of NADPH, so the decreased binding of NADPH will trigger the decreased catalytic ability of the mutant. In addition, the variant D652N of full-length MSR exhibits a change in coenzyme specificity with only NADH being capable of driving turnover. This result is direct evidence to confirm that Asp<sup>652</sup> is a key binding residue for NADPH on MSR.

Another residue Trp<sup>697</sup> is believed to be involved in the electron transfer reaction of MSR. Two mutants, W697A and W697H, were produced to probe the importance of this position and investigate whether these changes were reflected in the steady-state and pre-steady-state kinetic experiments. Comparison with the data obtained from the wild-type full-length MSR, the  $k_{\text{cat}}$  for W697A and W697H decreased about 10 fold and 24 fold and the  $K_m$  increased about 1.6 fold and 1.3 fold. These results show that both the binding affinity of NADPH and the catalytic ability of these two mutants have been affected. These results were confirmed by stopped-flow spectrophotometry experiments on W697A and W697H where the rate for electron transfer was decreased about 2 fold. One possible explanation is the variant of MSR forms a stable complex with NADP<sup>+</sup> and increases the inhibition of NADP<sup>+</sup>, so the catalytic ability is decreased.

The redox potential is an important factor in the electron transfer reaction of MSR. Compared with the redox potential data with the wild type protein of the FAD/NADPH binding domain, the redox potentials of the FAD of the mutants D652A, D652R and D652N are more positive with shifts of about 90 to 100 mV for the ox/sq FAD and about 50 mV for sq/hq FAD. This result is consistent with the stopped-flow experimental data which showed a slow hydride transfer rate for these two mutants. In addition, these results reveal that the environment of FAD has been disturbed by performing site directed mutagenesis. However, the PDA spectrum of

the mutants in the stopped-flow experiments also demonstrates the electron transfer mode for the mutants is similar to that of the wild type protein. It consists of three steps:  $A \rightleftharpoons B \rightleftharpoons C \rightleftharpoons D$  for the full-length MSR and mutants (D652A, W697A, and W697H) and one step mode for the FAD/NADPH binding domain of MSR with mutants D652A, D652R, and D652N. In addition, the semiquinone FAD and semiquinone FMN were detected in the stopped-flow experiments for full-length MSR and its mutant, but no semiquinone FAD was found in the stopped-flow kinetic studies on the wild-type FAD/NADPH binding domain of MSR and its mutants.

The mutants on the residue Asp<sup>652</sup> of MSR consists of two groups. One group includes D652A, D652R, D652N of the FAD/NADPH binding domain of MSR; another group has D652A, D652R, D652N of the full length MSR. Although all these mutants are focused on residue Asp<sup>652</sup>, the purification of the mutants D652A, D652R, D652N of the full length MSR were more complicated and difficult. So some experiments were not designed to complete.

Collectively, these results suggested that the mutagenesis on these two residues Asp<sup>652</sup>, Trp<sup>697</sup>, results in some change in the protein structure but not enough to abolish the catalytic ability and electron transfer ability of MSR. Some kinetic, pre steady-state kinetic and thermodynamic changes were observed. These changes provide good evidence to support Asp<sup>652</sup> and Trp<sup>697</sup> as being pivotal determinants in the structure and function for MSR. Clearly, the observed effects on catalysis might arise for changes in electrostatics and/or conformational differences. The next logical phase of the study would be to determine the crystal structures of the mutant proteins to offer further insight into the observed effects.

## **Chapter FIVE**

### **EPR, ENDOR, ESEEM and ELDOR on MSR**

## 5.1 Introduction

The redox potentials of the FMN and FAD cofactors of MSR allow for the formation of one electron and two electron reduced states containing the FMN semiquinone, and FMN and FAD semiquinones respectively. Flavin semiquinones bear an unpaired electron and can therefore be studied using EPR spectroscopy and the related techniques of pulsed ENDOR, ESEEM and pulsed ELDOR spectroscopy (see Chapter two **section 2.8**). These techniques provided data on the environment of the flavin cofactors and the change in inter-flavin distance caused by the binding of effectors such as  $\text{NADP}^+$  and the isolated activation domain of methionine synthase (AD). The latter is relevant to the conformational sampling mechanism proposed to operate in diflavin reductases including P450 reductase (CPR) and nitric oxide synthase (NOS), as described in Chapter one **Sections 1.3** and **Section 1.4**.

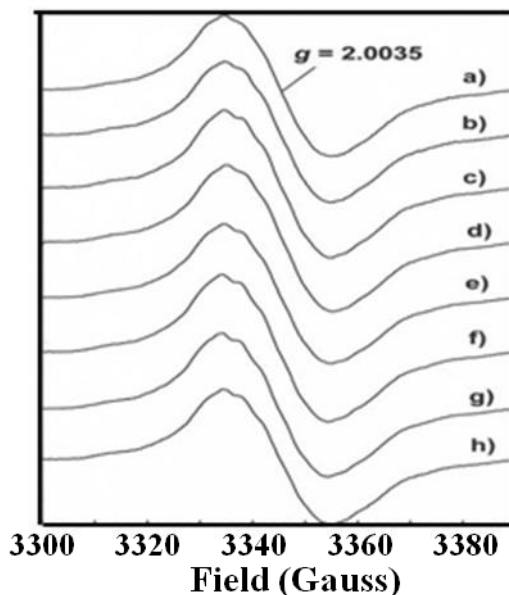
## 5.2. Results

### 5.2.1. EPR spectroscopy

X-band continuous wave EPR spectra of dithionite reduced MSR are shown in **Figure 5.1**. The first four spectra (a, b, c, d) show ‘one electron reduced’ MSR containing a proportion of FMN semiquinone; the second four spectra (e, f, g, h) show the ‘two electron reduced’ state of MSR, which contains FMN semiquinone and FAD semiquinone. The midpoint potential of the two electron reduced state determined that there is an equilibrium between the semiquinone FMN and semiquinone FAD rather than the formation of 100% semiquinone at either cofactor. The spectra b, c, d, and f, g, h, show the EPR of the complexes of MSR with 2',5'-ADP,  $\text{NADP}^+$  and the isolated activation domain of MS (AD) respectively. These

complexes were designed to form a 1:1 complex based on the dissociation constants of every component in every complex.

The X-band EPR spectrum of one electron reduced MSR (spectra a, b, c, d) is characterized by a single line with  $g=2.0035$  and a peak to trough width of 20.1 G. This is a typical spectrum for the neutral flavin semiquinone radical. These parameters were not changed in the complex of MSR with 2', 5'-ADP, NADP<sup>+</sup> and AD. The EPR spectrum of the two electron reduced MSR showed the same feature at  $g=2.0035$  with a peak to trough line width of 20.5 G. This spectrum confirms the formation of flavin semiquinone, and it also suggests that the line width of the EPR spectrum of the FAD semiquinone is slightly wider than that of the FMN semiquinone. As is observed in one electron reduced MSR, the formation of a complex of MSR with 2', 5'-ADP, NADP<sup>+</sup> does not affect the EPR spectrum.



**Figure 5.1 X-band continuous wave EPR spectra of dithionite reduced MSR:** a) one electron reduced: b) one electron reduced + 2', 5'-ADP: c) one electron reduced + NADP+: d) one electron reduced + AD: e) two electron reduced: f) two electron reduced + 2', 5'-ADP: g) two electron reduced + NADP+: h) two electron reduced + AD. Experimental parameters: microwave power 10  $\mu$ W; modulation amplitude 1 G; modulation frequency 100 KHz; temperature 80 K.

In addition, these EPR spectra also show several other features of neutral flavin semiquinones. Firstly, ‘tails’ to high and low field of the central line appear where the spectrum deviated from what might be expected of the first derivative of a Gaussian line and there is a small ‘step’ in the maximum at approximately 3338G. Both of these features arise from the partially resolved hyperfine coupling to H<sup>1</sup> and <sup>14</sup>N atoms of the flavin, mostly N(5)H, N(5) and C(8)-methyl atoms. Unfortunately, the resolution of the EPR spectrum does not permit accurate measurement and assignment of these hyperfine coupling constants.

In summary, EPR spectra confirm the formation of semiquinone FMN and FAD at low temperature and it is consistent with the same formation at room temperature observed using optical spectroscopy.

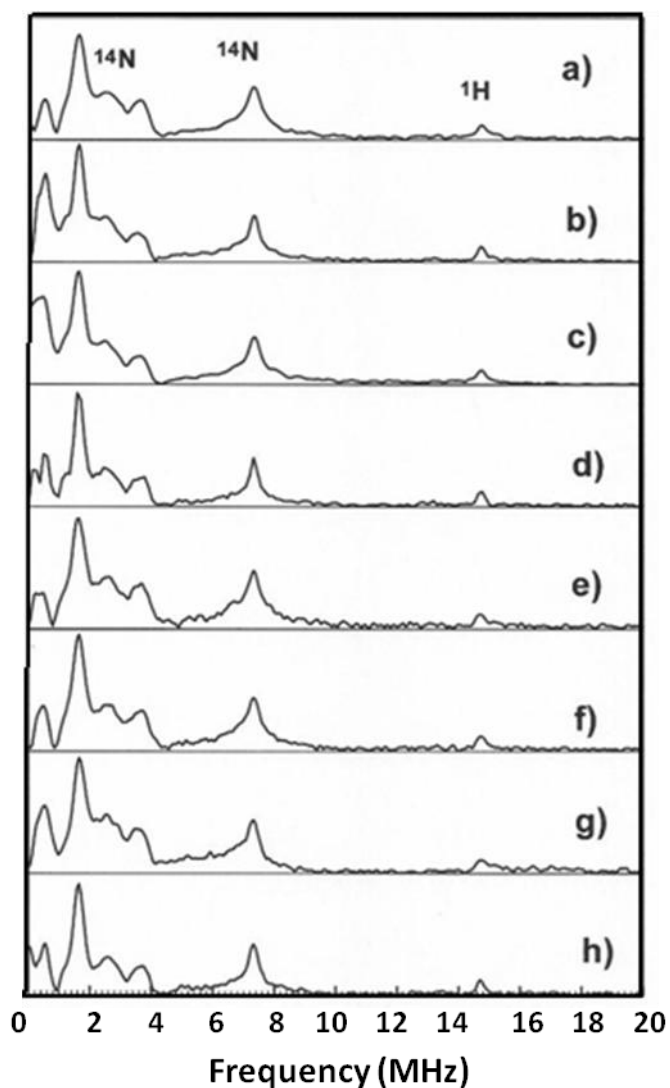
### **5.2.2. ESEEM spectroscopy**

ESEEM spectroscopy is a method of measuring the hyperfine coupling between atomic nuclei and unpaired electrons. ESEEM spectra are produced by the Fourier transformation of the modulation of spin echoes and ESEEM is particularly sensitive to small hyperfine coupling to nuclei with low Larmor frequencies and nuclear spin greater than ½ ( $I > 1/2$ ) such as <sup>14</sup>N or <sup>2</sup>H .

The X-band two pulse ESEEM spectra of dithionite reduced MSR are shown in **Figure 5.2**. Each spectrum is split into three regions. The first region, from 0 to 5 MHz, provides the information on the quadrupole and hyperfine coupling of <sup>14</sup>N atoms weakly coupled to the unpaired flavin semiquinone electron; the second region, from 6 to 9 MHz provides the information on the hyperfine coupling of <sup>14</sup>N



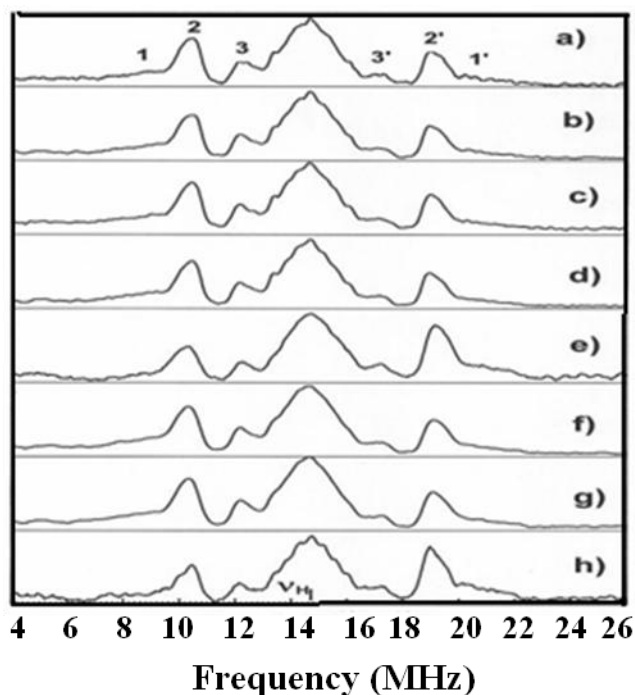
atoms to the unpaired flavin semiquinone electron; the third region, from 14 to 16 MHz provides information on the weak hyperfine coupling of  $^1\text{H}$  atoms to the unpaired flavin semiquinone electron. Previous ESEEM studies of other flavoproteins have shown that the 0 to 6 MHz region is dominated by contributions from the flavin semiquinone N(1) and N(3) atoms with  $^{14}\text{N}$  hyperfine coupling constants of 1-2 MHz. The 6 to 9 MHz region is dominated by a peak at 7.3 MHz which is assigned to the hyperfine constant to N(10)  $^{14}\text{N}$  hyperfine coupling. The small feature in the 14 to 16 MHz region at 14.7 MHz arises from weakly coupled  $^1\text{H}$  atom, which is possibly assigned to N(3)H. Since ESEEM is not particularly good at detecting large hyperfine coupling to nuclei with spin of  $\frac{1}{2}$  ( $I=\frac{1}{2}$ ), only this weak feature is observed for  $^1\text{H}$  nuclei. Although there are some limitations to the ESEEM method, the identical ESEEM spectra suggest that the environments of N(1), N(3) and N(10) are identical for both the FMN and FAD flavin semiquinones and also that all of these atoms are not affected by the binding of 2', 5'-ADP,  $\text{NADP}^+$  and AD.



**Figure 5.2. X-band two pulse ESEEM spectra of dithionite reduced MSR:** a) one electron reduced: b) one electron reduced + 2', 5'-ADP:c) one electron reduced + NADP+: d) one electron reduced + AD: e) two electron reduced: f) two electron reduced + 2', 5'-ADP: g) two electron reduced + NADP+: h) two electron reduced + AD. Experimental parameters: see Materials and Methods for pulse sequence; temperature 80 K; 60 scans were concatenated.

### 5.2.3. ENDOR spectroscopy

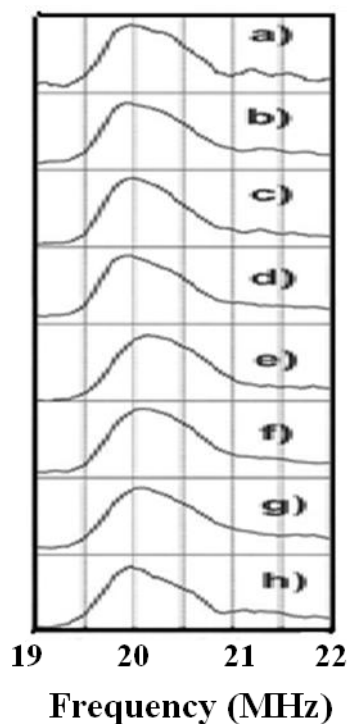
Electron Nuclear Double Resonance (ENDOR) spectroscopy can be used to measure the hyperfine coupling between atomic nuclei and unpaired electrons. Compared to ESEEM, ENDOR allows the detection of large hyperfine couplings to nuclei with nuclear spin  $\frac{1}{2}$  ( $I=\frac{1}{2}$ ), such as  $^1\text{H}$ . **Figure 5.3** shows the X-band echo detected Davies ENDOR spectra of MSR. The hyperfine coupling to  $^1\text{H}$  and unpaired electron are symmetrical around the central matrix feature which occurs at the nuclear Larmor frequency for  $^1\text{H}$ ,  $\nu_{\text{H}}$ , at 14.7 MHz under the conditions employed in these experiments. Three hyperfine couplings are observed and their assignments to flavin semiquinone protons are listed in **Table 5.1**. The most prominent lines in these spectra, (2, and 2'), arise from the 8-methyl group of the flavin semiquinone dimethylbenzene ring. These lines also show the most variation in the complexes of MSR with 2', 5'-ADP,  $\text{NADP}^+$  and AD and the addition of a second electron to MSR. The high frequency lines for pair 2, were therefore plotted on an expanded scale to make their line shape more easily discernable, Figure 5.4. The 8-methyl group lines consist of two components, an intense  $A_{\perp}$  component and a weaker  $A_{\parallel}$  component. The  $A_{\parallel}$  component gives rise to a shoulder and a slightly larger hyperfine coupling than  $A_{\perp}$ . These two components are a consequence of the cylindrical symmetry of the 8-methyl group hyperfine coupling, the axis of symmetry being the C (8) to methyl group bond. The difference between the  $A_{\perp}$  and  $A_{\parallel}$  can be indicative of the rate of methyl group rotation with a faster rotation rate making the difference smaller. The  $^1\text{H}$  hyperfine couplings are proportional to the share of the unpaired electron, the 'unpaired electron spin density', at the attached carbon in the singly occupied molecular orbital (SOMO) of the flavin semiquinone.



**Figure 5.3. X-band pulsed Davies ENDOR spectra of dithionite reduced MSR:** a) one electron reduced: b) one electron reduced + 2', 5'-ADP: c) one electron reduced + NADP+: d) one electron reduced + AD: e) two electron reduced: f) two electron reduced + 2', 5'-ADP: g) two electron reduced + NADP+: h) two electron reduced + AD. Experimental parameters: see Materials and Methods for pulse sequence; temperature 80 K; 100 scans were concatenated.

Hyperfine coupling constants (MHz)	1	2	$A_{\perp}/A_{\parallel}$	3
a) 1 electron reduced	11.5	8.5/9.2		5.1
b) 1 electron reduced + 2', 5'-ADP	11.5	8.5/9.2		5.1
c) 1 electron reduced + NADP <sup>+</sup>	11.5	8.6/9.1		5.1
d) 1 electron reduced + AD	11.5	8.5/9.2		5.1
e) 2 electron reduced	12.0	8.7/9.5		5.1
f) 2 electron reduced + 2', 5'-ADP	12.0	8.7/9.5		5.1
g) 2 electron reduced + NADP <sup>+</sup>	12.0	8.7/9.5		5.1
h) 2 electron reduced + AD	12.0	8.6/9.6		5.1
Assignment	C(1')H	8-methyl		C(6)H

**Table 5.1. The data of three observed hyperfine couplings and their assignments to flavin semiquinone protons.**



**Figure 5.4, an expansion of the high frequency methyl lines, 2', of Figure 5.3.**

Comparing the hyperfine coupling constants, it was found that in the one electron reduced state the unpaired electron spin densities at C (8), C (6) and C (1') of the FMN flavin semiquinone are identical in MSR and in its 2', 5'-ADP and AD complexes. However, there is a small change in the complex with NADP<sup>+</sup> in the 8-methyl anisotropy which suggests the methyl group may rotate more freely in this complex. In two electron reduced MSR, (**Figure 5.3** and **Figure 5.4, e-h**), there are slightly different 8-methyl group hyperfine couplings. This phenomenon can be explained by the presence of two overlapping 8-methyl group lines; one line arises from the FMN semiquinone which occurs in the EPR spectra of the one electron reduced MSR and the other new line originates from the FAD cofactor. The observed increase in the 8-methyl hyperfine coupling constants of the two electron reduced MSR samples suggests that the 8-methyl hyperfine coupling of the FAD semiquinone is larger than that of the FMN cofactor, so moving the overlapped

combination of FMN and FAD lines to a higher apparent hyperfine coupling. In addition, a more pronounced ‘apparent’ anisotropy of the 8-methyl coupling is shown, i.e. this line becomes wider while the  $A_{\perp}$  moves towards that observed for the FMN flavin semiquinone. This suggests that the binding of AD to the two electron reduced states increases the separation between the 8-methyl hyperfine coupling constants of the FMN and FAD flavin semiquinones, with the increasing of the FAD 8-methyl hyperfine coupling.

Throughout this study, the hyperfine coupling for the C(1') and C(6) remained relatively constant. The hyperfine coupling for the C(1') on the second electron reduced MSR increased, but the line associated with it was broad and difficult to measure. This increase probably indicates an overlap between the C(1')H line of the FMN and the FAD flavin semiquinones. Since the hyperfine coupling for the C(6)H remained constant, there is little change in the overall unpaired electron spin density on the dimethylbenzene ring for either of the cofactors on binding of 2', 5'-ADP, NADP<sup>+</sup> or AD. This result suggests that the observed changes in the 8-methyl group hyperfine couplings come from the 8-methyl group's dynamics.

#### **5.2.4. ELDOR**

Electron electron double resonance (ELDOR or DEER), can be used to measure the distance between two unpaired electrons. The X-band four pulse ELDOR spectra on the two electron reduced MSR, and the complexes of MSR and 2', 5' -ADP, NADP<sup>+</sup> and AD were collected and are shown in **Figure 5.5**. These spectra were obtained from the Fourier transform of the spin echo from the four pulse ELDOR experiment. The x axis provides a measure of the dipolar coupling,

$\nu_{DD}$ , between two unpaired electrons.  $\nu_{DD}$  is related to the distance between the two electrons,  $r$ .

$$\nu_{DD}(\theta, r) = \frac{g_1 g_2 \mu_0 \mu_B^2}{4\pi h} \frac{1}{r} (3 \cos^2 \theta - 1)$$

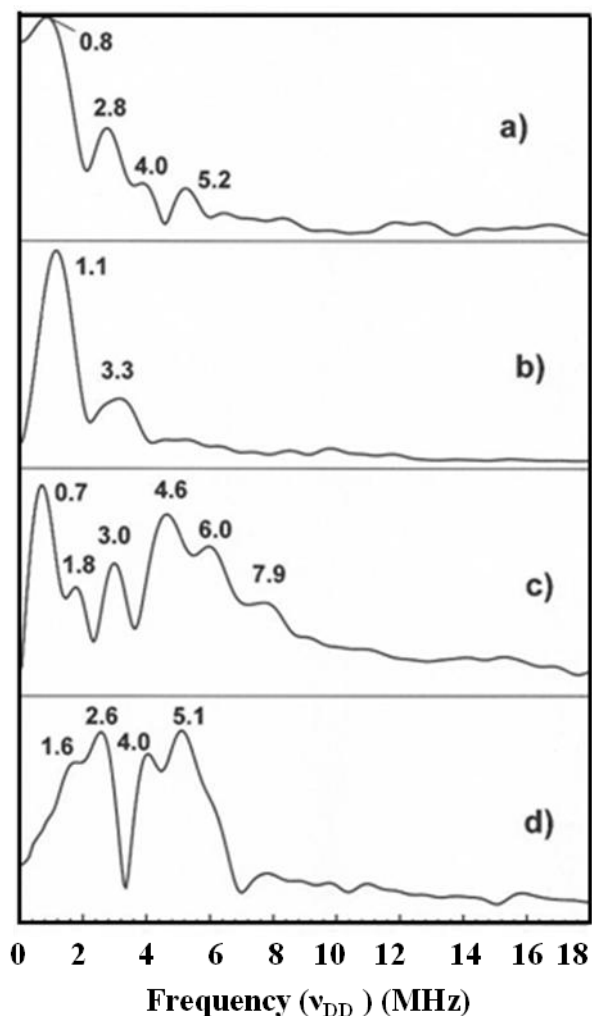
**Equation 5.1**

$$r = \sqrt[3]{\frac{52.16}{\nu_{DD}}}$$

**Equation 5.2**

Where  $\nu_{DD}$  is in MHz and  $r$  is in nm.

The distances between the FAD and FMN flavin semiquinone in the two electron reduced state of MSR obtained from the ELDOR spectra are shown in **Table 5.2**. Several inter-flavin distances were determined from each of the ELDOR spectra. The relative integrals of lines in the spectrum are important as they provide an indication of the number of molecules in each conformation. Consideration of the distance data along with the relative integrals shows that there are always multiple conformations of MSR and these conformations and their relative proportions change with substrate binding.



**Figure 5.5** X-band continuous wave EPR spectra of dithionite reduced MSR: a) two electron reduced: b) two electron reduced + 2,5-ADP: c) two electron reduced + NADP<sup>+</sup>: d) two electron reduced + AD. Experimental parameters: pulse sequence given in Materials and Methods; temperature 80 K; 400 scans were concatenated.

	$\nu_{DD}$ (MHz)	Distance, r (nm)	Relative integral
<b>2 electron reduced</b>	0.8, 2.8, 4.0, 5.2	3.9, 2.7, 2.3, 2.1	0.55, 0.24, 0.09, 0.12
<b>2 electron reduced + 2', 5'-ADP</b>	1.1, 3.3	3.6, 2.5	0.77, 0.23
<b>2 electron reduced + NADP<sup>+</sup></b>	0.7, 1.8, 3.0, 4.6, 6.0, 7.9	4.2, 3.1, 2.6, 2.2, 2.0, 1.9	0.23, 0.10, 0.14, 0.23, 0.19, 0.11
<b>2 electron reduced + AD</b>	1.6, 2.6, 4.0, 5.1	3.2, 2.7, 2.3, 2.1	0.20, 0.26, 0.24, 0.3

**Table 5.2** The distances data between the FAD and FMN flavin semiquinone in the two electron reduced state of MSR obtained from the ELDOR spectra.

### 5.3. Discussion



Continuous wave EPR spectra show the formation of neutral `blue` flavin semiquinones in both the FMN and FAD cofactors of MSR under all the conditions tested. MSR has been shown to form neutral flavin semiquinones in optical spectroscopy at room temperature. It is therefore evident that in EPR experiments carried out at a temperature of 80 K the protonation state of the flavin is unaffected and can be compared with the data obtained at room temperature.

ESEEM spectra report hyperfine coupling to  $^{14}\text{N}$  atoms of the flavin cofactors. These  $^{14}\text{N}$  atoms are located within the isoalloxazine end of the cofactor. The hyperfine coupling is a measure of the unpaired electron spin density at these nitrogen atoms and it is affected by the hydrogen bonding to the isoalloxazine end of flavin. The ESEEM spectra on MSR show that binding of 2', 5'-ADP,  $\text{NADP}^+$  and AD do not change the hydrogen bonding to the isoalloxazine end of the FMN and FAD cofactors.

ENDOR spectra of one electron and two electrons reduced MSR are similar. However, the difference between the 8-methyl hyperfine couplings of the FMN and FAD cofactors can be discerned. The significance of this difference is not clear and probably reflects the difference in the structures of FMN and FAD binding sites. In addition, the unpaired electron spin density distribution is also influenced by hydrogen bonding to the flavin cofactor reflecting part of the pattern of hydrogen bonding between the protein and the cofactor.

The 8-methyl hyperfine coupling of one electron reduced MSR, which contains the FMN flavin semiquinone, is affected by the binding of  $\text{NADP}^+$ . This suggests that the environment of the FMN cofactor is changed by the binding of  $\text{NADP}^+$ . The 8-methyl line becomes narrower, i.e there is a smaller anisotropy,

indicating an increase in the rotation of the 8-methyl group, although the actual rate of rotation cannot be determined quantitatively from the spectra. This suggests there is a change in the arrangement of the protein around the dimethylbenzene portion of the FMN cofactor, possibly increasing the solvent accessibility and leading to less steric hindrance at the methyl group. These data are consistent with and indicative of the movement of the FMN-binding domain within the diflavin reductase structure and function model.

The 8-methyl hyperfine coupling of the two electron reduced MSR, which contains FMN semiquinone and FAD semiquinone, is changed by the binding of AD. Compared to the data from the one electron reduced MSR, this change can be attributed to the FAD semiquinone. This suggests that the binding of AD affects the environment of the FAD cofactor. This data does not exclude the possibility of the change in the environment around the FMN cofactor while binding with AD, however, this change cannot be detected by ENDOR spectroscopy.

The ELDOR spectra of the two electron reduced MSR show the changes in the distance between FMN and FAD semiquinone with the binding of 2', 5'-ADP, NADP<sup>+</sup> and AD. The data clearly show that there are several inter-flavin distances measured from each ELDOR spectra. This suggests that MSR exist in several conformations at 80K. Each conformation represents an energy minimum and a 'frustrated' energy landscape where the lack of thermal energy at 80 K maintains the protein in a number of separate conformations which cannot convert at that temperature. The isolated MSR mainly exists in the conformations in which the two flavins are located far apart, 3.6-2.7 nm. The addition of 2', 5'-ADP maintains the equilibrium and possibly increases the distance between FAD and FMN cofactors. However, the binding of the NADP<sup>+</sup> moves the conformational equilibrium towards

shorter inter-flavin distances, between 2.7 and 1.8 nm. The binding of AD also moves the equilibrium towards short inter-flavin distances, but with a pattern of conformations that differ from that exhibited by NADP<sup>+</sup> bound MSR.

These results are consistent with the currently accepted model of diflavin reductase action in which the binding of substrates triggers the movements of the FMN-binding domain. In the case of the binding of NADP<sup>+</sup> and MS, it enables the FMN-binding domain to accept electrons from the FAD-binding domain and then donate to MS. The current model for electron transfer in the human MS-MSR system [118] suggests that the major interaction stabilising the MS-MSR complex occurs between the MS activation domain, AD, and the FMN binding domain. The nature of the equilibrium that governs conformation change in MSR has not previously been investigated. The ELDOR data presented in **Section 5.2.4** suggests that the equilibrium is not a simple ‘binary’ one, having two states ‘free’ and ‘bound’, but rather several conformational states can be identified suggesting that a conformational sampling mechanism may be operating. Surprisingly, given the models for the MS-MSR interaction exemplified by **Figure 9** in [118], the ELDOR data shows that the FAD to FMN distance decreases on binding to AD, relative to the distance between the flavin cofactors in the ‘resting’ enzyme with no effectors bound. This suggests that some revision of the current model of MS-MSR interactions is required, with consideration given to the location of the FAD domain within the MS-MSR complex. The MSR:AD complex has been shown to be less stable than the MSR-FMN-binding domain:AD complex [118] and this may be explained by the presence of the FAD domain in relatively close proximity to the FMN-binding domain in the MSR:AD complex (see **Section 1.4.4**). Moreover the presence of the FAD-binding domain of MSR affects the AD binding stoichiometry

[118], it being two AD to one MSR, but a one to one stoichiometry when only the FMN-binding domain of MSR was used. This also suggests that the FAD-binding domain of MSR plays a role in MSR-AD, and therefore MSR-MS, interactions, in keeping with the ELDOR data showing that the binding of AD shortens the distance between the FAD and FMN binding domains of MSR.

**CHAPTER SIX**  
**CRYSTALLOGRAPHY OF THE ACTIVATION DOMAIN OF**  
**METHIONINE SYNTHASE**

## 6.1. Introduction

Human MSR is a 78 kDa flavoprotein and its physiological function is to regenerate the active form of cobalamin-dependent methionine synthase by passing one electron from FMN, a cofactor of MSR, to cobalamin, the cofactor of MS. Structural studies on MS have suggested that MS is a multi-domain cobalamin-dependent enzyme which consists of four domains: from N to C terminus, a homocysteine binding domain, a CH<sub>3</sub>-H<sub>4</sub>folate binding domain, a cobalamin binding domain and a S-adenosylmethionine binding domain, which is also termed the activation domain of MS [30]. The activation domain of MS interacts with the FMN-binding domain of MSR. Research on the complex of these two domains has shown that mutagenesis of putative interface residues of human MS and MSR, Lys<sup>1071</sup> and Lys<sup>987</sup>, decreases the binding affinity between these two domains. High ionic strength conditions can also lower the binding affinity [118]. These results illustrate that the electrostatic interaction heavily affects the binding affinity of the complex between MS and MSR. In addition, isothermal titration calorimetry measurements of the binding stoichiometry of the FMN binding domain with the activation domain of MS revealed a stoichiometry of 1:2, and the midpoint reduction potential of the complex was not affected relative to the MSR on binding activation domain [118]. Also, kinetic data for electron transfer in MSR was similar for MSR alone and the MSR-MS complex [118]. Currently, most of the structural information for human MS has been inferred based on the structure of *E. coli* MetH [30], but the structure of the activation domain of human MS was successfully solved in the Scrutton group [2]. The crystal structure of the activation domain of MS solved at 1.6 Å resolution consists of one C-shaped structure with an  $\alpha$  and  $\beta$  region mixed core which are mainly dominated by a twisted  $\beta$ -sheet with a  $\beta$ -mender region. This structure is

similar to the structure of MetH, however, the distinct difference between the human MS and MetH is that there is an extended  $3_{10}$ -containing loop in human MS. This structure is perhaps related to their different binding stoichiometry.

In an attempt to clearly understand the structural relationship between MS and MSR a structure for the complex of the two proteins is required. After purification of the activation domain of MS and full-length MSR, these two domains were mixed in a 2:1 stoichiometry to perform crystallization of the complex of the activation domain of MS and MSR. In an attempt to determine the structure of the full length MSR and to overcome the difficulties met in the purification of MSR, two expression plasmids were constructed: the first plasmid contains one GST tag, cDNA of MSR and one (His)<sub>6</sub> tag. The MSR protein which was expressed by this plasmid in *E. coli* BL21(DE3) can potentially be purified by two affinity chromatography procedures, using the GST tag and (His)<sub>6</sub> tag on the MSR protein. The glutathione-Sepharose 4B column binds the MSR-GST fusion protein. After incubation with thrombin, the GST tag is cleaved from MSR; thereafter the Ni-NTA His resin column can be used to purify the MSR protein via the (His)<sub>6</sub> tag. This two-step affinity chromatography method quickly accomplishes the purification of MSR and should avoid the problem of proteolysis which has been observed in previous purifications of MSR. The second expression plasmid is designed to express MSR in *Pichia Pastoris*, which is a yeast-expression system that combines the advantages of both prokaryotic and eukaryotic expression systems [154]. As an example, the methylotrophic yeast *Pichia pastoris* provides high yield of recombinant proteins which can be grown in high cell densities using minimal media and offers a cost-effective method for <sup>13</sup>C-labelled protein production for NMR structural analyses. The gene of the target protein expressed in *Pichia pastoris* can be regulated strongly

and tightly by the alcohol oxidase1 (AOX1) promoter. The construction of these two plasmids was confirmed by sequencing of the expression plasmids and Western Blot analysis of the expressed protein.

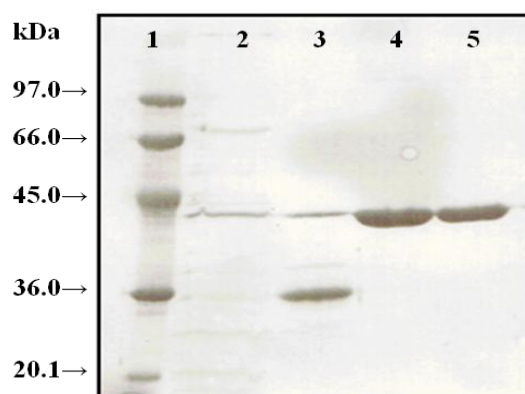
In this chapter, the results of the purification and crystallization of the activation domain of MS and the construction of the two MSR expression plasmids are demonstrated and discussed.

## **6.2. Results**

### **6.2.1. Expression and purification of the activation domain of MS**

The activation domain of MS was previously cloned in plasmid pET23d with a C-terminal His-tag. This plasmid was transformed to BL21(DE3) and the protein of the activation domain of MS was expressed. The expressed protein was purified according to the method of Wolthers *et al* [2]. The purified protein was analysed by 10% SDS-PAGE electrophoresis. Compared to the protein marker ladder, the molecular mass of the sample was consistent with the molecular mass deduced from the amino acid sequences of the activation domain of MS confirming that the purified sample was the activation domain of MS with the purity of a single band in 10% SDS-PAGE electrophoresis. This purified protein was dialysed against buffer overnight and stored -80 °C with 10 % glycerol for use in crystallography experiments.



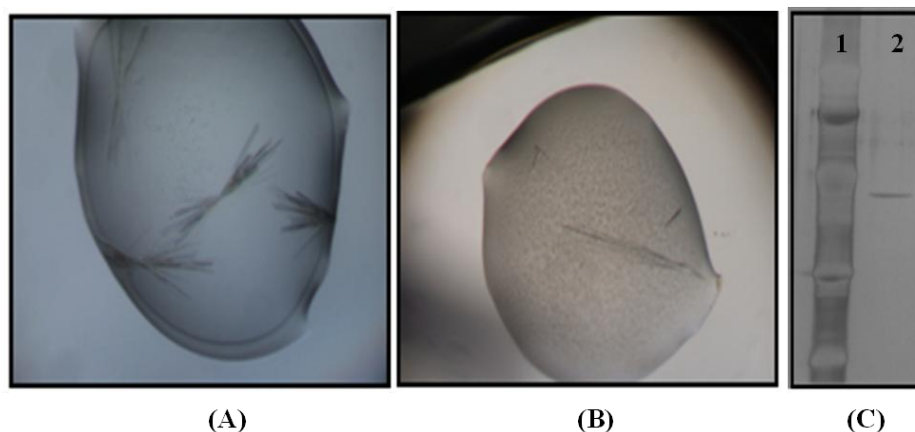


**Figure 6.1 10 % SDS/PAGE electrophoresis of the activation domain of MS.** Lane 1: molecular marker with molecular weight of 97.0, 66.0, 45.0, 36.0, 20.1 and 14.4 kDa. Lane 2: the cell lysates after sonification; Lane 3: the protein collected from the Ni-NTA resin column; Lane 4: the protein collected from the Q-Sepharose column.

### 6.2.2. Crystallography of the activation domain of MS

The previously determined crystal structure for activation was that of a mutant form which aided crystallogenesi. In this work attempts were made to grow crystals of the wild-type activation domain. A crystallography experiment on the activation domain of MS was carried out using the sitting drop vapour diffusion method at 19 °C. The protein sample at a concentration of 15 mg/mL was mixed with the detergents in PEG/Ion Screen Solution for Crystal Growth of HAMPTON RESEARCH Corp on the Mosquito robot machine. The sealed crystal screening plates were stored in the 19 °C fridge for about one week. One week later, needle-like crystals had grown under three conditions. 1).0.1 mM tris-sodium citrate pH5.5, 20% w/v PEG3000; 2). 0.1 M tris-sodium citrate 15% w/v PEG3000 and 3). 0.2 M sodium malonate 20% w/v PEG 3350. Some crystals were picked out with a loop and washed with buffer in the reservoir and ddH<sub>2</sub>O. The crystals were then dissolved and run on a 12% SDS-PAGE gel. The resulting electrophoresis gel was developed with a silver staining kit. The band of the dissolved crystals in the SDS electrophoresis gel have a molecular mass of ~38 kDa, which is consistent with the

calculated molecular mass of the activation domain of MS, so these crystals were the protein crystal of the wild type activation domain of MS (**Figure 6.2**). Despite obtaining crystals, they were not suitable for diffraction analysis and future work will need to refine conditions to obtain crystals of diffraction quality.



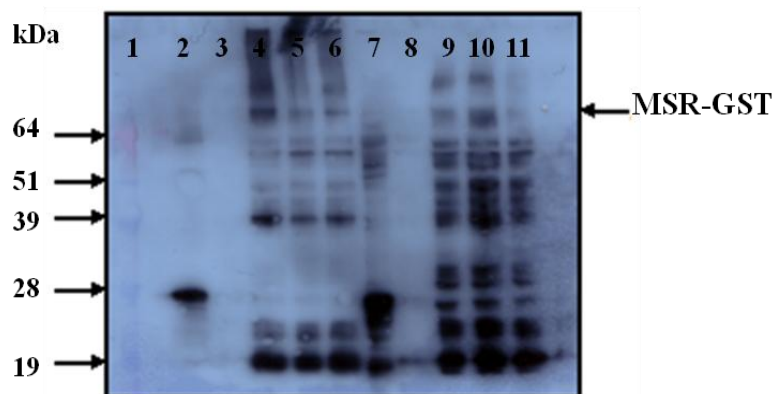
**Figure 6.2** The crystals of the activation domain of MS. (A) & (B): photographs of the crystals of the activation domain of MS. (C). SDS-PAGE gel of the dissolved crystal of MS. Lane 1 is a low molecular weight marker (Amersham) comprised of proteins with the molecular weight of 97.0, 66.0, 45.0, 36.0, 20.1 and 14.4 kDa respectively. Lane 2 is the dissolved crystal protein.

### 6.2.3. The construction of two MSR expression plasmids.

In this chapter two new plasmid constructs were made: the first pET41aMSR was created to encode a N-terminal GST and a C-terminal His tag in an attempt to aid rapid purification of MSR, thereby preventing proteolysis. Expression from this construct is described in section 6.2.3.1. The second plasmid (pMSRGST) was created to facilitate expression in *Pichia pastoris*. Given the time available it was not possible to analyse extensively expression of MSR from each of these constructs. A preliminary analysis is reported for pET41aMSR (Figure 6.3); although the construction of pMSRGST is reported there was insufficient time to explore expression in *Pichia pastoris*.

### 6.2.3.1. The construction of pET41a and its expression of MSR.

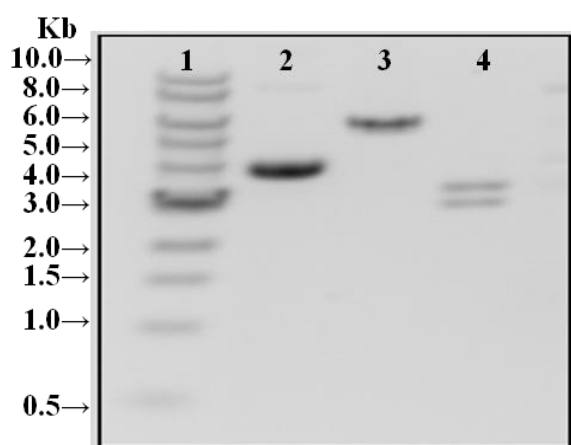
The plasmid, containing MSR cDNA, GST tag and (His)<sub>6</sub> tag (**Figure 2.1**) was verified by restriction enzyme digestion. The plasmid was transformed into *E. coli* BL21 to express MSR. A Western blot experiment validated the expression of the MSR protein (**Figure 6.3**). From the result of the Western blot analysis some bands below the MSR-GST band suggest that proteolysis of MSR-GST has occurred at some period during the cell growth. Further analysis of purified MSR expressed from this construct will now need to be performed to ascertain the level (if any) of proteolysis in the final purified protein product. Preliminary attempts to express the double tagged protein indicated that the level of recombinant protein expression was much lower than that for the GST-MSR fusion protein used for studies reported elsewhere in this thesis.



**Figure 6.3: Western Blot analysis for the expression of MSR containing two tags produced in *E. coli* BL21.** Lane 1 protein marker; Lane 2 and Lane 7 are the plasmid pET41a without IPTG at 16 hours and 3 hours; Lane 3, Lane 4, Lane 5 and Lane 6 are the cell lysate at 16 hours after the adding IPTG to a final concentration of 0 mM, 0.1 mM, 0.5mM, 1 mM; Lane 8, Lane 9, Lane 10 and Lane 11 are the cell lysate at 3 hours after the adding IPTG to a final concentration at 0 mM, 0.1 mM, 0.5 mM, 1 mM..

### 6.2.3.2. The construction of pMSRGST

The newly constructed plasmid pMSRGST (**Figure 2.2**) was verified by the restriction enzymes digestion reaction with NotI and NcoI, or PmeI alone, at 37 °C for 2 hours. The size of the restriction fragments observed by 1 % agarose electrophoresis confirmed that the clone was consistent in design. The sequencing result (**Figure 6.4**) from Company MWG confirmed the sequence integrity of this plasmid. Restriction digest analysis and DNA sequencing indicated that the new construct had been made successfully. Future work will now need to explore if the GST-MSR fusion protein can be synthesised in active form in *Pichia pastoris*.



**Figure 6.4: The digestion result of the construct expression vector containing GST tag, 6×His tag and MSR cDNA.** Lane 1: 1 Kb DNA ladder with molecular weight of 10.0, 8.0, 6.0, 5.0, 4.0, 3.0, 2.0, 1.5, 1.0 and 0.5 Kb; Lane 2: the construct plasmid, Lane 3: plasmid digested by NotI, Lane 4: plasmid digested by NotI and NcoI.



purification was completed and confirmed. Further research is now needed in the area of protein expression, to identify a new purification protocol and the production of full length MSR crystals.

The work described in this chapter therefore supports further on-going studies of MSR and the MS-MSR complex. A key challenge is to build a more detailed structural picture of the complex and its component domains. This will require provision of highly purified proteins in a form suitable for structural determination. It is hoped that the progress on crystallogenesi and plasmid construct development will assist in this long term goal.

## **CHAPTER SEVEN**

### **DISCUSSION**

## 7.1. Discussion

This PhD research program on MSR includes research on the crystal structure of the FAD/NADPH binding domain of MSR, kinetic and thermodynamic studies on the mutants of the FAD/NADPH binding domain of MSR and full-length MSR and the electron magnetic resonance spectroscopy, EPR, ENDOR, ESEEM and ELDOR on full-length MSR.

In studies of the crystal structure of the FAD/NADPH binding domain of MSR, the expressed recombinant protein was purified by affinity and anion-exchange chromatography to produce a protein that crystallized and diffracted to 1.9 Å. This protein crystal was subjected to X-ray diffraction studies, and the crystal structure was built. The study identified the binding sites for cofactors NADPH and FAD. As with other members in the diflavin reductase, MSR consists of two domains: the FMN binding domain in the N-terminal region and the FAD/NADPH binding domain on the C-terminal. One important structural feature of MSR is the extended hinge region which includes 82 residues. It is suggested that this long hinge region is involved in the large scale motion of the FMN binding domain of MSR, which is believed to play a part in the transfer of electrons from FAD to MS. The expected interflavin electron transfer rate for this diflavin reductase family is about  $10^7$  to  $10^8$  s<sup>-1</sup> if one uses the crystal structure of CPR or NOS to calculate theoretical values for electron transfer based on Marcus theory. However, the interflavin electron transfer rate for MSR is only 0.2 s<sup>-1</sup> [68], suggesting that electron transfer is not rate limiting and that conformational motion controls the rate of interflavin electron transfer. This idea is consistent with the ELDOR studies reported in Chapter five that indicate the FMN domain of MSR is mobile with respect to the FAD domain supporting the idea that conformational motion is an important part of the



interflavin electron transfer mechanism. These dynamic features are believed to be related to the physiological function of MSR. MSR only functions to regenerate the inert MS every 200 to 1000 catalytic cycles, and therefore catalysis can be slow. The rate of hydride transfer from NADPH to FAD in MSR is also relatively slow suggesting that high catalytic turnover is not important for physiological function.

Based on the crystal structure of the FAD/NADPH binding domain of MSR, the kinetic and thermodynamic studies on mutants of the FAD/NADPH binding domain and full-length MSR were completed. The mutants of MSR focus on two residues Asp<sup>652</sup> and Trp<sup>697</sup>. The Asp<sup>652</sup> is only 4-5Å distance to the pyrophosphate moiety of the substrate NADPH. The mutants at this position were designed to change the electrostatic charge and residue volume at this position by converting the natural residue to a series of variants (D652A, D652R and D652N). These mutants strongly decreased both the binding affinity of NADPH and the turnover numbers. The positive shift in the redox potentials of the FAD of the mutants was attributed to the slowness of the electron transfer rate from NADPH to FAD. Another residue Trp<sup>697</sup>, which is a conserved residue in the diflavin reductase family, packs on the face of isoalloxazine ring of FAD to form  $\pi$ - $\pi$  interaction with FAD. Combined with the binding residues for the 2'-phosphate of NADPH, this Trp<sup>697</sup> involves the stabilization of the binding of NADPH and also affects the selectivity with different coenzymes, such as NADPH and NADH. The mutants possessing changes at this position showed decreased catalytic ability of MSR and the emission of tryptophan fluorescence consistent with removal of the tryptophan side chain. This perhaps can be explained by the fact that the replacements from tryptophan to alanine and histidine have the isoalloxazine ring more exposed to water which further triggers the change of redox potential of FAD, resulting in a greater energy cost on the

electron transfer to the physiological electron acceptor. All these results verify that these two residues Asp<sup>652</sup> and Trp<sup>697</sup> are key determinants in the reductive half reaction of MSR.

Recent studies in structural biology have revealed that conformational change plays a significant role on the catalysis on the diflavin reductase family. To investigate the effect of conformational change on full length MSR, EPR, ENDOR, ESEEM and ELDOR techniques were applied to the wild type full-length MSR and to complexes of MSR-NADP, MSR-2'5'ADP, MSR-the activation domain of MS. The results of EPR, ENDOR, and ESEEM all confirmed the existence of the semiquinone form of FAD and FMN during the catalytic turnover. ELDOR provided the distance change between the two semiquinones which is a reliable indication for the conformational change of MSR. Combined data indicate the highly dynamic properties of MSR as inferred from the presence of the long interdomain linker between the FAD and FMN binding domains.

## **7.2. Further investigation**

In order to clearly understand the relationship between the structure and function of MSR, more biochemical experiments need to be carried out in future.

Using the crystallization conditions developed for the successful crystallization on the FAD/NADPH binding domain of MSR, the FMN binding domain of MSR and the full length MSR can be considered. To solve the difficulty in the full length MSR, the new expression plasmids which contain GST tag and (His)<sub>6</sub> tag together, can be expressed in *E.coli* system and *Pichia Pastoris*, further improvement on the purification and crystallization can be completed. Another

crystallization experiment on the complex of MSR-AD of MS is also suggested in future.

Based on the electronic structural research on MSR, using techniques such as EPR, ENDOR, ESEEM and ELDOR, more advanced interdisciplinary experiments on the dynamics structure of MSR should be carried out. The measurement of the relaxation time to determine the distance between the FMN semiquinone and FAD semiquinone has been finished, so the same method can be applied to measure the distance between the FMN semiquinone of MSR with the Co(II) cofactor of MS. Also, measurement of the distance change on these two cofactors with the addition of ligands such as  $\text{NADP}^+$  will provide some new illustration on the conformational change of the MS-MSR complex.

Focusing on the dynamic studies on the enzyme, the time dependent structural change in the MS-MSR catalysis process also could be researched. An advanced technology, fluorescence resonance energy transfer, FRET, could also be considered. FRET is a powerful technique used to measure the distance for 10Å to 75Å of two dyes [155]. At the single molecule level, single pair fluorescence resonance energy transfer, spFRET, has been successfully applied to the kinetic and conformational change of single domain proteins [156]. If spFRET were to be applied to the complex of MS-MSR, it could assist in completing the interprotein dynamic research on the larger protein complex.

## **REFERENCES**

- 1 Wolthers, K. R., Basran, J., Munro, A. W. and Scrutton, N. S. (2003) Molecular dissection of human methionine synthase reductase: Determination of the flavin redox potentials in full-length enzyme and isolated flavin-binding domains. *Biochemistry*. **42**, 3911-3920
- 2 Wolthers, K. R., Toogood, H. S., Jowitt, T. A., Marshall, K. R., Leys, D. and Scrutton, N. S. (2007) Crystal structure and solution characterization of the activation domain of human methionine synthase. *Febs J*. **274**, 738-750
- 3 Wolthers, K. R., Lou, X. D., Toogood, H. S., Leys, D. and Scrutton, N. S. (2007) Mechanism of coenzyme binding to human methionine synthase reductase revealed through the crystal structure of the FNR-like module and isothermal titration calorimetry. *Biochemistry*. **46**, 11833-11844
- 4 Navaza, J. (2001) Implementation of molecular replacement in AMoRe. *Acta Crystallogr D*. **57**, 1367-1372
- 5 Galli, C., MacArthur, R., AbuSoud, H. M., Clark, P., Stuehr, D. J. and Brudvig, G. W. (1996) EPR spectroscopic characterization of neuronal NO synthase (vol 35, pg 2804, 1996). *Biochemistry*. **35**, 7298-7298
- 6 Schweiger, A. and Jeschke, G. (2001) Principles of Pulse Electron Paramagnetic Resonance Spectroscopy
- 7 Kay, C. W. M., Elsasser, C., Bittl, R., Farrell, S. R. and Thorpe, C. (2006) Determination of the distance between the two neutral flavin radicals in augementer of liver regeneration by pulsed ELDOR. *J Am Chem Soc*. **128**, 76-77
- 8 Hay, S., Brenner, S., Khara, B., Quinn, A. M., Rigby, S. E. J. and Scrutton, N. S. (2010) Nature of the Energy Landscape for Gated Electron Transfer in a Dynamic Redox Protein. *J Am Chem Soc*. **132**, 9738-9745
- 9 [http://academic.brooklyn.cuny.edu/biology/bio4fv/page/coenzy\\_.htm](http://academic.brooklyn.cuny.edu/biology/bio4fv/page/coenzy_.htm). coenzymes and cofactors.
- 10 Jordan, F., Patel, M. S. and Editors. (2004) Thiamine: Catalytic Mechanisms in Normal and Disease States. [In: *Oxid. Stress Dis.*, 2004; 11]
- 11 <http://www.elmhurst.edu/~chm/vchembook/571cofactor.html>. coenzymes.
- 12 Palmer, T. (1981) *Understanding Enzymes*
- 13 Metzler, D. E. (2001) *Biochemistry: The Chemical Reactions of Living Cells, Volume 1; Second Edition*
- 14 Bryce, C. F. A. (1979) SAM - semantics and misunderstandings. *Trends Biochem. Sci.* (Pers. Ed.). **4**, N62-N63
- 15 Sigel, H. (1973) *Metal Ions in Biological Systems, Vol. 2: Mixed-Ligand Complexes*

- 16 Aggett, P. J. (1985) Physiology and Metabolism of Essential Trace-Elements - an Outline. *Clin Endocrinol Meta.* **14**, 513-543
- 17 Li, H. Y. and Poulos, T. L. (2005) Structure-function studies on nitric oxide synthases. *J Inorg Biochem.* **99**, 293-305
- 18 Prohaska, J. R. (2008) Role of copper transporters in copper homeostasis. *Am J Clin Nutr.* **88**, 826s-829s
- 19 Brugna, M., Tasse, L. and Hederstedt, L. (2010) In vivo production of catalase containing haem analogues. *Febs J.* **277**, 2663-2672
- 20 Doleh, L. and Romani, A. (2007) Biphasic effect of extra-reticular Mg<sup>2+</sup> on hepatic G6P transport and hydrolysis. *Arch Biochem Biophys.* **467**, 283-290
- 21 Ilies, M., Di Costanzo, L., North, M. L., Scott, J. A. and Christianson, D. W. (2010) 2-Aminoimidazole Amino Acids as Inhibitors of the Binuclear Manganese Metalloenzyme Human Arginase I. *J Med Chem.* **53**, 4266-4276
- 22 Cerqueira, N. M. F. S. A., Gonzalez, P. J., Brondino, C. D., Romao, M. J., Romao, C. C., Moura, I. and Moura, J. J. G. (2009) The Effect of the Sixth Sulfur Ligand in the Catalytic Mechanism of Periplasmic Nitrate Reductase. *J Comput Chem.* **30**, 2466-2484
- 23 Kaluarachchi, H., Chan-Chung, K. C. and Zamble, D. B. Microbial nickel proteins. *Natural Product Reports.* **27**, 681-694
- 24 Akil, M., Gurbuz, U., Bicer, M., Sivrikaya, A., Mogulkoc, R., Baltaci, A.K. (2010) Effect of Selenium Supplementation on Lipid Peroxidation, Antioxidant Enzymes, and Lactate Levels in Rats Immediately After Acute Swimming Exercise Biological Trace Element Research
- 25 Maurmann, L. and Bose, R. N. (2010) Unwinding of zinc finger domain of DNA polymerase I by cis-diamminedichloroplatinum(II). *Dalton T.* **39**, 7968-7979
- 26 Muller Ingrid, B., Bergmann, B., Groves Matthew, R., Couto, I., Amaral, L., Begley Tadhg, P., Walter Rolf, D. and Wrenger, C. (2009) The vitamin B1 metabolism of *Staphylococcus aureus* is controlled at enzymatic and transcriptional levels. *PloS one.* **4**, e7656
- 27 Kirkland, J. B. (2003) Niacin and carcinogenesis. *Nutrition and Cancer.* **46**, 110-118
- 28 Kanouchi, H., Shibuya, M., Tsukamoto, S., Fujimura, Y., Tachibana, H., Yamada, K. and Oka, T. (2010) Comparisons of uptake and cell surface binding among pyridoxal, pyridoxine, and pyridoxamine in RAW264.7 cells. *Nutrition.* **26**, 648-652
- 29 Bryk, R., Arango, N., Venugopal, A., Warren, J. D., Park, Y. H., Patel, M. S., Lima, C. D. and Nathan, C. (2010) Triazaspirodimeoxybenzoyls as Selective Inhibitors of Mycobacterial Lipoamide Dehydrogenase. *Biochemistry.* **49**, 1616-1627

- 30 Ludwig, M. L. and Matthews, R. G. (1997) Structure-based perspectives on B-12-dependent enzymes. *Annu Rev Biochem.* **66**, 269-313
- 31 Gasser, B., Dragosits, M. and Mattanovich, D. (2010) Engineering of biotin-prototrophy in *Pichia pastoris* for robust production processes. *Metabolic Engineering*. **In Press, Corrected Proof**
- 32 Leonardi, R., Zhang, Y. M., Rock, C. O. and Jackowski, S. (2005) Coenzyme A: Back in action. *Prog Lipid Res.* **44**, 125-153
- 33 Joosten, V. and van Berkel, W. J. H. (2007) Flavoenzymes. *Curr Opin Chem Biol.* **11**, 195-202
- 34 Mack, M. and Grill, S. (2006) Riboflavin analogs and inhibitors of riboflavin biosynthesis. *Appl Microbiol Biot.* **71**, 265-275
- 35 Bugg, T. and Editor. (1996) Introduction to Enzyme and Coenzyme Chemistry
- 36 Chiang, P. K., Gordon, R. K., Tal, J., Zeng, G. C., Doctor, B. P., Pardhasaradhi, K. and McCann, P. P. (1996) S-adenosylmethionine and methylation. *Faseb J.* **10**, 471-480
- 37 Noll, K. M., Rinehart, K. L., Tanner, R. S. and Wolfe, R. S. (1986) Structure of Component-B (7-Mercaptoheptanoylthreonine Phosphate) of the Methylcoenzyme-M Methylreductase System of *Methanobacterium-Thermoautotrophicum*. *P Natl Acad Sci USA.* **83**, 4238-4242
- 38 Balch, W. E. and Wolfe, R. S. (1979) Specificity and Biological Distribution of Coenzyme M (2-Mercaptoethanesulfonic Acid). *J Bacteriol.* **137**, 256-263
- 39 Crane, F. L. (2001) Biochemical functions of coenzyme Q10. *Journal of the American College of Nutrition.* **20**, 591-598
- 40 Wijayanti, N., Katz, N. and Immenschuh, S. (2004) Biology of heme in health and disease. *Curr Med Chem.* **11**, 981-986
- 41 Meister, A. and Anderson, M. E. (1983) Glutathione. *Annu Rev Biochem.* **52**, 711-760
- 42 Mendel, R. R. and Bittner, F. (2006) Cell biology of molybdenum. *Bba-Mol Cell Res.* **1763**, 621-635
- 43 Pai, E. F., Karplus, P. A. and Schulz, G. E. (1988) Crystallographic Analysis of the Binding of Nadph, Nadph Fragments, and Nadph Analogues to Glutathione-Reductase. *Biochemistry.* **27**, 4465-4474
- 44 Medina, M. (2009) Structural and mechanistic aspects of flavoproteins: photosynthetic electron transfer from photosystem I to NADP(+). *Febs J.* **276**, 3942-3958

- 45 Berg, I. A., Kockelkorn, D., Ramos-Vera, W. H., Say, R. F., Zarzycki, J., Hugler, M., Alber, B. E. and Fuchs, G. (2010) Autotrophic carbon fixation in archaea. *Nat Rev Microbiol.* **8**, 447-460
- 46 Brutnell, T. P., Wang, L., Swartwood, K., Goldschmidt, A., Jackson, D., Zhu, X., Kellogg, E., and Van Ecka, J. (2010) *Setaria viridis*: A Model for C4 Photosynthesis. *The Plant Cell*
- 47 Cabezas, H., Raposo, R. R. and Melendez-Hevia, E. (1999) Activity and metabolic roles of the pentose phosphate cycle in several rat tissues. *Mol Cell Biochem.* **201**, 57-63
- 48 Sassi, N., Paul, C., Martin, A., Bettaieb, A. and Jeannin, J.-F. (2010) Lipid a-induced responses in vivo. *Advances in experimental medicine and biology.* **667**, 69-80
- 49 Wei, C.-C., Motl, N., Levek, K., Chen, L. Q., Yang, Y.-P., Johnson, T., Hamilton, L. and Stuehr, D. J. (2010) Conformational states and kinetics of the calcium binding domain of NADPH oxidase 5. *Open Biochemistry Journal.* **4**, 59-67
- 50 Myasoedova, K. N. and Timofeev, K. N. (2010) Conformational Changes near the Cytochrome P450 Active Site upon Binding of Two Different Ligands. *Biochemistry-Moscow.* **75**, 899-904
- 51 Rather, L. J., Knapp, B., Haehnel, W. and Fuchs, G. (2010) Coenzyme A-dependent Aerobic Metabolism of Benzoate via Epoxide Formation. *J Biol Chem.* **285**, 20615-20624
- 52 Hatanosa, F., Takagi, Y. and Shikita, M. (1973) Hydrogen Transfer from Nadph to Steroid by Testicular 20-Alpha-Hydroxysteroid Dehydrogenase - Stereospecificity and Isotope-Effect. *J Biochem-Tokyo.* **74**, 1065-1067
- 53 Kono, H., Rusyn, I., Yin, M., Gabele, E., Yamashina, S., Dikalova, A., Kadiiska, M. B., Connor, H. D., Mason, R. P., Segal, B. H., Bradford, B. U., Holland, S. M. and Thurman, R. G. (2000) NADPH oxidase-derived free radicals are key oxidants in alcohol-induced liver disease. *J Clin Invest.* **106**, 867-872
- 54 Hoban, P. R., Walton, M. I., Robson, C. N., Godden, J., Stratford, I. J., Workman, P., Harris, A. L. and Hickson, I. D. (1990) Decreased Nadph - Cytochrome-P-450 Reductase-Activity and Impaired Drug Activation in a Mammalian-Cell Line Resistant to Mitomycin-C under Aerobic but Not Hypoxic Conditions. *Cancer Research.* **50**, 4692-4697
- 55 Randaccio, L., Geremia, S., Demitri, N. and Wuerges, J. (2010) Vitamin B-12: Unique Metalorganic Compounds and the Most Complex Vitamins. *Molecules.* **15**, 3228-3259
- 56 Lenhert, P. G. and Hodgkin, D. C. (1961) Structure of 5,6-Dimethylbenzimidazolylcobamide Coenzyme. *Nature.* **192**, 937-938
- 57 Blakley, R. L. (1969) *The Biochemistry of Folic Acid and Related Pteridines* (Frontiers of Biology, Vol. 13)



- 58 Michel, C., Buckel, W. and Linder, D. (1991) Purification of the Coenzyme B12-Containing 2-Methyleneglutarate Mutase from *Clostridium-Barkeri* by High-Performance Liquid-Chromatography. *Journal of Chromatography*. **587**, 93-99
- 59 Shen, A. L. and Kasper, C. B. (2000) Differential contributions of NADPH-cytochrome P450 oxidoreductase FAD binding site residues to flavin binding and catalysis. *J Biol Chem*. **275**, 41087-41091
- 60 Wolthers, K. R. and Scrutton, N. S. (2004) Electron transfer in human methionine synthase reductase studied by stopped-flow spectrophotometry. *Biochemistry*. **43**, 490-500
- 61 Ghisla, S., Massey, V., Lhoste, J. M. and Mayhew, S. G. (1974) Fluorescence and Optical Characteristics of Reduced Flavines and Flavoproteins. *Biochemistry*. **13**, 589-597
- 62 Ghisla, S. and Massey, V. (1989) Mechanisms of Flavoprotein-Catalyzed Reactions. *European Journal of Biochemistry*. **181**, 1-17
- 63 Muller, F., Walker, W. H., Massey, V., Brustle, M. and Hemmerich, P. (1972) Light-Absorption Studies on Neutral Flavin Radicals. *European Journal of Biochemistry*. **25**, 573-&
- 64 Sancho, J. (2006) Flavodoxins: sequence, folding, binding, function and beyond. *Cellular and Molecular Life Sciences*. **63**, 855-864
- 65 Mukherjee, T., Zhang, Y., Abdelwahed, S., Ealick, S. E. and Begley, T. P. (2010) Catalysis of a Flavoenzyme-Mediated Amide Hydrolysis. *J Am Chem Soc*. **132**, 5550-5551
- 66 Tu, S. C., Lei, B. F., Liu, M. Y., Tang, C. K. and Jeffers, C. (2000) Probing the mechanisms of the biological intermolecular transfer of reduced flavin. *Journal of Nutrition*. **130**, 331s-332s
- 67 Awad, S., Henderson, G. B., Cerami, A. and Held, K. D. (1992) Effects of Trypanothione on the Biological-Activity of Irradiated Transforming DNA. *International Journal of Radiation Biology*. **62**, 401-407
- 68 Murataliev, M. B., Feyereisen, R. and Walker, A. (2004) Electron transfer by diflavin reductases. *Biochimica Et Biophysica Acta-Proteins and Proteomics*. **1698**, 1-26
- 69 Damiani, M. J., Yalloway, G. N., Lu, J., McLeod, N. R. and O'Neill, M. A. (2009) Kinetic Stability of the Flavin Semiquinone in Photolyase and Cryptochrome-DASH. *Biochemistry*. **48**, 11399-11411
- 70 Wang, Z., Chernyshev, A., Koehn, E. M., Manuel, T. D., Lesley, S. A. and Kohen, A. (2009) Oxidase activity of a flavin-dependent thymidylate synthase. *Febs J*. **276**, 2801-2810
- 71 Despicic, P. O. and Maloy, S. (1993) Puta Protein, a Membrane-Associated Flavin Dehydrogenase, Acts as a Redox-Dependent Transcriptional Regulator. *P Natl Acad Sci USA*. **90**, 4295-4298

- 72 Mallett, T. C., Wallen, J. R., Karplus, P. A., Sakai, H., Tsukihara, T. and Claiborne, A. (2006) Structure of coenzyme A-disulfide reductase from *Staphylococcus aureus* at 1.54 angstrom resolution. *Biochemistry*. **45**, 11278-11289
- 73 Niederpruem, D. J. and Hackett, D. P. (1958) The Oxygen Affinity of a Flavin Oxidase Involved in the Respiration of *Streptococcus Faecalis*. *Plant Physiology*. **33**, 113-115
- 74 Eswaramoorthy, S., Bonanno, J. B., Burley, S. K. and Swaminathan, S. (2006) Mechanism of action of a flavin-containing monooxygenase. *P Natl Acad Sci USA*. **103**, 9832-9837
- 75 Karplus, P. A., Daniels, M. J. and Herriott, J. R. (1991) Atomic-Structure of Ferredoxin-Nadp<sup>+</sup> Reductase - Prototype for a Structurally Novel Flavoenzyme Family. *Science*. **251**, 60-66
- 76 Watenpugh, K. D., Sieker, L. C. and Jensen, L. H. (1973) Binding of riboflavine 5'-phosphate in a flavoprotein. Flavodoxin at 2.0 Ang. resolution. *Proc. Nat. Acad. Sci. U. S. A.* **70**, 3857-3860
- 77 Gutierrez, A., Munro, A. W., Grunau, A., Wolf, C. R., Scrutton, N. S. and Roberts, G. C. K. (2003) Interflavin electron transfer in human cytochrome P450 reductase is enhanced by coenzyme binding - Relaxation kinetic studies with coenzyme analogues. *European Journal of Biochemistry*. **270**, 2612-2621
- 78 Zhang, J., Martasek, P., Paschke, R., Shea, T., Masters, B. S. S. and Kim, J. J. P. (2001) Crystal structure of the FAD/NADPH-binding domain of rat neuronal nitric-oxide synthase - Comparisons with NADPH-cytochrome P450 oxidoreductase. *J Biol Chem*. **276**, 37506-37513
- 79 Finn, R. D., Basran, J., Roitel, O., Wolf, C. R., Munro, A. W., Paine, M. J. I. and Scrutton, N. S. (2003) Determination of the redox potentials and electron transfer properties of the FAD- and FMN-binding domains of the human oxidoreductase NR1. *European Journal of Biochemistry*. **270**, 1164-1175
- 80 Haines, D. C., Tomchick, D. R., Machius, M. and Peterson, J. A. (2001) Pivotal role of water in the mechanism of P450BM-3. *Biochemistry*. **40**, 13456-13465
- 81 Crane, B. R., Siegel, L. M. and Getzoff, E. D. (1995) Sulfite Reductase Structure at 1.6 Angstrom - Evolution and Catalysis for Reduction of Inorganic Anions. *Science*. **270**, 59-67
- 82 Wada, F., Shibata, H., Goto, M. and Sakamoto, Y. (1968) Participation of Microsomal Electron Transport System Involving Cytochrome P-450 in Omega-Oxidation of Fatty Acids. *Biochim Biophys Acta*. **162**, 518-524
- 83 Gusarov, I., Starodubtseva, M., Wang, Z. Q., McQuade, L., Lippard, S. J., Stuehr, D. J. and Nudler, E. (2008) Bacterial nitric-oxide synthases operate without a dedicated redox partner (vol 283, pg 13140, 2008). *J Biol Chem*. **283**, 19164-19164

- 84 Kurzban, G. P. and Strobel, H. W. (1986) Preparation and Characterization of Fad-Dependent Nadph-Cytochrome P-450 Reductase. *J Biol Chem.* **261**, 7824-7830
- 85 Thaete, L. G., Siegel, D., Malkinson, A. M., Forrest, G. L. and Ross, D. (1991) Nad(P)H-Quinone Oxidoreductase (Dt-Diaphorase) Activity and Messenger-Rna Content in Normal and Neoplastic Mouse Lung Epithelia. *Int J Cancer.* **49**, 145-149
- 86 Iyanagi, T. (1990) On the Mechanism of One-Electron Reduction of Quinones by Microsomal Flavin Enzymes - the Kinetic-Analysis between Cytochrome-B5 and Menadione. *Free Radical Res Com.* **8**, 259-268
- 87 Weber, M. M., Lenhoff, H. M. and Kaplan, N. O. (1956) Reduction of Inorganic Iron and Cytochrome-C by Flavin Enzymes. *J Biol Chem.* **220**, 93-104
- 88 Vermilion, J. L. and Coon, M. J. (1978) Identification of the High and Low Potential Flavins of Liver Microsomal Nadph-Cytochrome P-450 Reductase. *J Biol Chem.* **253**, 8812-8819
- 89 Yoshimoto, A. and Sato, R. (1968) Studies on Yeast Sulfite Reductase .I. Purification and Characterization. *Biochim Biophys Acta.* **153**, 555-575
- 90 Wang, M., Roberts, D. L., Paschke, R., Shea, T. M., Masters, B. S. S. and Kim, J. J. P. (1997) Three-dimensional structure of NADPH-cytochrome P450 reductase: Prototype for FMN- and FAD-containing enzymes. *P Natl Acad Sci USA.* **94**, 8411-8416
- 91 Gruez, A., Pignol, D., Zeghouf, M., Coves, J., Fontecave, M., Ferrer, J. L. and Fontecilla-Camps, J. C. (2000) Four crystal structures of the 60 kDa flavoprotein monomer of the sulfite reductase indicate a disordered flavodoxin-like module. *J Mol Biol.* **299**, 199-212
- 92 Watt, W., Tulinsky, A., Swenson, R. P. and Watenpaugh, K. D. (1991) Comparison of the Crystal-Structures of a Flavodoxin in Its 3 Oxidation-States at Cryogenic Temperatures. *J Mol Biol.* **218**, 195-208
- 93 Komori, H., Seo, D., Sakurai, T. and Higuchi, Y. (2010) Crystallization and preliminary X-ray studies of ferredoxin-NADP(+) oxidoreductase encoded by *Bacillus subtilis* yumC. *Acta Crystallogr F.* **66**, 301-303
- 94 Gutierrez, A., Lian, L. Y., Wolf, C. R., Scrutton, N. S. and Roberts, G. C. K. (2001) Stopped-flow kinetic studies of flavin reduction in human cytochrome P450 reductase and its component domains. *Biochemistry.* **40**, 1964-1975
- 95 Dunford, A. J., Rigby, S. E. J., Hay, S., Munro, A. W. and Scrutton, N. S. (2007) Conformational and thermodynamic control of electron transfer in neuronal nitric oxide synthase. *Biochemistry.* **46**, 5018-5029
- 96 Miller, R. T., Martasek, P., Omura, T. and Masters, B. S. S. (1999) Rapid kinetic studies of electron transfer in the three isoforms of nitric oxide synthase. *Biochem Bioph Res Co.* **265**, 184-188

- 97 Knight, K. and Scrutton, N. S. (2002) Stopped-flow kinetic studies of electron transfer in the reductase domain of neuronal nitric oxide synthase: re-evaluation of the kinetic mechanism reveals new enzyme intermediates and variation with cytochrome P450 reductase. *Biochem J.* **367**, 19-30
- 98 Garcin, E. D., Bruns, C. M., Lloyd, S. J., Hosfield, D. J., Tiso, M., Gachhui, R., Stuehr, D. J., Tainer, J. A. and Getzoff, E. D. (2004) Structural basis for isozyme-specific regulation of electron transfer in nitric-oxide synthase. *J Biol Chem.* **279**, 37918-37927
- 99 Shen, A. L., Porter, T. D., Wilson, T. E. and Kasper, C. B. (1989) Structural-Analysis of the Fmn Binding Domain of NADPH-Cytochrome P-450 Oxidoreductase by Site-Directed Mutagenesis. *J Biol Chem.* **264**, 7584-7589
- 100 Bastiaens, P. I. H., Bonants, P. J. M., Muller, F. and Visser, A. J. W. G. (1989) Time-Resolved Fluorescence Spectroscopy of NADPH Cytochrome-P-450 Reductase - Demonstration of Energy-Transfer between the 2 Prosthetic Groups. *Biochemistry.* **28**, 8416-8425
- 101 Olteanu, H., Wolthers, K. R., Munro, A. W., Scrutton, N. S. and Banerjee, R. (2004) Kinetic and thermodynamic characterization of the common polymorphic variants of human methionine synthase reductase. *Biochemistry.* **43**, 1988-1997
- 102 Munro, A. W., Noble, M. A., Robledo, L., Daff, S. N. and Chapman, S. K. (2001) Determination of the redox properties of human NADPH-cytochrome P450 reductase. *Biochemistry.* **40**, 1956-1963
- 103 Noble, M. A., Munro, A. W., Rivers, S. L., Robledo, L., Daff, S. N., Yellowlees, L. J., Shimizu, T., Sagami, I., Guillemette, J. G. and Chapman, S. K. (1999) Potentiometric analysis of the flavin cofactors of neuronal nitric oxide synthase. *Biochemistry.* **38**, 16413-16418
- 104 Roman, L. J., Martasek, P., Miller, R. T., Harris, D. E., de la Garza, M. A., Shea, T. M., Kim, J. J. P. and Masters, B. S. S. (2000) The C termini of constitutive nitric-oxide synthases control electron flow through the flavin and heme domains and affect modulation by calmodulin. *J Biol Chem.* **275**, 29225-29232
- 105 Craig, D. H., Chapman, S. K. and Daff, S. (2002) Calmodulin activates electron transfer through neuronal nitric-oxide synthase reductase domain by releasing an NADPH-dependent conformational lock. *J Biol Chem.* **277**, 33987-33994
- 106 Hannemann, F., Bichet, A., Ewen, K. M. and Bernhardt, R. (2007) Cytochrome P450 systems - biological variations of electron transport chains. *Bba-Gen Subjects.* **1770**, 330-344
- 107 Porter, T. D. (1991) An Unusual yet Strongly Conserved Flavoprotein Reductase in Bacteria and Mammals. *Trends Biochem Sci.* **16**, 154-158
- 108 Isenberg, I. and Szentgyorgyi, A. (1958) Free Radical Formation in Riboflavin Complexes. *P Natl Acad Sci USA.* **44**, 857-862

- 109 Dohr, O., Paine, M. J. I., Friedberg, T., Roberts, G. C. K. and Wolf, C. R. (2001) Engineering of a functional human NADH-dependent cytochrome P450 system. *P Natl Acad Sci USA*. **98**, 81-86
- 110 Hubbard, P. A., Shen, A. L., Paschke, R., Kasper, C. B. and Kim, J. J. P. (2001) NADPH-cytochrome P450 oxidoreductase - Structural basis for hydride and electron transfer. *J Biol Chem*. **276**, 29163-29170
- 111 Gutierrez, A., Paine, M., Wolf, C. R., Scrutton, N. S. and Roberts, G. C. K. (2002) Relaxation kinetics of cytochrome P450 reductase: Internal electron transfer is limited by conformational change and regulated by coenzyme binding. *Biochemistry*. **41**, 4626-4637
- 112 Watkins, D. and Rosenblatt, D. S. (1989) Functional Methionine Synthase Deficiency (Cble and Cblg) - Clinical and Biochemical Heterogeneity. *Am J Med Genet*. **34**, 427-434
- 113 Leclerc, D., Wilson, A., Dumas, R., Gafuik, C., Song, D., Watkins, D., Heng, H. H. Q., Rommens, J. M., Scherer, S. W., Rosenblatt, D. S. and Gravel, R. A. (1998) Cloning and mapping of a cDNA for methionine synthase reductase, a flavoprotein defective in patients with homocystinuria. *P Natl Acad Sci USA*. **95**, 3059-3064
- 114 Galkin, A. A. G., O. Y., Dubinskii, A. A., Kabdin, N. N., Krymov, V. N., Kurochkin, V. I., Lebedev, Y. S., Oransky, L. G., Shuvalov, V. F. (1977) EPR Spectrometer in 2-mm Range for Chemical Research. *Instrum. Experim. Techn*. **20**, 1229
- 115 Poulos, T. L., Sheriff, S. and Howard, A. J. (1987) Cocystals of Yeast Cytochrome-C Peroxidase and Horse Heart Cytochrome-C. *J Biol Chem*. **262**, 13881-13884
- 116 Orville, A. M., Lountos, G. T., Finnegan, S., Gadda, G. and Prabhakar, R. (2009) Crystallographic, Spectroscopic, and Computational Analysis of a Flavin C4a-Oxygen Adduct in Choline Oxidase. *Biochemistry*. **48**, 720-728
- 117 Banerjee, R. V., Frasca, V., Ballou, D. P. and Matthews, R. G. (1990) Participation of Cob(I)Alamin in the Reaction Catalyzed by Methionine Synthase from *Escherichia-Coli* - a Steady-State and Rapid Reaction Kinetic-Analysis. *Biochemistry*. **29**, 11101-11109
- 118 Wolthers, K. R. and Scrutton, N. S. (2007) Protein interactions in the human methionine synthase - Methionine synthase reductase complex and implications for the mechanism of enzyme reactivation. *Biochemistry*. **46**, 6696-6709
- 119 Fujii, K., Galivan, J. H. and Huennekens, F. M. (1977) Activation of Methionine Synthase - Further Characterization of Flavoprotein System. *Arch Biochem Biophys*. **178**, 662-670
- 120 Jarrett, J. T., Amaratunga, M., Drennan, C. L., Scholten, J. D., Sands, R. H., Ludwig, M. L. and Matthews, R. G. (1996) Mutations in the B-12-binding region of methionine synthase: How the protein controls methylcobalamin reactivity. *Biochemistry*. **35**, 2464-2475
- 121 Drennan, C. L., Huang, S., Drummond, J. T., Matthews, R. G. and Ludwig, M. L. (1994) How a Protein Binds B-12 - a 3.0-Angstrom X-Ray Structure of B-12-Binding Domains of Methionine Synthase. *Science*. **266**, 1669-1674

- 122 Evans, J. C., Huddler, D. P., Hilgers, M. T., Romanchuk, G., Matthews, R. G. and Ludwig, M. L. (2004) Structures of the N-terminal modules imply large domain motions during catalysis by methionine synthase. *P Natl Acad Sci USA*. **101**, 3729-3736
- 123 Dixon, M. M., Huang, S., Matthews, R. G. and Ludwig, M. (1996) The structure of the C-terminal domain of methionine synthase: Presenting S-adenosylmethionine for reductive methylation of B-12. *Structure*. **4**, 1263-1275
- 124 Li, Y. N., Gulati, S., Baker, P. J., Brody, L. C., Banerjee, R. and Kruger, W. D. (1996) Cloning, mapping and RNA analysis of the human methionine synthase gene. *Hum Mol Genet*. **5**, 1851-1858
- 125 Olteanu, H., Munson, T. and Banerjee, R. (2002) Differences in the efficiency of reductive activation of methionine synthase and exogenous electron acceptors between the common polymorphic variants of human methionine synthase reductase. *Biochemistry* **41**, 13378-13385
- 126 Resenblatt. (1995) *The Metabolic and Molecular Bases of Inherited Disease*, seventh edition-3-volume set. Edited by Charles R. Scriver, Arthur L. Beaudet, William S. Sly, and David Valle
- 127 Fenton, W. A. a. R., D.S. (1995) *The Metabolic and Molecular Bases of Inherited Disease*, seventh edition-3-volume set. Edited by Charles R. Scriver, Arthur L. Beaudet, William S. Sly, and David Valle
- 128 Leclerc, D., Campeau, E., Goyette, P., Adjalla, C. E., Christensen, B., Ross, M., Eydoux, P., Rosenblatt, D. S., Rozen, R. and Gravel, R. A. (1996) Human methionine synthase: CDNA cloning and identification of mutations in patients of the cblG complementation group of folate/cobalamin disorders. *Hum Mol Genet*. **5**, 1867-1874
- 129 Watkins, D. and Rosenblatt, D. S. (1988) Genetic-Heterogeneity among Patients with Methylcobalamin Deficiency - Definition of 2 Complementation Groups, Cble and Cblg. *J Clin Invest*. **81**, 1690-1694
- 130 Steen, C., Rosenblatt, D. S., Scheying, H., Braeuer, H. C. and Kohlschutter, A. (1997) Cobalamin E (cblE) disease: A severe neurological disorder with megaloblastic anaemia, homocystinuria and low serum methionine. *J Inherit Metab Dis*. **20**, 705-706
- 131 Wilson, A., Leclerc, D., Rosenblatt, D. S. and Gravel, R. A. (1999) Molecular basis for methionine synthase reductase deficiency in patients belonging to the cblE complementation group of disorders in folate/cobalamin metabolism. *Hum Mol Genet*. **8**, 2009-2016
- 132 Brown, T. A. (1991) *The essential techniques in molecular biology*. *Essent. Mol. Biol.* **1**, 1-11
- 133 Madl, T., Felli, I. C., Bertini, I. and Sattler, M. (2010) Structural Analysis of Protein Interfaces from C-13 Direct-Detected Paramagnetic Relaxation Enhancements. *J Am Chem Soc*. **132**, 7285-7287

- 134 Fand, S. B. and Spencer, R. P. (1964) Off-Peak Absorption Measurements in Feulgen Cytophotometry. *J Cell Biol.* **22**, 515-520
- 135 Otwinowski, Z. and Minor, W. (1997) Processing of X-ray diffraction data collected in oscillation mode. *Method Enzymol.* **276**, 307-326
- 136 Murshudov, G. N., Vagin, A. A. and Dodson, E. J. (1997) Refinement of macromolecular structures by the maximum-likelihood method. *Acta Crystallogr D.* **53**, 240-255
- 137 Roussel, A. C., C. . (1991) TURBO-FRODO Version 1.1 release B.
- 138 Emsley, P. and Cowtan, K. (2004) Coot: model-building tools for molecular graphics. *Acta Crystallogr D.* **60**, 2126-2132
- 139 Hevel, J. M., White, K. A. and Marletta, M. A. (1991) Purification of the Inducible Murine Macrophage Nitric-Oxide Synthase - Identification as a Flavoprotein. *J Biol Chem.* **266**, 22789-22791
- 140 Dixon, M. (1953) The Determination of Enzyme Inhibitor Constants. *Biochem J.* **55**, 170-171
- 141 Dawson, R. M. C. (1986) *Data for Biochemical Research.* 3rd Ed
- 142 Odom, B., Hanneke, D., D'Urso, B. and Gabrielse, G. (2006) New measurement of the electron magnetic moment using a one-electron quantum cyclotron. *Phys Rev Lett.* **97**, 30801
- 143 Carrington, A., McLachlan, A. D. and Editors. (1967) *Introduction To Magnetic Resonance; With Applications to Chemistry and Chemical Physics*
- 144 Steinhoff, H. J. (2002) Methods for study of protein dynamics and protein-protein interaction in protein-ubiquitination by electron paramagnetic resonance spectroscopy. *Front Biosci.* **7**, C97-C110
- 145 Kendrew, J. C., Bodo, G., Dintzis, H. M., Parrish, R. G., Wyckoff, H. and Phillips, D. C. (1958) 3-Dimensional Model of the Myoglobin Molecule Obtained by X-Ray Analysis. *Nature.* **181**, 662-666
- 146 Fletterick, R. J., Bates, D. J. and Steitz, T. A. (1975) Structure of a Yeast Hexokinase Monomer and Its Complexes with Substrates at 2.7-Å Resolution. *P Natl Acad Sci USA.* **72**, 38-42
- 147 Shefter, E. (1968) Structural Studies on Complexes 2 - Crystal Molecular Structure of a 1-1 Caffeine and 5-Chlorosalicylic Acid Complex. *J Pharm Sci.* **57**, 1163-1168
- 148 Rini, J. M., Schulzegahmen, U. and Wilson, I. A. (1992) Structural Evidence for Induced Fit as a Mechanism for Antibody-Antigen Recognition. *Science.* **255**, 959-965

- 149 Bossartwhitaker, P., Chang, C. Y., Novotny, J., Benjamin, D. C. and Sheriff, S. (1995) The Crystal-Structure of the Antibody N-10-Staphylococcal Nuclease Complex at 2.9 Angstrom Resolution. *J Mol Biol.* **253**, 559-575
- 150 Coker, S. F., Lloyd, A. J., Mitchell, E., Lewis, G. R., Coker, A. R. and Shoolingin-Jordan, P. M. (2010) The high-resolution structure of pig heart succinyl-CoA:3-oxoacid coenzyme A transferase. *Acta Crystallogr D.* **66**, 797-805
- 151 Hall, G. and Emsley, J. (2010) Structure of human thioredoxin exhibits a large conformational change. *Protein Sci.* **19**, 1807-1811
- 152 Mcpherson, A. (1990) Current Approaches to Macromolecular Crystallization. *European Journal of Biochemistry.* **189**, 1-23
- 153 Solomon, B. and Levin, Y. (1976) Flavin-protein interaction in bound glucose oxidase. *Journal of Solid-Phase Biochemistry.* **1**, 159-171
- 154 Buckholz, R. G. and Gleeson, M. A. G. (1991) Yeast Systems for the Commercial Production of Heterologous Proteins. *Bio-Technol.* **9**, 1067-1072
- 155 Jovin, T. M. A.-J., D.J. (1989) FRET microscopy: digital imaging of fluorescence resonance energy transfer *Cell Structure and Function by Microspectrofluometry.* (eds. Kohen, E., Hirschberg, J.G. & Ploem, J.S.) 99-117
- 156 Slaughter, B. D., Unruh, J. R., Allen, M. W., Urbauer, R. J. B. and Johnson, C. K. (2005) Conformational substates of calmodulin revealed by single-pair fluorescence resonance energy transfer: Influence of solution conditions and oxidative modification. *Biochemistry.* **44**, 3694-3707